To the Graduate Council:
I am submitting herewith a dissertation written by Daniel W. Holley entitled "Synthesis and Characterization of Branched Polyelectrolytes: Star-branched NaPSS". I have examined the final electronic copy of this dissertation for form and content and recommend that it be accepted in partial fulfillment of the requirements for the degree of Doctor of Philosophy, with a major in Chemistry.

Jimmy W. Mays
Major Professor

We have read this dissertation and recommend its acceptance:

Mark Dadmun

Bin Zhao

Bin Hu

Accepted for the Council:

Carolyn R. Hodges
Vice Provost and Dean of the
Graduate School

(Original Signatures are on file with official student records.)

# Synthesis and Characterization of Branched Polyelectrolytes: Star-branched NaPSS

**A Dissertation**

**Presented for the**

**Doctor of Philosophy Degree**

**The University of Tennessee, Knoxville**

**Daniel W. Holley**

**December 2009**

# Dedication

This work is dedicated to the memory of Leah Nicole Holley, my sister and friend.

# Acknowledgements

I would like to thank my dissertation committee for their patience and time, as well as my advisor, Dr. Jimmy Mays, for things too numerous to list. I would also like to thank all of the members of the Mays group, past and present, for their support and guidance. In addition, the following people assisted in the scientific work, or listened to me complain about polyelectrolytes:

| Scientific | Non-scientific |
| --- | --- |
| Duraij Baskaran | Hillary Fleenor |
| Jin Chuan Yang | Patricia Mays |
| David Uhrig | |
| Ravi Aggarwal | |
| Andrew Goodwin | |
| Tom Malmgren | |

# Abstract

In this thesis, we examined the effect of branching on the solution characteristics of polyelectrolytes using a set of star-branched NaPSS. The polystyrene precursors to these polyelectrolytes were synthesized using anionic polymerization allowing for the production of three distinct groups of star-branched polystyrenes with varying functionality and arm length.

Following sulfonation, several methods commonly employed in the literature for evaluation of sulfonation degree we established that sulfonation was quantitative. TGA was also demonstrated to reveal important characteristics of the sample.

We used aqueous SEC coupled with a multiple angle light scattering detector to determine several molecular characteristics of the star-branched NaPSS samples. Linear NaPSS synthesized via radical polymerization and sulfonation of polystyrene were characterized and important differences between NaPSS synthesized by the two methods were established. Dynamic light scattering experiments established a qualitative link between the presence of a slow diffusive mode and the degree of sulfonation. The branching parameter *g* was determined for the star-branched NaPSS samples and compared to theoretical predictions.

Static light scattering experiments were performed to elucidate the effect of $C_s$ on the $R_g$, where it was determined that $R_g \sim C_s^{-0.11}$ for the whole range of samples. The apparent persistence length was determined and relations were established for its variation as a function of $C_s$, *f* and degree of arm polymerization. Additionally, no agreement was found between theoretical predictions of *g* and experimentally determined ones. A method was developed that enabled the determination of molecular dimensions

of star-branched NaPSS using AFM with a high degree of agreement with the radii established using scattering methods on solutions of the polymers.

The intrinsic viscosity could reliably be determined in solutions with $C_s$ using either a Huggins or Wolf equation. For solutions with no $C_s$, the Huggins equation fit over the data at low $C_p$ was confirmed by AFM measurements of the dimensions of the polyelectrolyte and comparisons to the radius determined from the intrinsic viscosities calculated using the two equations to be more accurate. The values of g' were calculated for solutions of the NaPSS stars in water and compared with theory.

# Table of Contents


**PART 1: INTRODUCTION ..... 1**

***Issues Related to Polyelectrolyte Characterization ..... 3***
*Model Polyelectrolyte Synthesis via Sulfonation ..... 3*
*Bi-modal Distribution of Relaxation Times ..... 4*
*The Viscosity Polyelectrolyte Effect ..... 5*

***Polyelectrolyte Theory ..... 5***
*Linear Chains ..... 6*
*Star Polyelectrolytes in the Osmotic Regime ..... 9*

***Branched Polyelectrolytes-Experimental Studies ..... 10***
*Star-Branched Poly(acrylic acid) ..... 10*
*Star-Branched Sodium Poly(styrenesulfonate) ..... 12*
*Other Branched Architectures ..... 13*
*Frozen Micelles ..... 14*

***Motivation for Work ..... 16***

***Appendix ..... 19***

***References ..... 23***

**PART 2: THEORETICAL BACKGROUND AND EXPERIMENTAL DETAILS OF SYNTHESIS AND CHARACTERIZATION ..... 27**

***Living Polymerization ..... 28***

***Anionic Polymerization ..... 30***
*Star Polymer Synthesis ..... 31*
*Linking Reagents ..... 32*

***Sulfonation ..... 33***

***Characterization Theory ..... 35***
*Size Exclusion Chromatography ..... 35*
*Aqueous Size Exclusion Chromatography ..... 37*
*Static Light Scattering ..... 38*
*Dynamic Light Scattering ..... 41*

*Experimental* ..... *42*
*Anionic Polymerization-Vacuum Line* ..... *43*
*Anionic Polymerization-Reagents* ..... *43*
*Anionic Polymerization-Procedure* ..... *46*
*Sulfonation-Procedure* ..... *51*
*Characterization-SLS* ..... *53*
*Characterization-AFM* ..... *54*

*Appendix* ..... *58*

*References* ..... *65*

**PART 3: SYNTHESIS AND CHARACTERIZATION OF STAR-BRANCHED POLYELECTROLYTES ..... 68**

*Abstract* ..... *69*

*Introduction* ..... *70*

*Experimental* ..... *73*

*Results and Discussion* ..... *76*
*Synthesis and Characterization of Precursor Polystyrenes* ..... *76*
*Sulfonation Degree Characterization* ..... *78*
*Aqueous SEC Results* ..... *84*

*Summary and Conclusions* ..... *93*

*Appendix* ..... *95*

*References* ..... *115*

**PART 4: STATIC LIGHT SCATTERING STUDY OF STAR-BRANCHED NAPSS IN AQUEOUS SOLUTIONS OF VARYING IONIC STRENGTH ..... 118**

*Abstract* ..... *119*

*Introduction* ..... *119*

*Experimental* ..... *122*

*Results and Discussion* ..... *124*
*Static Light Scattering-$R_g$, $R_h$, $A_2$* ..... *124*

*Persistence Length* ..... *127*
*Branching ratio g* ..... *130*
*Dynamic Light Scattering* ..... *132*
*Atomic Force Microscopy* ..... *133*

***Summary and Conclusions*** ..... ***135***

***Appendix*** ..... ***136***

***References*** ..... ***148***

**PART 5: VISCOMETRIC PROPERTIES OF STAR-BRANCHED NAPSS IN SOLUTIONS OF VARYING IONIC STRENGTH** ..... **151**

***Abstract*** ..... ***152***

***Introduction*** ..... ***153***

***Experimental*** ..... ***154***

***Theory*** ..... ***156***

***Results and Discussion*** ..... ***158***
***Intrinsic Viscosity – Solutions with $C_s$*** ..... *158*
***Intrinsic Viscosity – No $C_s$ Solutions*** ..... *160*
***Viscometric Radius ($R_v$)*** ..... *162*
***Atomic Force Microscopy - $R_{afm}$ and $R_v/R_h$*** ..... *163*
***Branching ratio g'*** ..... *166*

***Summary and Conclusions*** ..... ***169***

***Appendix*** ..... ***171***

***References*** ..... ***186***

**PART 6: FINAL CONCLUSIONS AND SUMMARY** ..... **189**

***Final Conclusions*** ..... ***190***

***Future Work*** ..... ***193***

**VITA** ..... **195**

# List of Figures

Figure 1: Examples of common synthetic polyelectrolytes. 1.) the bromine salt of quaternized poly(4-vinylpyridine), an example of a strong cationic polyelectrolyte. 2.) sodium poly(styrenesulfonate), an example of a strong anionic polyelectrolyte. 3.) sodium poly(acrylic acid), an example of a weak anionic polyelectrolyte. ..... 20

Figure 2: Plot of the apparent diffusion coefficient ($D_{app}$) vs. log [NaBr], showing the evolution of a bimodal distribution of relaxation times upon decreasing $C_s$. [9] ..... 21

Figure 3: Plot of the reduced viscosity vs. the concentration for NaPSS of varying degrees of polymerization, displaying the increase in $\eta_{red}$ ($\eta_{red} = \eta_{rel}$-1/$C_p$) with decreasing $C_p$, known as the viscosity polyelectrolyte effect.[37] ..... 22

Figure 4: Vacuum Line Diagram ..... 59

Figure 5: Synthesis of Star-branched polystyrene ..... 60

Figure 6: Star Polystyrene Synthesis Apparatus ..... 61

Figure 7: Polystyene Sulfonation and Neutralization ..... 62

Figure 8: Closed-Loop Filtration Schematic ..... 63

Figure 9: Atomic Force Microscopy Schematic ..... 64

Figure 10: SEC elugrams of 40 star series in THF, showing the decrease in Retention Time with an increase in both molecular weight and *f*. ..... 96

Figure 11: Elution Profile of 54p, showing an efficient separation of the portions of the sample on the basis of molecular weight. ..... 99

Figure 12: Titration of 54s, showing a sharp transition expected for titration of a strong acid by a strong base. ..... 100

Figure 13: $^1$H NMR of 54s in $D_2O$, showing peak assignments and integrations relative to the 3 $H_c$ protons on the polymer backbone. ..... 101

Figure 14: Thermogravimetric Analysis of 54s, displaying the parameters discussed in the text. ..... 102

Figure 15: ASEC-MALLS elugram of 1.18Mstd, displaying a multimodal peak and nonlinear evolution of molecular weight with elution volume. ..... 105

Figure 16: ASEC-MALLS elugram of NaPSSrad2, showing a linear evolution of molecular weight with elution volume, indicative of homogeneity. ..... 106

Figure 17: ASEC-MALLS Elugram of 52s, showing an almost linear evolution of molecular weight with elution volume. ..... 108

Figure 18: ASEC-MALLS of 46s, showing 90° light scattering and refractive index signals. ..... 109

Figure 19: Comparison of $R_g$ vs. *f* between polystyrene (PS) precursors and NaPSS stars for 6 series of star polymers, showing a slightly larger increase of $R_g$ with *f* for the NaPSS series of stars. ..... 110

Figure 20: $R_g$ vs. $M_w$ for the 6 series. ..... 111

Figure 21: Berry Plot of 56s in 0.1M NaCl. ..... 137

Figure 22: Sample 54s in (a) water and (b) 1M NaCl aqueous solution, showing change with change in $C_s$. ..... 143

Figure 23: Sample 54s cast on mica from water. The colored lines illustrate the method of measuring $R_{afm}$ described in detail in the text. ..... 144

Figure 24: (a) AFM image of the sample 54s cast on mica from 1M NaCl solution showing the raised core region surrounded by a "sombrero" rim. (b) Graph corresponding to lines and crosshairs, with dotted lines corresponding to position of crosshairs on image. The distances measured between crosshairs placed at periphery and the core are 29 nm, 28 nm, and 26 nm for the blue, red, and green markers respectively. ..... 146

Figure 25: AFM image of sample 66s cast from 0.01M NaCl aqueous solvent onto mica, copied from 2D Single Molecules program. The green lines tracing the star arms are manually drawn. ..... 147

Figure 26: Typical Huggins plot of the concentration dependence of $\eta_{red}$ for 54s in solutions of varying $C_s$, showing the decrease in [η] with increasing $C_s$. ..... 172

Figure 27: Plot showing ln $\eta_{rel}$ vs. $C_p$ fitted using Wolf equation (Equation 17). ..... 174

Figure 28: Huggins plots of the 50s series of polymers in water, showing extrapolation of low concentrations to infinite dilution. ..... 175

Figure 29: ln $\eta_{rel}$ vs. $C_p$ for sample 2.69Mstd, fitted using Wolf equation (Equation 17). ..... 177

Figure 30: AFM image of sample 62s, cast from a dilute aqueous solution with no $C_s$. 179

Figure 31: AFM images of dilute aqueous solutions of star NaPSS, showing possible aggregation at different length scales. (a) shows 46s at a length scale of 1.3 μm, the average lateral diameter of the domains is ~0.7 μm. (b) is an expanded view of the same

sample at a length scale of 10 μm, showing domains and individual chains. (c) is an image of a dilute aqueous solution of 44s at a 20 μm length scale. ..... 181

Figure 32: $\eta_{red}$ vs. $C_p$ for aqueous solutions of 50s series of samples, showing the viscosity polyelectrolyte effect. The lines drawn are guides for the eye only. ..... 182

Figure 33: : $\eta_{red}$ vs. $C_p$ for aqueous solutions of 60s series of samples, showing viscosity polyelectrolyte effect. The lines drawn are guides for the eye only. ..... 183

Figure 34: $\eta_{red}$ vs. $C_p$ plots for 40s series of samples, showing rapid changes in slope at the lowest $C_p$. A log-log scale is employed, and the lines are guides for the eye only.. 184

# List of Tables

Table 1: Molecular Characteristics of Star Polystyrenes ..... 97

Table 2: Radii of Star Polystyrenes ..... 98

Table 3: Characterization of Sulfonation Degree for Star-branched and Linear NaPSS103

Table 4: TGA Results for Star-branched and Linear NaPSS ..... 104

Table 5: Aqueous SEC Results for Linear NaPSS ..... 107

Table 6: Aqueous SEC Results for Star-branched NaPSS ..... 112

Table 7: Dynamic Light Scattering of Linear and Star-branched NaPSS ..... 113

Table 8: g Values for Star-branched NaPSS and Polystyrene Precursors ..... 114

Table 9: Static Light Scattering of Star-branched NaPSS in Aqueous 1M NaCl ..... 138

Table 10: Static Light Scattering of Star-branched NaPSS in Aqueous 0.1 M NaCl .... 139

Table 11: Static Light Scattering of Star-branched NaPSS in 0.01 M NaCl ..... 140

Table 12: Combinatorial Wormlike Chain Parameters ..... 141

Table 13: Experimental and Theoretical *g* values for NaPSS star polymers in aqueous solvents of varying ionic strength ..... 142

Table 14: $R_{afm}$ Averages in Solutions of Varying $C_s$ ..... 145

Table 15: Intrinsic Viscosities and Wolf Coefficients for Aqueous Solutions of Star-branched NaPSS at Various $C_s$ ..... 173

Table 16: Intrinsic Viscosities and Coefficients for Aqueous Solutions of Star-branched NaPSS determined by Huggins and Wolf Extrapolations ..... 176

Table 17: Values of the Viscometric Radius $R_v$ for Solutions of Star-branched NaPSS in Solvents of Varying Ionic Strength with $R_{afm}$ ..... 178

Table 18: $R_v/R_h$ Values for Solutions of Star-branched NaPSS in Aqueous Solvent of Varying Ionic Strength ..... 180

Table 19: Experimental and Theoretical g' values for Solutions of Star-branched NaPSS in Water and Polystyrene Precursors in THF ..... 185

# Part 1: Introduction

One of the materials that is essential to modern life is a class of chemical compounds known as polymers, which are composed of many small chemical repeating units known as monomers covalently connected together to form a macromolecular chain. Polymers can exhibit a wide variation in their chemical and physical properties upon seemingly small changes in their monomeric functionality and microscopic chemical structure. The properties of polymers can be tailored through selection of different types of monomers and through architectural control. This variation of polymers properties makes synthetic polymeric materials useful in applications ranging from controlled drug delivery to bulletproof vests, and is due to factors including but not limited to molecular weight, molecular weight distribution, branching, monomer composition, morphology, tacticity, microstructure, and functionality. Although polymers can be subdivided into many different categories based upon factors such as polymerization method, polymerization mechanism, and potential function, the category of polymers known as polyelectrolytes, which are water soluble ionic polymers resembling biomacromolecules in their complexity and function in aqueous systems, is of primary interest in this thesis.[1]

Polyelectrolytes are polymer chains that bear a large percentage of groups that disassociate in water or other polar solvent and in turn acquire an electrical charge.[2] Depending on the nature of the ionic groups, polyelectrolytes are broadly classified into anionic and cationic polymers, and can be further classified as strong or weak polyelectrolytes. Examples of typical strong anionic, strong cationic and weak anionic polyelectrolytes are given in Figure 1. Strong polyelectrolytes dissociate spontaneously in solution, whereas weak polyelectrolytes require interaction with small molecules in

solution in order for dissociation to occur. This dissociation and the resulting molecular structure that arises from it, namely regions of like charge connected in a chain, with a cloud of counterions that vary in their degree of association with the charged polymer backbone gives rise to the many characteristic differences observed between solutions of neutral polymers and polyelectrolytes. In the next section a number of problems in the polyelectrolyte field are described for the purpose of illustrating these differences.

## *Issues Related to Polyelectrolyte Characterization*

### *Model Polyelectrolyte Synthesis via Sulfonation*

Sodium poly(styrene sulfonate) (NaPSS) is the polymer most often regarded in the literature as a model polyelectrolyte. In the typical case, NaPSS is synthesized using anionic polymerization of styrene to produce narrow molecular weight distributed polystyrene and subsequently sulfonated utilizing a number of different conditions.[3] The details of the sulfonation reaction will be covered in detail in a subsequent chapter, but are left out here for the sake of clarity. The sulfonation degree of NaPSS is determined via titration, elemental analysis or nuclear magnetic resonance spectroscopy (NMR), and the NaPSS is then analyzed with the assumption that the sulfonated material is nearly monodisperse.[4-6] However, it is occasionally noted that the materials subjected to the harsh conditions of sulfonation may contain significant amounts of crosslinks and intramolecular or intermolecular linkages formed via sulfone formation. Sulfones are very stable compounds formed from highly reactive $SO_3H$ groups that can only be decomposed by melting with alkaline hydroxides. Even a small number of sulfone linkages can have a profound effect on the solution properties of the NaPSS obtained using post polymerization sulfonation.[7] Moreover, there is still some debate as to the

characterization of the degree of sulfonation obtained via these post-polymerization processes. This factor is important, as the properties of sulfonated materials can have a strong dependence on the degree of sulfonation.[8] These problems associated with sulfonation become even more complex in the case of NaPSS with a branched architecture.

***Bi-modal Distribution of Relaxation Times***

A second interesting characteristic of polyelectrolyte solutions, first reported by Lin, Lee and Schurr in 1978, relates to an experimental technique known as dynamic light scattering (DLS).[9] In this study, it was observed that aqueous solutions of L-lysine subjected to progressively lower concentrations of added salt ($C_s$) displayed bimodal distributions of their relaxations times below a certain critical $C_s$ that is related to the concentration of polyelectrolyte ($C_p$) in the solution. The graph illustrating this relationship is reprinted in Figure 2. In more recent studies that had the technological advantage of auto-correlators capable of handling multimodal distributions, the relaxation times in the bimodal regime were quantified.[4,5,10-13] The shorter relaxation time, referred to hereafter as the fast mode, is generally taken to reflect "diffusive properties of single macroions or at least large segments of single macroions.", even though this would require a whole polyelectrolyte chain or segments of a polyelectrolyte chain to traverse several thousand angstroms at rates close to those of small ions or solvents.[14] The longer relaxation time, referred to hereafter as the slow mode, is generally accepted to represent multimacroion domains or aggregates of polyelectrolytes, as shown by small angle neutron experiments.[15] However, this mode is still a topic of considerable debate, as indicated by Sehgal and Seery and Sedlak.[11,12] The following quote illustrates the

difficulties associated with interpreting the experimental results: "Nevertheless, eigenmodes (and associated decay rates) in general can be identified with simple types of motions (that can be easily visualized) only in very special cases."[11]

***The Viscosity Polyelectrolyte Effect***

A third problem unique to polyelectrolyte solutions is related to viscosity, and is generally referred to as the viscosity "polyelectrolyte effect". In aqueous solutions of low ionic strength ($C_s$ approaching zero), it has been observed that highly charged polyelectrolytes exhibit an increase in reduced viscosity ($\eta_{red}$) with decreasing $C_p$, sometimes displaying a peak.[6,16-19] This phenomenon, which is illustrated in Figure 3, is in contrast to solutions of neutral polymers, which exhibit a linear relationship between these two parameters even at low concentrations, and can be safely extrapolated to infinite dilution to determine the intrinsic viscosity ($[\eta]$) using the Huggins equation;

$$\eta_{red} = [\eta] + k'[\eta]^2 C_p \quad (1)$$

where $k'$ is the Huggins coefficient, which varies depending on a variety of experimental conditions. Although this transition is usually attributed to the expansion of polyelectrolyte chains to occupy more volume in solution, the theoretical interpretation of this phenomenon is still controversial, and with the experimental difficulties associated with characterizing polyelectrolytes under conditions of low $C_s$, is likely to remain so.

## *Polyelectrolyte Theory*

As the examples in the previous section illustrate, the properties of linear polyelectrolyte solutions are still a matter of some debate, especially in comparison to the properties of solutions of linear neutral polymers. Considering this, it should come as no surprise that the properties of branched polyelectrolytes are even less well understood, in

spite of intense interest from theoreticians.[20-22] Since star-branched polymers are often used as models for the effects of branching on solution properties, many publications have dealt with both the theory and modeling of such systems. Recently, Rubinstein and Shusharina published a work that describes a comprehensive scaling theory for solutions of star-branched polyelectrolytes.[22] In order to demonstrate several key theoretical concepts of polyelectrolyte solutions, the next two sections will examine linear and star-branched polyelectrolytes using the theory described in the aforementioned publication.

***Linear Chains***

The electrostatic blob model, a scaling theory first proposed by deGennes, is the basis for much of the theory surrounding the behavior of polyelectrolyte stars in solution.[23] It is important to note here that scaling theories such as the one used by deGennes show qualitative trends between various parameters, rather than an exact quantitative relationship between them. In the scaling model a flexible linear polymer chain having *N* Kuhn segments each of *b* in length is dissolved in a polar liquid with a dielectric permittivity ε at temperature $T$.[24] The term Kuhn segment comes from theoretical treatments of polymer chains using the random flight model, and denotes a division of the polymer chain into statistical segments that are freely jointed in relation to each other. Concentration of the polymer is expressed in terms of the Kuhn segment number density, *c*. The fraction of charged Kuhn segments in an individual polymer chain is denoted by *f*, and carrying an elementary charge *e*. Keeping these parameters in mind, a polyelectrolyte chain can be visualized as a collection of electrostatic blobs connected in a linear array. The size of these blobs is given by

$$\xi_{el} \approx b(uf^2)^{-1/3} \tag{2}$$

with $u = l_B/b$. $l_B$ is an important constant of a given polyelectrolyte system called the Bjerrum length, and is defined as follows:

$$l_B = \frac{e^2}{\varepsilon k_B T} \tag{3}$$

where $k_B$ is the Boltzmann constant.[2] The Bjerrum length is defined as the distance at which the electrostatic interaction between two like charges becomes close in magnitude to the thermal energy. Under these conditions, which neglect the effect of counterions entirely, the size of the polymer chain is given by

$$R_{lin}^{d} \approx \frac{b^2 N}{\xi_{el}} \approx bN(uf^2)^{\frac{1}{3}} \tag{4}$$

Though simple, the preceding model of polyelectrolyte conformation cannot be applied to experimental conditions because it neglects an important phenomenon unique to solutions of polyelectrolytes. The assumption in the previous model is that the counterions of the charged portions of the chain are dispersed homogeneously throughout the solution and thus have no significant effect on the electrostatic blobs. This assumption is not valid under most experimental conditions, where relatively large Bjerrum lengths drive the counterions into close association with the oppositely charged sections of the polyelectrolyte chain.[25,26] This phenomenon, known as counterion condensation, effectively reduces the overall charge of the chain and thereby affects its overall conformation. In order to model this phenomenon, we must consider the electrostatic energy of interaction of a counterion with the chain of blobs. For this, the polyelectrolyte chain can be modeled as a charged cylinder and the energy of interaction can be described by

$$\mathrm{E}_{ei} = \left( {ep_0}/{\varepsilon} \right) \ln r \tag{5}$$

where r is the distance of the charge from the cylinder and $p_0$, called the linear charge density, is as follows:

$$p_0 \approx \frac{ef^{1/3}}{bu^{1/3}} \tag{6}$$

When $p_0 > e/l_B$, the conditions appropriate for condensation of the counterions exist. This situation, which is commonly referred to as the Manning condition for condensation, and can be expressed as

$$u^2 f > 1 \tag{7}$$

Due to the effective reduction in charge that occurs under these conditions, the electrostatic blob must become larger to be on the order of the thermal energy, therefore

$$\xi_{el}^{c} \approx b(uf^2\beta^2)^{-1/3} \approx l_B \tag{8}$$

where $\beta$ is defined as the fraction of counterions remaining uncondensed to the chain. An estimate of the quantity $\beta$ is given by

$$\beta \approx 1/(u^2 f) \tag{9}$$

under the conditions appropriate for counterion condensation. Some algebraic manipulation of the preceding equations reveals that $\xi_{el}^{c}$ is approximately the size of $l_B$. Naturally, since the size of the electrostatic blob has changed because of counterion condensation, the overall size of the chain has also changed, and is now represented as

$$R_{lin}^{c} = bN/u \tag{10}$$

This concludes the description of the theory of conformation of linear polyelectrolytes in water with no added salt, and provides a basis for the following description of star polyelectrolyte conformation.

***Star Polyelectrolytes in the Osmotic Regime***

According to Rubinstein, three structural regimes have been identified for star polyelectrolytes in dilute solution with no added salt.[22] These are the polyelectrolyte, osmotic, and quasi-neutral regimes. For the purposes of this Introduction, only the osmotic regime under conditions of counterion condensation will be described, since this is the regime that has the most experimental relevance. The crossover condition from the experimentally inaccessible polyelectrolyte regime to the osmotic regime is defined as the condition where

$$l_B \frac{pNf}{R} > 1 \tag{11}$$

where $p$ is the number of arms per star, $N$ is the number of Kuhn segments per arm, $f$ is the fraction of charged segments, and $R$ is the radius of the star. This delineates the point where it is energetically more favorable to condense counterions into the spherical volume of the star to reduce electrostatic repulsion between segments rather than to stretch the arms further. It should be noted that that condensation into the volume of the star is not the same as counterion condensation onto the star arms, leading to a situation where the aforementioned fraction β of the counterions remains "free" in the spherical volume of the star, with the rest of the counterions condensed on the chain in the same manner as in the linear case. In fact, it is found that in the osmotic regime, under conditions of counterion condensation, the blob size ($\xi^{os}$) and the star radius ($R_{OS}$) are described as

$$\xi^{OS} \approx b(uf^2\beta^2)^{-1/3} \approx l_B \quad (12)$$

$$R_{OS} \approx bN/u \quad (13)$$

A comparison with equations (8) and (10) above reveals that, surprisingly, both the blob and overall size of an arm in a polyelectrolyte star is exactly the same as that of a linear chain of the same degree of polymerization as the arm. Numerous other concentration regimes exist for polyelectrolyte stars, both in the absence and presence of $C_s$. These regimes will be described in the text when they are applicable to experimental results.

## *Branched Polyelectrolytes-Experimental Studies*

Although the problems described in the previous section have been extensively studied in the case of linear polyelectrolyte chains, very few experimental studies have been performed involving polyelectrolytes with branched architectures. This is particularly true of those architectures with controlled degrees of branching, such as combs and stars. In this section a review of the current literature on branched polyelectrolytes will be presented, with a particular emphasis on controlled architectures and solution properties of branched polyelectrolytes.

### *Star-Branched Poly(acrylic acid)*

A number of experimental studies have been performed on polyacrylate stars synthesized by various methods. In general, these studies involve the synthesis of acrylate or methacrylate linear polymers via atom transfer radical polymerization (ATRP), and subsequent linking to a difunctional monomer such as divinylbenzene (DVB) or a multifunctional linking reagent to make star branched polyacrylates and polymethacrylates. These polyacrylate stars are then hydrolyzed to produce poly (acrylic

acid) (PAA) or poly(methacrylic acid) (PMAA) stars, which are considered to be weak polyelectrolytes. In order to study the formation of a crystalline ordering of highly branched stars near the overlap concentration C*, Furukawa and Ishizu synthesized two poly(acrylic acid) stars with arm functionality (*f*) of 30 and 97.[27] They found that the stars behaved as soft spheres in solution, and that the solutions formed a bcc (body centered cubic) crystalline ordering above the C*. Moinard et al., performed experiments on a similar system comprised of four- and six-arm PAA based stars, with different counterions ($Na^+$, $Cs^+$, and $Rb^+$)[28]. The authors performed static and dynamic light scattering experiments on these polymer solutions to determine their average molar mass ($M_w$), radius of gyration ($R_g$), second virial coefficient ($A_2$), hydrodynamic radius ($R_h$), and persistence length $L_p$, which is defined as the length of the polymer chain over which correlations in the direction of the tangent are lost and is an informal measure of the stiffness of the chain. The viscosity polyelectrolyte effect, as well as a bimodal distribution of relaxation times in DLS, was also observed in these solutions. It was noted that the relative increase in $\eta_{red}$ with decreasing $C_p$ is not as large as in the case of the linear PAA systems studied. While a thorough examination of solution properties of the samples available was performed in this work, the breadth of conclusions that could be reached in regards to variables such as *p* and *N* of the stars was somewhat limited due to the small set of samples that were used. The small size of the stars, resulting in $R_g$'s that are close to the theoretical limit of detection by light scattering (< 20nm), is also problematic. In a similar work, Muller et al. examined the osmotic coefficients and the titration curves of a series of PAA stars with different functionalities and arm lengths synthesized by atom transfer radical polymerization.[29] They found that the titration

curves were shifted to higher pH with increasing *p* due to increasing osmotic pressure and segment density inside the stars. They also found that the osmotic coefficient, defined as

$$\phi = \frac{\Pi_m}{\Pi_{cal}} \tag{14}$$

where $\Pi_m$ denotes the measured osmotic pressure and $\Pi_{cal}$ is the calculated osmotic pressure according to van't Hoff's law, decreases with increasing arm functionality. One difficulty with this work, as with all studies of weak acids such as PAA, is that the ionization degree of the polyelectrolyte changes significantly with the pH of the solution, making it more difficult to study solution properties solely as a function of the ionic strength. This is not true in the case of NaPSS, which has a degree of ionization nearly independent of solution pH. The current literature available on regularly branched examples of NaPSS will be examined in the next section.

***Star-Branched Sodium Poly(styrenesulfonate)***

The first reported synthesis and characterization of star-branched NaPSS was in a work by Mays.[30] In this work, star-branched polystyrene of low polydispersity was synthesized by an arm-first method using anionic polymerization, and these polymers were sulfonated to produce star polyelectrolytes. DLS experiments on these samples revealed that the $R_h$ of star-branched materials were much less sensitive to $C_s$ than linear materials of the same $M_w$. In 2001, Heinrich and coworkers studied a collection of star-branched NaPSSs utilizing small-angle X-ray scattering.[31] The purpose of this work was to study the previously mentioned ordering phenomenon of polyelectrolyte stars near C* with NaPSS stars of a much lower functionality ($f$ ~12) than those of Furukawa and Ishizu. The main conclusion reached from this work was that the ordering phenomenon which was observed in polystyrene (PS) stars was also observed in the NaPSS stars,

although over a larger range of concentrations. In fact the degree of ordering was seen to increase as the $C_p$ decreased past C*, an effect that was attributed to electrostatic interactions. This result supports the conclusion that crystalline order can be achieved in solutions of polyelectrolyte stars with less functionality than is required for solutions of neutral polymer stars, as the ordering is seen to be at least partially due to electrostatic interactions in this case. It is worthy of note that the star-branched NaPSS studied in this work were partially sulfonated (an average of ~69% for the three samples studied) and presented an "amphiphilic character" in aqueous solutions.

***Other Branched Architectures***

In addition to the star-branched architectures mentioned above, a couple of works involving other branched architectures deserve mention. The first of these works was presented by Fernyhough and co-workers, who describe the synthesis and characterization of NaPSS with a comb architecture.[32] The degree of sulfonation of the combs was verified by NMR and titration, and aqueous size exclusion chromatography (ASEC) confirmed that the structure of the polystyrene combs was maintained through the sulfonation process. The $M_w$ and sulfonation degree of the sulfonated combs was reported, but no other data was presented regarding the solution properties of the polyelectrolytes. A work on somewhat similar structures was recently published by Lienkamp and co-workers.[33] The authors of this work synthesized end-functionalized cylindrical NaPSS brushes by utilizing anionic polymerization of the backbone followed by atom transfer radical polymerization (ATRP) of dodecyl and ethyl sulfonate esters to produce the brush arms. The synthesized copolymer contained a hydrophobic *p*-methylstyrene backbone with arms consisting of partially hydrolyzed

polystyrenesulfonate dodecyl and ethyl esters. For the majority of copolymers characterized in this work the degree of hydrolysis of the esters was ~66%. The authors performed extensive characterization of these materials using static and dynamic light scattering as well as cryo-TEM, all of which indicated that the materials have a high tendency to aggregate in solution. This high tendency to aggregate limits the conclusions that can be reached regarding the solution properties as a function of the branching degree of individual polyelectrolyte molecules.

***Frozen Micelles***

In recent years a large body of literature has accumulated regarding the phenomenon of micellization of diblock copolymers consisting of both charged and neutral block segments in aqueous solution. A micelle is an ordered aggregate of molecules driven by the incompatibility of one portion of the molecule with the surrounding solvent selective for the other portion. In aqueous solution, charged/neutral diblock copolymers form micelles when the $C_p$ reaches a certain minimum concentration called the critical micelle concentration (cmc). Because these amphiphilic block copolymers often self-assemble into spherical star-like structures in solution, the resulting micelles are sometimes regarded as models for star-branched polyelectrolytes. While there are a number of publications on this subject, the author would like to mention some examples that have most often been referenced in the literature concerning star polyelectrolyte theory. In the first often-cited example, Muller and coworkers examined the behavior of micellar solutions of asymmetric diblock copolymers made of deuterated sodium poly(styrenesulfonate) ($NaPSS_d$) and of poly(ethylene-*alt*-propylene) (PEP) or of poly(tert-*butyl*-styrene) (PtBS).[34] In aqueous solution these copolymers form micelles

with a core radius ($R_c$) that was found to be concentration independent over a wide range, resulting in structures with a "frozen core". The authors focused on concentrated solutions of the micelles, and found that there are two intensity peaks in the plot of neutron-scattered intensity versus the scattered wave vector ($q$) at concentrations well above the C*. The first peak shifted as $C_p^{1/3}$ while the second shifted as $C_p^{1/2}$. The origin of the second peak was given two possible explanations. The first was that it was due to the interpenetration of the micelles, and the second was that it was due to the contraction of some arms inside the micelle. Experiments of a similar nature carried out by Korobko and coworkers on a system composed of diblock copolymers of poly(styrene-*b*-acrylic acid) indicated that in fact the radii of the micelles decreases at concentrations around the C* and finally that interdigitation occurs at concentration much beyond this.[35] At this point it is pertinent to make some observations regarding the perception of these micellar systems as models for polyelectrolyte stars:

1. The versatility of these systems as far as the functionality and length of the arms is limited by the necessity to have appropriate segmental lengths of hydrophibic and hydrophilic blocks in order to achieve aggregation leading to stable micelles in solution.
2. Although the volume of the hydrophobic core of these micelles is small relative to the volume of the star, it might be possible for it to affect the conformation of the star. A phenomenon involving linear polyelectrolytes has been reported, where hydrophobic patches on the same polymer chain resulting from partial sulfonation have aggregated, resulting in a more collapsed conformation in solution relative to

the fully sulfonated species[8]. A similar situation could exist in the case of these micelles, though an experimental test of this hypothesis has not been performed.

3. An examination of the literature reviewed above will reveal that, while a variety of scattering methods have been applied to micellar systems in order to elucidate their solution properties, these studies have concentrated on the regime of $C_p$ close to the C*. The reason for this is a fundamental property of these frozen micelle solutions: The star-like structures they form in solution are stable only within a certain range of $C_p$ and $C_s$ [36]. Naturally this limits the scope of the solution properties that can be studied with these branched polyelectrolytes.

## *Motivation for Work*

As has been demonstrated above, a systematic and comprehensive study of the solution properties of star-branched polyelectrolytes has not yet been performed. Therefore, due to the large degree of interest shown by theoreticians, as well as the need to understand structurally similar biological systems, we propose the synthesis and characterization of a series of star-branched NaPSS. The proposed work is organized into the following steps:

- The synthesis of DVB-linked polystyrene stars that vary in the parameters of *f* and *N* using anionic polymerization, and full characterization of these molecules for verification of model architecture. This will consist of the determination of $M_n$,$M_w$, $R_g$, $R_h$,[η] and polydispersity for these samples using SEC coupled with light scattering and viscosity detectors.
- The sulfonation of the polystyrene stars to produce NaPSS star-branched molecules suitable for examining the effect of variation of *f* and *N* on the solution

properties of star-branched polyelectrolytes. Full characterization of the degree of sulfonation will be effected by all currently available means, including titration, $^1$H NMR, and elemental analysis. The results from these methods will also be compared to results obtained by TGA.

- Aqueous gel-permeation chromatography will be used to determine determine $M_n$,$M_w$, $R_g$ and polydispersity of the NaPSS stars, and these results will be compared with the previous results determined for the polystyrene precursors as well as theoretically calculated values. $R_h$ values for the NaPSS stars will be determined and the values of the ratio $R_g/R_h$ and the branching parameter $g$ will be compared with the values determined for the neutral precursors and with theory.
- Examination of the variation of solution properties with $C_s$ will be completed by a series of static light scattering (SLS) experiments performed at various $C_s$. The information obtained from these experiments will be the $A_2$, $M_w$, and $R_g$ all as functions of $C_s$, $f$, and $N$ which will be compared with theoretical predictions of polelectrolyte stars in the dilute osmotic regime with added salt.
- DLS experiments will also be performed to determine the variation of $R_h$ with $C_s$ and to determine the $R_g/R_h$ ratio, which will be compared with theoretically determined values. These experiments will also allow for the examination of possible bimodal relaxation times in solutions of NaPSS stars.
- Atomic force microscopy (AFM) experiments will be performed using the NaPSS star solutions previously used for both SLS and DLS. The experiments will verify the architecture of the molecules as well as provide an estimate of their size in

solution. These parameters determined using this method will be compared to the parameters determined via the use of SLS and DLS.

- Viscosimetric properties of the NaPSS solutions will be determined using both the linear Huggins equation, as well as a new method recently proposed by Wolf in solutions with varying amounts of $C_s$, and will be correlated to structural parameters such as *f* and *N*.
- Additional viscosimetric measurements will be performed using solutions with no $C_s$, and these results will be evaluated using the Huggins and Wolf equations. The comparison of the [η] determined using these theories will be compared with literature values determined for linear analogues of the same $M_w$, allowing for the determination of the viscosimetric branching parameter g' . These values will be compared with the values from theoretical predictions as well as the previously determined g' for the neutral precursors.
- Novel AFM measurements of NaPSS solutions with no $C_s$ will be performed in the $C_p$ regime wherein the viscosity polyelectrolyte effect occurs. This will allow for the direct examination of the relative size of the NaPSS stars in this regime.

In order to perform the synthesis and characterization described in the preceding points, a large number of experimental techniques and instrumental setups will be used. These are described in detail in the following chapter.

***Appendix***

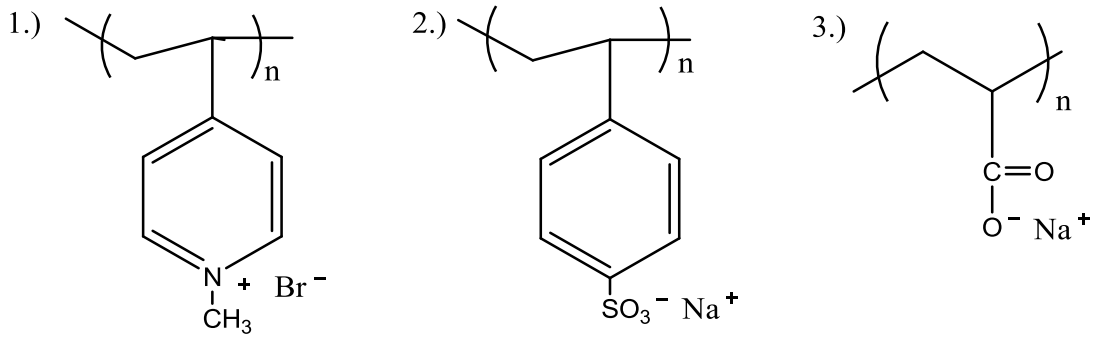



**Figure 1: Examples of common synthetic polyelectrolytes. 1.) the bromine salt of quaternized poly(4-vinylpyridine), an example of a strong cationic polyelectrolyte. 2.) sodium poly(styrenesulfonate), an example of a strong anionic polyelectrolyte. 3.) sodium poly(acrylic acid), an example of a weak anionic polyelectrolyte.**

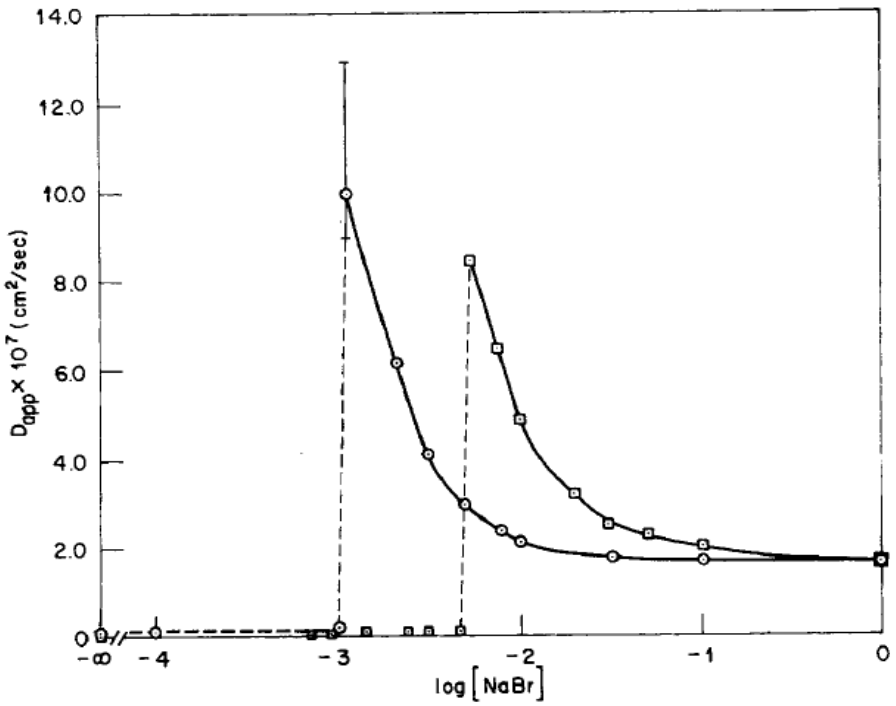



**Figure 2: Plot of the apparent diffusion coefficient ($D_{app}$) vs. log [NaBr], showing the evolution of a bimodal distribution of relaxation times upon decreasing $C_s$. [9]**

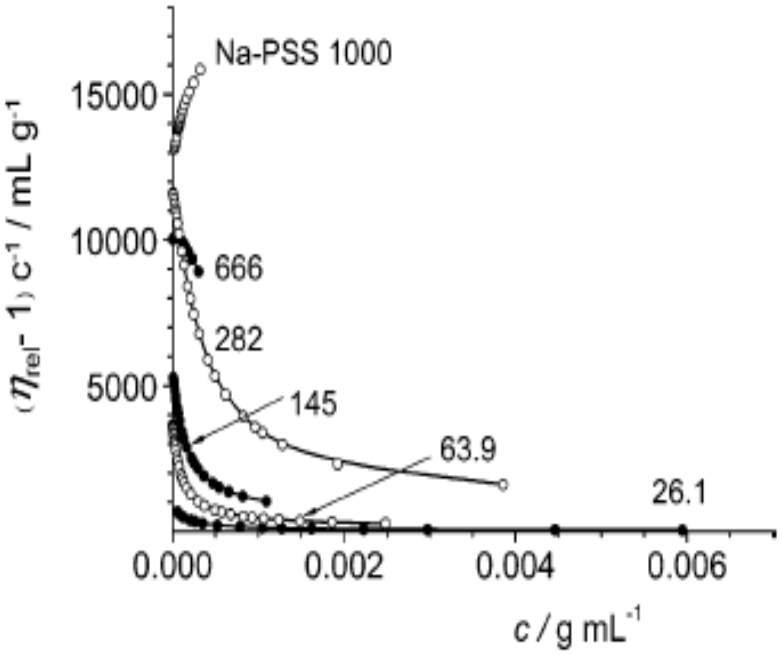



**Figure 3: Plot of the reduced viscosity vs. the concentration for NaPSS of varying degrees of polymerization, displaying the increase in $\eta_{red}$ ($\eta_{red} = \eta_{rel}$-1/$C_p$) with decreasing $C_p$, known as the viscosity polyelectrolyte effect.**[37]

## *References*

(1) Odian, G. *Principles of Polymerization*; Third ed. ed.; John Wiley and Sons Inc.: New York, 1991.

(2) Mandel, M. *Physical Properties of Polyelectrolyte Solutions*; ed.; Volume a cura del Settore Editoriale AIM: Pisa, 1992, p 1.

(3) Kuccaronera, F.; Janccaron, J. *Polymer Engineering & Science* **1998**, *38*, 783-792.

(4) Muthukumar, M. *The Journal of Chemical Physics* **1997**, *107*, 2619-2635.

(5) Serhatli, E.; Serhatli, M.; Baysal, B. M.; Karasz, F. E. *Polymer* **2002**, *43*, 5439-5445.

(6) Yang, J. Y.; Liu, N.; Yu, D. H.; Peng, C. J.; Liu, H. L.; Hu, Y.; Jiang, J. W. *Industrial & Engineering Chemistry Research* **2005**, *44*, 8120-8126.

(7) Akhil, K. S.; Sandip, R.; Juvekar, V. A. *Polymer International* **2007**, *56*, 167-174.

(8) Spiteri, M. N.; Williams, C. E.; F.Boue *Macromolecules* **2007**, *40*, 6679-6691.

(9) Lin, S.-C.; Lee, W. I.; Schurr, M. J. *Biopolymers* **1978**, *17*, 1041-1064.

(10) Cong, R.; Temyanko, E.; Russo, P. S.; Edwin, N.; Uppu, R. M. *Macromolecules* **2006**, *39*, 731-739.

(11) Sedlak, M. *Langmuir* **1999**, *15*, 4045-4051.

(12) Sedlak, M.; Amis, E. J. *The Journal of Chemical Physics* **1992**, *96*, 826-834.

(13) Tanahatoe, J. J.; Kuil, M. E. *J. Phys. Chem. B* **1997**, *101*, 9233-9239.

(14) Topp, A.; Belkoura, L.; Woermann, D. *Macromolecules* **1996**, *29*, 5392-5397

(15) Ermi, B. D.; Amis, E. J. *Macromolecules* **1998**, *31*, 7378-7385.

(16) Cohen, J.; Priel, Z. *Polymer Communications* **1989**, *30*, 223-224.

(17) Cohen, J.; Priel, Z.; Rabin, Y. *The Journal of Chemical Physics* **1988**, *88*, 7111-7116.

(18) Roure, I.; Rinaudo, M.; Milas, M.; Frollini, E. *Polymer* **1998**, *39*, 5441-5445.

(19) Vink, H. *Polymer* **1992**, *33*, 3711-3716.

(20) Jusufi, A.; Likos, C. N.; Lowen, H. *The Journal of Chemical Physics* **2002**, *116*, 11011-11027.

(21) Misra, S.; Mattice, W. L.; Napper, D. H. *Macromolecules* **1994**, *27*, 7090-7098.

(22) Shusharina, N. P.; Rubinstein, M. *Macromolecules* **2008**, *41*, 203-217.

(23) de Gennes, P. G. *Scaling Concepts in Polymer Physics*; Cornell University Press: Ithaca, NY, 1979.

(24) Dobrynin, A. V.; Rubinstein, M. *Macromolecules* **1999**, *32*, 915-922.

(25) Manning, G. S. *The Journal of Chemical Physics* **1969**, *51*, 924-933.

(26) Manning, G. S. *Acc. Chem. Res.* **1979**, *12*, 443-449.

(27) Furukawa, T.; Ishizu, K. *Macromolecules* **2005**, *38*, 2911-2917.

(28) Moinard, D.; Borsali, R.; Taton, D.; Gnanou, Y. *Macromolecules* **2005**, *38*, 7105-7120.

(29) Plamper, F. A.; Becker, H.; Lanzendörfer, M.; Patel, M.; Wittemann, A.; Ballauff, M.; Müller, A. H. E. *Macromolecular Chemistry and Physics* **2005**, *206*, 1813-1825.

(30) Mays, J. W. *Polymer Communications* **1990**, *31*, 170-172.

(31) Heinrich, M.; Rawiso, M.; Zilliox, J. G.; Lesieur, P.; Simon, J. P. *The European Physical Journal E - Soft Matter* **2001**, *4*, 131-142.

(32) Fernyhough, C. M.; Young, R. N.; Ryan, A. J.; Hutchings, L. R. *Polymer* **2006**, *47*, 3455-3463.

(33) Lienkamp, K.; Noe, L.; Breniaux, M. H.; Lieberwirth, I.; Groehn, F.; Wegner, G. *Macromolecules* **2007**, *40*, 2486-2502.

(34) Muller, F.; Delsanti, M.; Auvray, L.; Yang, J.; Chen, Y. J.; Mays, J. W.; Demé, B.; Tirrell, M.; Guenoun, P. *The European Physical Journal E - Soft Matter* **2000**, *3*, 45-53.

(35) Korobko, A. V.; Jesse, W.; Lapp, A.; Egelhaaf, S. U.; van der Maarel, J. R. C. *The Journal of Chemical Physics* **2005**, *122*, 024902.

(36) Astafieva, I.; Zhong, X. F.; Eisenberg, A. *Macromolecules* **1993**, *26*, 7339-7352.

(37) Eckelt, J.; Knopf, A.; Wolf, B. A. *Macromolecules* **2008**, *41*, 912-918.

# Part 2: Theoretical Background and Experimental Details of Synthesis and Characterization

There are essentially two routes to the synthesis of NaPSS. The first route involves the polymerization of the sodium styrenesulfonate monomer (NaSS). This synthesis has been performed via conventional free radical polymerization as well as, more recently, controlled radical polymerization methods such as reversible addition-fragmentation chain transfer (RAFT), nitroxide mediated polymerization (NMP) and atom transfer radical polymerization (ATRP).[1-3] Among the aforementioned controlled radical polymerization methods, RAFT produces the best results in terms of polydispersity and molecular weight, but even this method is limited to very low molecular weights (<30k) with a polydispersity around 1.2. Conventional free radical polymerization of NaSS is able to produce polymers of much higher molecular weight, but the polydispersity of these polymers is high as is usually the case when this type of polymerization is used. Due to these limitations, the synthesis of NaPSS with controlled architectures is currently restricted to synthesis by the second route: synthesis of a polystyrene precursor of low polydispersity utilizing a living polymerization method, followed by post-polymerization modification via sulfonation. This synthesis is the subject of the following sections.

## *Living Polymerization*

In order to synthesize polystyrene of sufficiently low polydispersity that it can be used as a model polymer, it is necessary to use one of the so-called "living" polymerization methods. These methods primarily include anionic polymerization, nitroxide mediated polymerization (NMP), atom transfer radical polymerization (ATRP), and reversible addition-fragmentation chain transfer (RAFT) polymerization , and according to Quirk [4] are characterized by the following experimental criteria:

1. The polymerization reaction continues until both the initial monomer used in the reaction as well as any monomer added after this time are incorporated into the living polymer.
2. The degree of polymerization (N) is a linear function of the percentage of monomer consumed.
3. The number of growing polymer chains does not change during the course of the reaction. This is true for controlled radical polymerizations, in the sense that the equilibrium between propagating and non-propagating chains is constant throughout the reaction, effectively resulting in a constant number of growing chains at a given time.
4. The average degree of polymerization, which is a direct function of the molecular weight, can be controlled by adjusting the stoichiometry of the reaction. This usually corresponds to adjusting the ratio of the moles of initial monomer to the moles of initiator to obtain polymer of a given N.
5. The polydispersity, defined as the weight average molecular weight ($M_w$) divided by the number average molecular weight ($M_n$), is low, though maximum value of this number is still the subject of some debate.
6. It is possible to create block copolymers by the addition of another, different monomer, after the first monomer has been consumed by the polymerization.
7. It is possible to quantitatively functionalize the end of the polymer chain by a reaction conducted after the monomer has been consumed.
8. A plot of the rate of propagation versus time should be linear throughout the extent of the reaction.

Although all of the controlled radical polymerization methods mentioned above do meet these experimental criteria, and are therefore methods that can be used to synthesize polystyrene of a low polydispersity and controlled molecular architecture, they are inconvenient for the synthesis of NaPSS stars for a number of reasons that will be described in detail in the following sections. Therefore anionic polymerization is the method chosen for the synthesis of NaPSS stars in this thesis, and as such, is the focus of the following section.

## *Anionic Polymerization*

The method of polymer synthesis known as living anionic polymerization was first demonstrated by Szwarc in 1956.[5,6] In a later publication, Szwarc elegantly demonstrated the living nature of the anionic polymerization of styrene.[7] In this work, a special reaction vessel fitted with two ampoules containing diluted styrene monomer, one ampoule containing sodium napthalenide initiator, and a long tube containing a glass-encased weight. After breaking one ampoule containing styrene and the initiator ampoule, the reaction proceeds with a bright red color indicating that initiation of the polymerization has occurred. After waiting a sufficient amount of time for the propagating chain ends to incorporate all of the initial styrene into the resulting polymer, the viscosity of the polymer solution was determined by manipulating the reactor to fill the tube with solution followed by determining the time taken for the weight to pass a mark on the tube. Once an estimate of the viscosity was determined, the second ampoule of styrene was broken and the propagation continues long enough to consume the monomer. The viscosity of the solution was determined in the same manner as before, and was found to be approximately ten times greater than the first solution. This

experiment demonstrated that chain extension occurs upon the addition of monomer to chain ends that have previously stopped propagating due to complete consumption of monomer, without significant termination or chain transfer occurring.

As the experiment described in the previous paragraph shows, the anionic polymerization of styrene is a well established method of making polystyrene quantitatively terminated with anionic end-groups capable of undergoing subsequent reaction. This is essential when the synthesis of well-defined molecular architectures such as star polymers is desired, and is the primary reason why anionic synthesis is still chosen as the primary technique for the synthesis of model architectures, in spite of the recent availability of experimentally more facile controlled radical polymerization techniques.

***Star Polymer Synthesis***

A star polymer is a polymer in which all of the polymer arms originate from a central graft point. There are two general pathways for the synthesis of star polymers. The first involves the use of multifunctional initiators to form the core of the star, from which the star arms are grown. This synthetic procedure has a number of difficulties associated with it because of the often limited solubility of the multifunctional initiators as well as the variable initiation efficiency of the initiation sites in the core. Both of these factors can lead to a broadening of the polydispersity of the product, and have the additional drawback of difficult characterization of the polymer arms, due to the difficulty in obtaining arm material. The second pathway to polystyrene star synthesis involves the use of multifunctional linking reagents to link together arms with

carbanionic ends. This reaction should yield star polymers with arms of the same length, with the additional advantage of facile characterization of the individual arms.

***Linking Reagents***

Many different linking reagents of various functionalities have been used in the literature.[4] These linking reagents fall into three broad types. The first type consists of polyfunctional halogenated hydrocarbon-type linking agents such as 1,2,4-tris(Chloromethyl)benzene, an agent that theoretically produces a three-arm star. These agents suffer from a significant drawback, in that, through the mechanism of lithium-halide exchange [8], linking reagents can couple, thereby producing linking centers of varied functionality and greatly increasing the polydispersity of the obtained polymers. The second group of linking reagents, consisting of multifunctional chlorosilane compounds, does not suffer from the aforementioned coupling reaction. However it has been found that the linking efficiency of these compounds with poly(styryl) lithium is poor, particularly with higher functionalities. More importantly for the work in this thesis, there is some evidence that the Si-C bond is not stable under sulfonation conditions.[9] The third type of linking agent is the difunctional monomer divinyl benzene (DVB). This linking agent forms polymer stars via a three step process.[10,11] The first step is the crossover of the reactive anionic center to the DVB. The second step is the polymerization of the DVB to form a block copolymer of DVB and styrene. The final step is the linking of poly(styryl) lithium to the polymerized DVB to form a star branched structure, with a "nodule" of DVB in the center. With this methodology, stars with *f* ranging from 3 to 56 have been reported in the literature. Theoretically, the ratio of the moles of DVB to the living chain ends should have a simple relation to the *f* obtained.

However, due to the variable composition of the technical grade of DVB used, which usually contains a mixture of *m*- and *p*- divinylbenzene, and the numerous other reaction variables involved, a simple relationship between the DVB/Li ratio and $f$ has not been established from an examination of the published literature.

## *Sulfonation*

Having established a valid method of synthesis for polystyrene stars, we would now like to focus on the conversion of these materials to NaPSS stars using the method of sulfonation. Sulfonation is "a substitution reaction used to attach an $-SO_3$ group on a molecule of an organic compound via a chemical bond to carbon or, less frequently, to a nitrogen atom of the chemical compound."[12] It has been found through studies of the sulfonation of small molecules that sulfonation proceeds much more readily for aromatic compounds as opposed to aliphatic compounds, even though the dissociation energy of the C-H bond is significantly higher in aromatic compounds.

The sulfonation of aromatic compounds, including polymers, proceeds via a typical $S_E2$ mechanism. The oxygen atoms in $SO_3$ pull electron density away from the sulfur atom, creating an electrophilic center that reacts with the region of highest $\pi$ electron density on the aromatic ring, generally the *para* position in polystyrene. A $\pi$ complex is formed between the $SO_3$ group and the aromatic ring, which subsequently undergoes relatively slow conversion to an arenium intermediate in the second rate-determining step. This intermediate quickly releases a proton to produce the final sulfonated product.

Sulfonation as a reaction suffers from two main detrimental side reactions, both of which are particularly important when model polyelectrolytes with full sulfonation and

unaltered conformation are desired. The first of these side reactions is the desulfonation reaction, in which a sulfonated product reacts with water to undergo hydrolysis to produce sulfuric acid and the aromatic starting material. This reaction is actually in equilibrium with the sulfonation process, and can be minimized in the sulfonated product by converting the sulfonic acid to the salt form, which does not undergo desulfonation. The second issue with the sulfonation reaction is the reaction of two of the highly reactive sulfonic acid species to form a sulfone crosslink in the polymer. Sulfones are very stable compounds whose presence in NaPSS can have obvious implications on the conformation of the polymer. Sulfone formation is best controlled by using dilute solutions for the polymerization and performing the sulfonation at relatively low temperature.

The large degree of interest in polymers with small percentages of charged groups, also known as ionomers, have resulted in the recent development of several new procedures for polymer analogous sulfonation. In one of these methods, described first by Makowski, a dichloroethane solution of polystyrene was reacted with acetyl sulfate to give very lightly sulfonated polystyrene.[13] This process was later extended by Baigl and coworkers to the synthesis of NaPSS with degrees of sulfonation ranging from 30% to 91%, although it was also reported that small amounts of crosslinking in the higher molecular weight samples (>1 million) were detected using aqueous SEC.[14] The method of sulfonation most commonly used to produce quantitatively sulfonated NaPSS was first reported by Vink.[15] In this procedure, a solution of polystyrene in cyclohexane was combined with a solution of phosphorous pentoxide ($P_2O_5$) and sulfuric acid ($H_2SO_4$) and stirred for 30 minutes at 40 $^oC$. The resulting product has a degree of sulfonation ranging

from 90 to 95%. This procedure was later modified by Smisek with the use of much lower polymer concentrations and doubling the concentration of phosphorous pentoxide, in order to reduce the amount of sulfone formation.[16] Due to the ability to produce NaPSS of high sulfonation degree with a limited degree of crosslinking, the Vink method of sulfonation was chosen for the polymers in this thesis. A full description of the experimental conditions used for this synthesis is described in a later section of this chapter.

## *Characterization Theory*

In order to verify that the synthesis of NaPSS stars was successful, a full characterization of both the neutral polystyrene precursors as well as the charged final product is necessary. In this section, the necessary background for a number of characterization techniques including organic size-exclusion chromatography (SEC), aqueous size-exclusion chromatography (ASEC), static light scattering (SLS), dynamic light scattering (DLS), and atomic force microscopy (AFM) are described. Other characterization techniques that were employed in this thesis include titration, elemental analysis, thermal gravimetric analysis (TGA), viscometry, membrane osmometry, nuclear magnetic resonance spectroscopy (NMR) and rheology and are described in the chapters wherein these techniques are used.

### *Size Exclusion Chromatography*

Due to its ease of use, simplicity, and compatibility with other analysis methods, size-exclusion chromatography (SEC) is the most often used analytical technique in the field of polymer science. A typical SEC system consists of a liquid chromatography pump, an injector, one or more SEC columns, one or more detectors, and a computer for

data collection and analysis. A typical SEC experiment is described in the following paragraphs.

A dilute solution (~1 mg/mL) of the polymer sample to be examined is injected into the constantly flowing solvent stream that is circulated throughout the SEC setup, with the time of the injection being marked electronically. The solution enters the SEC columns and is subsequently separated into fractions based on the hydrodynamic volume of the individual species in the polymer sample. The mechanism of this separation is based on the variable porosity of the crosslinked polystyrene beads, which effectively allow polymer molecules with larger hydrodynamic volumes to follow less tortuous paths through the SEC column. The result of this is that largest molecules elute from the column to the detectors first, followed by the other size fractions at later times. At this point the polymer sample, which has been fractionated according to hydrodynamic volume, elutes to the detectors in the SEC system. In the SEC systems used in this thesis, these detectors include a differential refractive index detector (RI), a static light scattering detector (SLS), a continuous viscometer detector (CV), and a dynamic light scattering detector (DLS). Given the value of the refractive index increment for the polymer being examined in the given solvent being used as the mobile phase, the concentration of each fraction or slice of a sample can be determined from the RI detector signal. With this concentration, the signals from the SLS, CV, and DLS detectors can be used to determine the radius of gyration ($R_g$), hydrodynamic radius ($R_h$), weight average molecular weight ($M_w$) and intrinsic viscosity ($[\eta]$) of narrow slices of the polymer sample. In addition to this, the shape of the RI curve can be analyzed to estimate the polydispersity of the sample.

Although calibration of the SEC system with narrow molecular weight distribution linear polystyrene standards to establish a $M_w$ versus elution volume plot has been useful in the past as a method to estimate the molecular weight of polymers, this technique is not applicable in the case of branched structures due to the varying dependence of $M_w$ on hydrodynamic volume as compared to the linear standards. As such, calibration curves such as these were not used in the analysis of samples in this thesis. Another method of SEC analysis called universal calibration was developed to overcome the limitations of straight calibration with linear standards just mentioned. This method utilizes the relationship of the Einstein viscosity law

$$[\eta] = C\frac{V_h}{M} \tag{15}$$

where $[\eta]$ is the intrinsic viscosity, $V_h$ is the hydrodynamic volume, C is a constant, and $M$ is the molecular weight. From a plot of $[\eta]M$ versus retention time for standards of low polydispersity, the relation between the hydrodynamic volume and the retention volume can be established. This relation can subsequently be used to determine the molecular weight of any polymer analyzed in the SEC system, assuming the polymer adopts a random coil conformation in solution. Since it is unlikely that highly branched species like star polymers adopt a random coil conformation in solution, the applicability of this method of analysis to star-branched polymers is questionable.

***Aqueous Size Exclusion Chromatography***

The steps outlined above assume that there is no interaction between the polymer sample and the column material. While this is true in the case of the polystyrene star precursors that are examined in this thesis, which are analyzed using tetrahydrofuran as

the mobile phase, it is often not true when aqueous mobile phases are used in the SEC experiment[17]. This variant of SEC is termed aqueous size exclusion chromatography (ASEC) and involves a number of complications beyond the ones usually encountered with SEC using an organic mobile phase, particularly when used with highly charged polyelectrolytes such as NaPSS. The first complication is the lack of well-defined NaPSS standards for calibration. This problem can be overcome by using a static light scattering detector for absolute molecular weight determination, rather than using a calibration curve. The second complication is called the polyelectrolyte effect and refers to the expansion of the polyelectrolyte at low polymer concentrations. This variability of the polyelectrolyte conformation makes efficient separation of the polyelectrolyte into fractions of different molecular weights difficult under these conditions. The third complication that occurs relates to the interaction of the polyelectrolyte with the column packing material. This can take the form of electrostatic repulsion between charged portions of the packing material and the polyelectrolyte, and may also include the hydrophobic adsorption of the polyelectrolyte on the packing material. Both the second and third complications can be overcome by the careful selection of column material and mobile phase. For the work in this thesis the column packing material was neutral, and the mobile phase was a mixture of acetonitrile and water with a high concentration of low molecular weight salt. This combination was chosen to reduce the polyelectrolyte effect and the adsorption of the polymer on the column.

***Static Light Scattering***

The static light scattering experiment can provide a wealth of information about the polymer chain, including the z-average radius of gyration ($R_g$), the weight average

molecular weight ($M_w$), and the second virial coefficient ($A_2$).[18] The relationship between these parameters is most often expressed with the following working equation:

$$\frac{Kc}{\Delta R\theta} = \frac{1}{M_w}\left[1 + \frac{16\pi^2 {n_0}^2}{3\lambda_0^2} R_g sin^2\left(\frac{\theta}{2}\right)\right] + 2A_2 c \qquad (16)$$

where $K = (n_0 \nu)^2 (4\pi^2/\lambda_0^4 N_0)$, $\lambda_0$ is the wavelength of light, $N_0$ is Avagodro's number, $n_0$ is the refractive index of the solvent, and $\nu$ is the refractive index increment for the polymer solution. $R\theta$, which is the quantity actually measured in the scattering experiment, is called the Rayleigh ratio and represents the excess scattering of light due to solute particles at an angle $\theta$. In a typical static light scattering experiment, a number of solutions with different concentrations of the polymer to be characterized are examined at various angles. The data are then plotted following the method developed by Zimm, using $Kc/(\Delta R\theta)$ as the ordinate and $\left( sin^2\left(\frac{\theta}{2}\right) + Ac\right)$ as the abcissa, with $A$ being an arbitrary constant chosen to spread the scattering curves out for easier viewing. These data are then extrapolated to θ = 0 and c = 0, and these extrapolated points are fitted in a linear manner and extrapolated to the ordinate. When this is done correctly, the fitted lines have a mutual intercept of $1/M_w$ and slopes corresponding to $\frac{16\pi^2 {n_0}^2}{3\lambda_0^2} R_g$ and $2A_2$ for the c = 0 and θ = 0 lines, respectively. Theoretically, Equation (2) is applicable to large, chemically regular, macromolecules of any dispersity with intermolecular interactions, and as such the Zimm method is the primary method of analysis for light scattering data in the polymer literature. Another popular method of analysis, particularly for very large particles, was proposed by Berry.[19] In this method, $Kc/(\Delta R\theta)^{\frac{1}{2}}$ is plotted as the ordinate, with the abscissa the same as in the Zimm

treatment. The same basic method of analysis as in the Zimm method is then used, with the advantage being the relative ease with which the extrapolated points can be fitted linearly. Recently, Andersson and coworkers published a work calculating the relative error of using the Debye, Berry, and Zimm methods of extrapolation on two idealized particle shapes: spheres and random coils.[20] They examined the two shapes over $R_g$ values ranging from 25 nm to 250 nm and calculated the relative error in extrapolation of each, using fitting curves with different order polynomials. They compared these calculations with an experiment on a very high $M_w$ poly(ethylene oxide) sample that was expected to display random coil behavior in water. The end result of the calculations was that, over the widest range of particle size and shape, the most robust fitting procedure was a linear curve fit over the lowest reliable angular data plotted using the Berry method. As polymers examined in this thesis cover a wide range of size due to both molecular weight and varying solvent conditions, this method was utilized for analysis of all of the static light scattering data.

While the theoretical treatments described above have been shown to be applicable to a large range of polymers under a wide variety of solvent conditions, their application to solutions of polyelectrolytes must be made with great care. It has been shown that the light scattering from aqueous solutions of polyelectrolytes at low concentrations of $C_s$ cannot be interpreted using a Zimm analysis because there is a peak in the plot of $Kc/(\Delta R_\theta)$ versus $sin^2\left(\frac{\theta}{2}\right)$ in these solutions. Since the addition of salt to these solutions causes the peak to gradually disappear, the origin of this peculiar scattering is attributed to electrostatic interactions between polyelectrolyte chains, resulting in an osmotically "stiff" solution that does not have the concentration

fluctuations that are the source of scattering from polymer solutions, resulting in a very weak excess scattering. Therefore, to reliably determine the chain parameters mentioned in the previous paragraph using a Zimm or Berry analysis, static light scattering experiments of aqueous polyelectrolyte solutions must be made with significant amounts of added salt.

This introduces another complication into the analysis: now the solution contains three components. In ternary systems, one component can preferentially absorb onto the solvent sheath surrounding the polymer, a phenomenon known as preferential adsorption. Essentially, the preferentially adsorbed solution component and the polymer are closely associated to form a sort of complex, which has a different refractive index than the polymer alone. Additionally, the solvent in polyelectrolyte solutions has a different refractive index than the pure solvent. If $\nu$ is measured in the conventional manner, with the refractive index of the pure solvent subtracted from the refractive index of the solution, large errors in the determination of $\nu$ will result. The solution to this problem lies in a careful dialysis of a concentrated polyelectrolyte solution against the solvent before $\nu$ is determined. This dialysis should establish constant chemical potential of all the components in the system. The concentrated solution in the dialysis tubing can then be diluted with the solution outside the bag to make a set of solutions that can be used to determine $\nu$. The solvent outside the dialysis bag is used to determine the solvent baseline in the differential refractive index experiment.

***Dynamic Light Scattering***

Dynamic light scattering measures temporal fluctuations of the intensity of scattered light caused by the concentration fluctuations in dilute solution, which are, in

turn, caused by solute Brownian movements. The scattering signals given by the solution at two different times can be correlated, and is expressed in the simplest case of an ensemble of identical, non-interacting, hard, and spherical particles by the following equation:

$$g(\tau) = A_0 + Aexp(-\Gamma t) \tag{17}$$

where $\Gamma = D_t q^2$. Here $q = 4\pi n sin(\theta/2)/\lambda$. The parameters are as follows: $D_t$ is the translational diffusion coefficient, $n$ is the index of refraction of the fluid, $\lambda$ is the wavelength of incident light, and $\theta$ is the angle of observation. $D_t$ is related to the hydrodynamic radius ($R_h$) by the following equation:

$$R_h = \frac{k_B T}{6\pi\eta D_t} \tag{18}$$

where $k_B$ is the Boltzmann constant, $T$ is the absolute temperature, and $\eta$ is the solvent viscosity. Some modifications to the theory outlined here are commonly used to take the polydispersity of experimentally encountered systems into account, such as fitting by the method of cumulants and the Laplace inversion of CONTIN. A detailed explanation of these methods is beyond the scope of this thesis.

## *Experimental*

The synthesis of polymers via the use of anionic polymerization is an experimentally challenging endeavor, particularly if the synthesis is performed under high vacuum. The characterization of polyelectrolytes, particularly in aqueous solutions, is also experimentally difficult. This section of the thesis will describe the experimental procedures and details of the anionic synthesis, followed by a detailed description of the

procedures and equipment used in the static light scattering characterization of the polyelectrolyte stars.

***Anionic Polymerization-Vacuum Line***

All of the anionic syntheses described in this thesis were performed using all-glass, custom made apparatuses coupled with a vacuum line capable of achieving a high vacuum. A diagram of the vacuum line used in this work is depicted in Figure 4. With the exception of the silicon oil diffusion pump and the stopcocks, the vacuum line consists entirely of pyrex glass tubing. J. Young teflon stopcocks are used to control the sections of the line that are under vacuum. The combination of the mechanical pump and the silicon oil diffusion pump is able to achieve a pressure of in the range of $10^{-5}$ Torr in the vacuum line. To achieve this pressure, rigorous maintenance of both pumps is required. In the case of the mechanical pump, this is performed by regularly changing the oil in the pump to remove the volatile organic components that inevitably accumulate there during the course of working with the line, as well as maintaining liquid nitrogen in the nitrogen trap between the diffusion pump and the mechanical pump. Keeping this trap full of nitrogen also helps maintain the oil in the diffusion pump, keeping organic components from combining with and decomposing the hot oil in the pump.

***Anionic Polymerization-Reagents***

For all of the anionic polymerizations performed in this thesis, benzene was used as the reaction solvent. In our lab, reagent grade benzene from Fisher Scientific is allowed to stir over concentrated sulfuric acid for no less than 1 week. This effectively removes trace contaminants such as toluene from the solvent. In the next step, the purified benzene is decanted and distilled over calcium hydride under a dry nitrogen

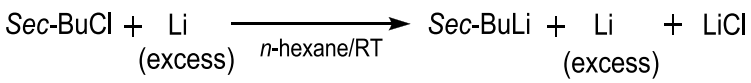
atmosphere to remove traces of water. The benzene purified in this manner can be stored in screw top glass bottles until needed for use on the vacuum line. The final purification step involves pouring this benzene into a glass cylinder fitted with ground glass joint, followed by the addition of unpurified n-butyl lithium and styrene. This mixture is then quickly attached to the line and degassed with several freeze-thaw cycles. These cycles consist of freezing the entire mixture completely with liquid nitrogen, then drawing a vacuum on the flask until a high vacuum is obtained. This is signaled by the absence of noise when a Tesla coil is brought into contact with the outer surface of the line. The absence of noise immediately upon opening the vacuum to the frozen benzene solution signals the end of the degassing step. Assuming the benzene is reasonably pure, a red color should develop in the cylinder, indicative of living oligostyrenyl lithium anions in the benzene solution. This red color serves as a facile indicator of the purity of the benzene in the cylinder throughout the course of its use.

The styrene monomer in this thesis was reagent grade material obtained from Sigma Aldrich. The first step of the purification process involves stirring the monomer over calcium hydride on the vacuum line overnight to remove moisture. This mixture is subsequently degassed following the same procedure outlined in the above paragraph, then distilled under vacuum to another flask fitted with ampoules. This flask contains dibutylmagnesium which was previously injected into the flask through a rubber septum, and opened to the vacuum to remove the hexane solvent contained in the dibutylmagnesium reagent solution. The resulting styrene/dibutylmagnesium solution is then allowed to react for at least two hours, with the evolution of a faint yellow color indicating the formation of styrenyl magnesium. Another degassing step is then followed

by the distillation of the styrene into the ampoules, which are subsequently frozen and removed from line under high vacuum via the process of heat-sealing a constriction. The ampoules of purified styrene are then stored in the freezer at ~-20 ℃ for later use. Usually, the styrene stored in this manner is safe to store for at least six months.

Divinylbenzene (DVB), which was obtained from Sigma Aldrich as a technical mixture of *para*-and *meta*- isomers is purified in a very similar manner to styrene. One difference in the process has to do with the high boiling point of DVB. Due to this, distillation of the monomer is difficult even under vacuum, and must be assisted by heating both the monomer solution and the pathway to the ampoule. The ampoule of DVB was then attached to a dilution apparatus, which contains a number of precalibrated ampoules attached to a large section for containing the solution. This apparatus is connected to the vacuum line and a known volume of benzene is distilled into it. After degassing the benzene, the dilution apparatus is removed from the vacuum line by heat-sealing the constriction. The DVB and benzene are then mixed by breaking the ampoule and manipulating the dilution apparatus. In this manner, a dilute solution of the DVB linking reagent can be stored in the freezer, and ampoules with the desired volume of solution can be obtained as needed. This step is necessary both because of the high tendency for undiluted DVB to self polymerize as well as the necessity to obtain very small quantities of DVB for use in linking reactions.

Sec-butyllithium (*sec*-BuLi) was used as the initiator in all of the anionic polymerizations in this thesis. A detailed description of the synthesis of this initiator has been presented many times before [21], so only a cursory description of the reaction is presented here. The equation describing this synthesis is




(19)

where *sec*-BuCl is sec-butylchloride, which is reacted with excess lithium (Li) in high vacuum conditions in an all-glass reactor to give the initiator. After synthesis and ampoulization of the concentrated sec-BuLi in hexane, an ampoule of the concentrated solution is attached to a dilution apparatus and diluted with benzene in a manner similar to the one described for DVB. The concentration of the initiator is checked by performing the anionic polymerization of styrene with a known amount of monomer and volume of initiator solution. From the molecular weight obtained from SEC, the initiator concentration can be calculated.

Methanol is used as the terminating agent in the polymerizations described here. The reagent grade material is obtained from Sigma Aldrich. The purification consists of carefully degassing the methanol on the vacuum line in a similar manner as described for benzene, then distilling small amounts of methanol into ampoules and heat sealing the constrictions.

***Anionic Polymerization-Procedure***

All of the anionic polymerizations performed in this thesis utilized the same polymerization reactor, which is depicted in Figure 6, and follow the general synthesis scheme depicted in Figure 5. The reactor was assembled from pyrex tubing and round-bottom flasks by glassblowing. Ampoules containing different components used in the polymerization are labeled and marked by color. Sec-BuLi is marked by yellow, styrene by blue, methanol by red, and DVB by green. All of the ampoulized materials were purified as previously described. The synthesis procedure follows the steps outlined below:

1. The apparatus depicted in Figure 6 is attached to the vacuum line using male and female ground glass joints. Through the manipulation of stopcocks, the apparatus is subjected to the vacuum and checked for pinholes using a Tesla coil. The coil will arc when placed close to the pinhole. Assuming no pinholes are discovered, the apparatus is then flame dried using a torch with a gentle flame. The removal of all residual moisture and the attainment of high vacuum in the apparatus is checked by placing the Tesla coil on any contiguous section of the vacuum line wherein the vacuum is currently being applied. If the noise from the Tesla coil does not change, high vacuum has been obtained.
2. After verifying that the vacuum is good, benzene is distilled into the reactor by opening the stopcocks between the benzene cylinder and the reactor and placing a liquid nitrogen bath around the reactor. After a known amount of benzene is distilled from the precalibrated cylinder, the stopcocks between the benzene and reactor are closed and the stopcocks between the reactor and the pumps are opened. The reactor is pumped down until high vacuum is obtained, and is subsequently removed from the vacuum line by heat sealing constriction 1. After the constriction cools, the benzene is then slowly thawed by placing the reactor under running water.
3. In order to clean the reactor of any contaminants that may later terminate the reaction prematurely, the breakseal to the sec-BuLi ampoule is broken and the reactor is manipulated so that solution contacts and the sec-BuLi reacts with any contaminants that are present on the surface of the glass. The amount of sec-BuLi solution used is calculated as 1.1 times the amount needed to achieve the desired

arm molecular weight. This is necessary because some of the sec-BuLi is sacrificed in this step.

4. To start the polymerization, the breakseal to the styrene ampoule is broken, and the reactor manipulated to mix the monomer and solution. Successful initiation of the polymerization is indicated by the appearance of a bright yellow color, which in all cases occurred immediately after breaking the styrene ampoule breakseal. This polymerization is allowed to continue for a time sufficient to incorporate all of the monomer into the polymer chain (4-24 hours depending on the chain length desired).
5. Approximately one third of the solution of living polystyrenyllithium chains is distributed into reaction vessel 1. Constriction 2 on this reaction vessel is then washed with solvent by applying a cloth towel dipped in liquid nitrogen and heat sealed to remove the reaction vessel from the main reactor. This process is repeated for reaction vessels 2 and 3, with a small amount of the solution being retained in the main reactor.
6. The living polystyrenyllithium chain ends remaining in the main reactor are terminated by breaking the breakseal of the methanol ampoule located on that reactor. The resulting polymer solution is then removed from the reactor by breaking open the main reaction vessel. This is followed by pouring the solution into a large volume of methanol to precipitate the polymer, then decanting the methanol and drying in a vacuum oven to obtain the dried polymer. Subsequent SEC analysis of the polymer confirms that polymerization has taken place and

establishes the $M_w$, $M_n$ and polydispersity of the polymer arms that are soon to be linked together in the linking vessels.

7. The linking reaction is performed by breaking the breakseal of the DVB ampoule of each linking vessel. These ampoules have varying amounts of DVB so that polystyrene stars with three different functionalities can be synthesized. Successful initiation of the DVB linking reagent is indicated by the immediate change of the solution from yellow to dark red upon breaking the DVB ampoule breakseal and manipulating the linking reactor to mix the solution. The linking reactor is then clamped and heated in a water bath at 40 ℃ and allowed to react, with constant stirring, for at least 48 hours. If necessary, the progress of the linking reaction can be found by taking an aliquot from the solution into the DVB ampoule and heat sealing the constriction connecting it to the linking reactor.
8. Once the completion of the linking reaction has been verified by either taking an aliquot of the reaction or waiting for an extensive period of time, the linking reaction is terminated by breaking the breakseal of the ampoule containing methanol. Termination of the reaction is indicated by the absence of color in the solution. The polymer solution is then poured into a large volume of methanol with stirring to effect precipitation and the polymer final product dried in a vacuum oven overnight.

All samples obtained in this manner were characterized using SEC to verify the efficiency of linking the arms to the core. Some samples exhibited such high linking efficiency that fractionation was not needed, indicated by a monomodal distribution in the SEC trace. However, most samples exhibited a bimodal trace, indicative of unlinked

chains. For these samples, it is necessary to perform a fractionation to remove this fraction of lower molecular weight chains. For the fractionation, toluene/methanol was used as the solvent/nonsolvent system to allow the separation of the star polymer from the unlinked arms based on molecular weight. The fractionation used here proceeded as described in the following paragraphs.

A dilute solution of the sample to be fractionated was made by dissolving the polymer sample in toluene. Typically, 20 grams of polymer was dissolved in 1.5 liters of toluene, making a solution that is around 1.3% percent polymer by weight. After the sample is completely dissolved, methanol is added to the quickly stirring solution in small aliquots until a slight blue color persists. This color is indicative of aggregation of the polymer chains into domains large enough to scatter light, and signals that the cloud point has been reached in the solution at the current temperature. At this point, the solution is slowly heated to 35 ℃, still with rapid stirring. As heating proceeds, small aliquots of methanol are added to the solution. Once 35 ℃ is reached, the solution should be clear, indicating no significant aggregation. The solution is now ready for transfer to the separation funnel where the rest of the fractionation takes place. Before transfer, the funnel is warmed with a gentle flame so that it will not be cooler than the polymer solution that is being added to it, which will result in non-equilibrium precipitation of the polymer on the walls of the funnel. The system is then allowed to cool slowly to room temperature. As cooling slowly proceeds over the course of several hours, the appearance of small gel particles in the lower portion of the separatory funnel indicates the separation of the solution into gel and sol phases. These phases correspond to the high molecular weight (stars) and lower molecular weight (unlinked chains) portions of

the polymer sample. Once the system has been allowed to equilibrate at room temperature overnight, aliquots of each phase are characterized by SEC. This characterization verifies the separation of the unlinked chains from the polystyrene stars, indicated by a single peak in the chromatogram at the previously noted elution time for the star fraction of the sample. If separation has not occurred the fractionation can be performed again. If separation has occurred, the bottom phase of the solution in the funnel is precipitated by allowing it to flow dropwise into a large volume of methanol. Methanol is decanted from the precipitated polymer, and the polymer is dried in a vacuum oven overnight. Dried samples had the appearance of a white powder and are stored in the freezer until needed.

***Sulfonation-Procedure***

As has been mentioned previously, a modified version of the sulfonation method described by Vink was chosen as the method used for sulfonation for the samples in this thesis. A description of a typical sulfonation procedure follows, and the synthesis scheme is depicted in Figure 7.

Approximately 1.5 grams of polymer sample is dissolved in 300 milliliters of dry cyclohexane in a beaker. Once the polymer is dissolved, the solution is heated to 40 ℃ and left to stir under a blanket of dry nitrogen. A 500 milliliter round bottom flask is loaded with 20 grams of $P_2O_5$ under a dry nitrogen atmosphere in a glove box. The flask is sealed and transferred to a fume hood to continue the reaction. At this point 200 milliliters of sulfuric acid ($H_2SO_4$) is slowly added to the flask with stirring under a nitrogen atmosphere. This results in the evolution of a great deal of heat and the eventual dissolution of the components into a homogeneous solution. This solution is allowed to

cool to 40 ℃ before the next step. Now, the polymer solution is added to the round bottom flask with rapid stirring, and the solution is allowed to stir for one hour with no heating. At first two distinct phases are observed, which blend together into a single homogenous, cloudy phase after about 30 minutes and persists for the duration of the reaction. About 50 grams of ice is added to the solution with stirring, after which the solution is transferred to a 500 milliliter separatory funnel. Eventually the solution separates into three phases: a top layer consisting mainly of cyclohexane, a small middle phase of sulfonated polystyrene with the consistency of chewing gum, and a bottom phase consisting mainly of sulfuric acid. The middle phase is separated from the other two and dissolved in 500 milliliters of deionized water. Pellets of sodium hydroxide are added to this solution until a pH of nine (monitored using pH indicator paper) is reached. After sulfonation, the solution must be dialized to remove low molecular weight salt from the desired polyelectrolyte. To this end, the polymer solutions are poured into dialysis tubing which is sealed and placed in a large volume of deionized water. The brand of dialysis tubing used is 3,500 kilodalton cutoff from Fisher Scientific, and the water purification system is a Barnstead Nanopure system with a 0.2 micron filter.. The resistivity of water from this system is normally ~18 ohm. Progress in the dialysis was checked using a Inotec conductivity meter to measure the conductivity of the dialysate. This dialysate was checked twice daily, with water changes if needed, until the conductivity of the dialysate was the unchanged after waiting 24 hours. On average, this process took ten days for each sample. After the dialysis is complete, the sample is removed from the dialysis tubing and freeze-dried in a Fisher Scientific freeze drier. The

dried polyelectrolyte star sample is then stored in the freezer until needed for subsequent characterization.

***Characterization-SLS***

Due to the highly polar nature of aqueous solutions, extraordinary measures must be taken to eliminate dust from these solutions. A diagram of the static light scattering apparatus used for the measurements in this thesis is shown in Figure 8. The system, previously described as a "closed loop filtration system", consists of a reservoir made from a disposable 5 milliliter plastic syringe body sealed with a rubber septum. The luer lock of the syringe was fitted with a 0.45 micrometer pore size polytetrafluoroethylene (PTFE) hydrophilic filter from Millipore. The next component in the system is a peristaltic pump purchased from Fisher Scientific, allowing the solution to be circulated through the system without a chance of contamination from pump components. The last component is the scattering cell, which consists of a scintillation vial from Whatman and another rubber septum. This cell is carefully placed in the macro-batch holder of the Wyatt DAWN EOS light scattering instrument used in these experiments. This instrument has detectors at 18 different angles, the response from which was normalized to the angle at approximately 90° using a solution of 20k $M_w$ poly(ethyleneoxide) in water as the isotropic scatterer. The scattering intensity was calibrated using toluene as the reference. All of the components in the filtration system were connected using PTFE tubing, allowing for the continuous filtration of solutions used for light scattering. After the system described above has been assembled, and the scattering cell has been properly aligned, approximately 20 mL of the aqueous solvent to be used is injected through the rubber septum sealing the syringe reservoir. This was done with the

peristaltic pump running in order to distribute the solvent through the system and verify that the minimum volume required for circulation has been injected. The solvent is circulated throughout the system until a stable baseline is reached, as verified by observing the scattering intensity signal plotted vs. time in the ASTRA software. Typically, this step took about 30 minutes to complete. The mass of solvent injected is measured by weighing the syringe used for injection before and immediately after injection. This mass is converted to volume in subsequent calculations via the predetermined density of the solvent. After the solvent is thoroughly filtered, a small volume (< 1 mL) of a concentrated NaPSS star stock solution was injected into the system through the rubber septum at the reservoir, and the system was allowed to circulate until a stable intensity signal is obtained in the ASTRA software. The exact mass of solution injected is determined in the same manner as for the solvent in the previous step. At this point, circulation of the solution is stopped to record the signal. The injection process was repeated four or five times in order to attain scattering intensities for five or six concentrations of each sample. Once the final concentration has been run, the filtered solution remaining in the system is stored in a screw-top polypropylene vial for further characterization by DLS and AFM. The components of the closed loop system were then disassembled and cleaned thoroughly with distilled water and compressed air.

***Characterization-AFM***

The instrument known as the atomic force microscope came about as a result of pioneering work done by G. Binnig and H. Rohrer at the IBM research laboratory in 1981. These scientists developed an instrument called the scanning tunneling microscope

(STM) which operates on the principle of a quantum mechanical effect known as the tunneling effect. Essentially, a sharp metallic tip is brought into close proximity with the sample surface and a voltage is applied between the tip and this surface. Upon moving the tip close enough to the surface, electrons are able to tunnel from the surface to the tip, producing a measurable current. This magnitude of this current is strongly dependent upon the distance of the tip from the sample, thus recording the changes in tip height needed to keep this current constant allows for an image of the topography of the sample to be produced.

The demonstrated success of the STM to image very small features led to the subsequent development of the group of instruments known collectively as scanning probe microscopes (SPM), all of which use a different interaction of the probe with the sample surface to produce an image of the surface. Perhaps the most commonly used instrument in this group is known as the atomic force microscope (AFM), which can be operated in three modes: contact, non-contact and tapping. In contact mode, the tip makes physical contact with the sample, with the contact force causing the cantilever to bend in response to topography changes. It is rarely used for polymer samples due to high probability that the tip will damage the sample as it is dragged across it. Non-contact mode utilizes a stiff, oscillating cantilever that is operated quite close to the sample, but not touching it. Typically the distance is 5-10 nm away from the surface, where long range van der Waals forces are prevalent. This mode is non-destructive, but is limited in that it cannot image large sample sizes because the topography changes inherent in this situation can cause damage to the tip or sample. By far the most popular mode of AFM for imaging of polymers, tapping mode utilizes oscillations of the

cantilever in closer proximity to the sample than non-contact mode, in a manner such that the tip intermittently taps the sample surface. This mode avoids inelastic surface deformation and is also able to image large sample sizes. The latter point is especially important for the single molecule imaging described in this thesis, because a large surface area of the sample must often be examined in order to provide a statistically significant number of measurements for the elucidation of molecular parameters.

Due to the reason cited above, AFM in the tapping mode was exclusively utilized for the work herein. An examination of Figure 9 will assist in a description of the components and principles of operation of the AFM in this mode. Basically, a piezo stack causes the cantilever tip to oscillate at its resonant frequency by vertically exciting the cantilever substrate. A laser bream focused on the cantilever reflects off the top portion and is subsequently detected by a quad photodiode array, which records the signal as a sinusoidal electronic signal. This signal is converted to a root mean square amplitude value, which is subsequently displaced in AC volts. Once the tip is carefully lowered to the point that it has intermittent contact with the surface while keeping the excitement of the cantilever by the piezo stack constant, the changes in amplitude of the oscillation of the tip due to the contact are recorded by the computer and interpreted as changes in the vertical height of the sample, as the sample is slowly moved under the tip by the piezoelectric translator. The recorded signal can also be interpreted to reveal other characteristics of the sample, such as phase imaging, which works by measuring the phase difference between the oscillations of the piezo stack and the detected oscillation. The contrast in this form of imaging is believed to result from differences in sample

stiffness and viscoelasticity. Details of the experimental procedure involved with AFM will be given in subsequent chapters.

# *Appendix*

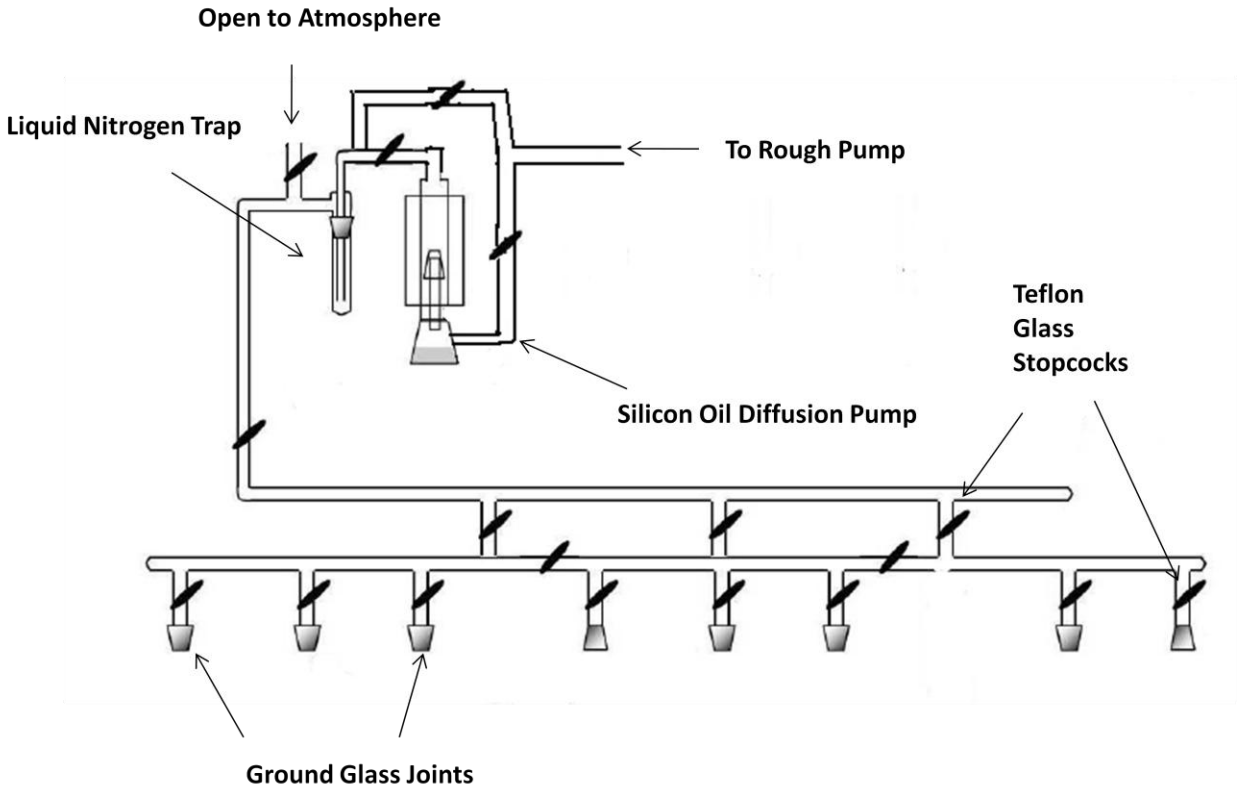



**Figure 4: Vacuum Line Diagram**

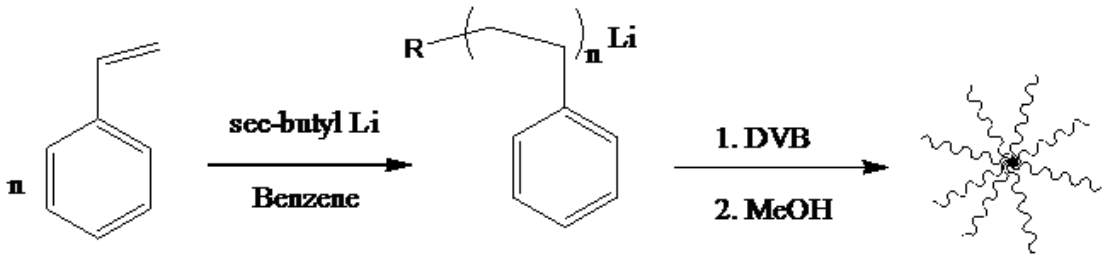



**Figure 5: Synthesis of Star-branched polystyrene**

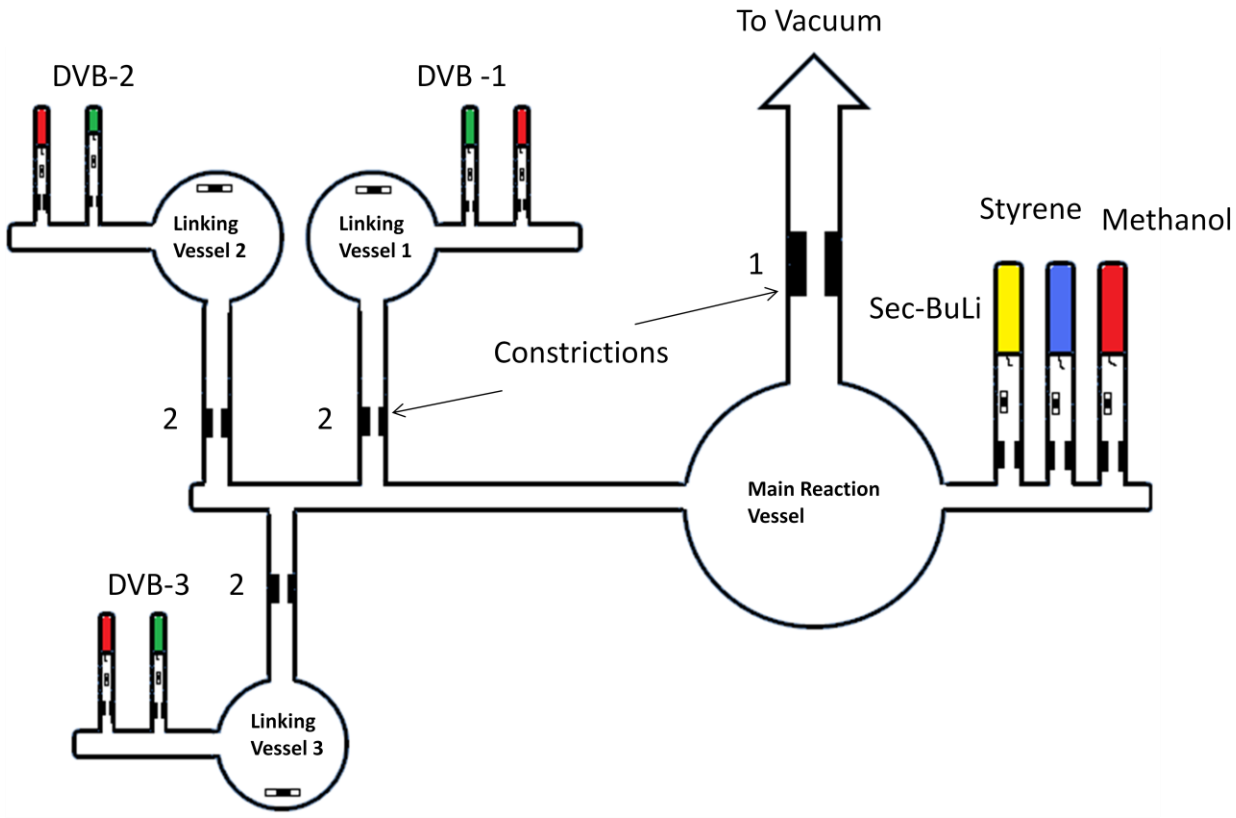



**Figure 6: Star Polystyrene Synthesis Apparatus**

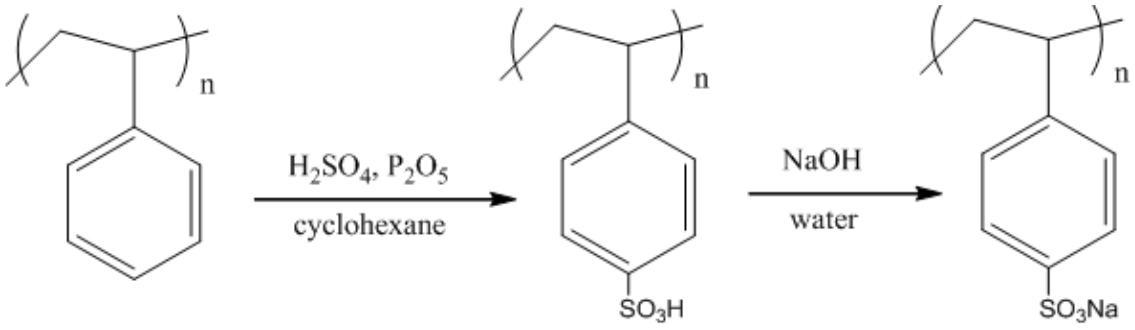



**Figure 7: Polystyene Sulfonation and Neutralization**

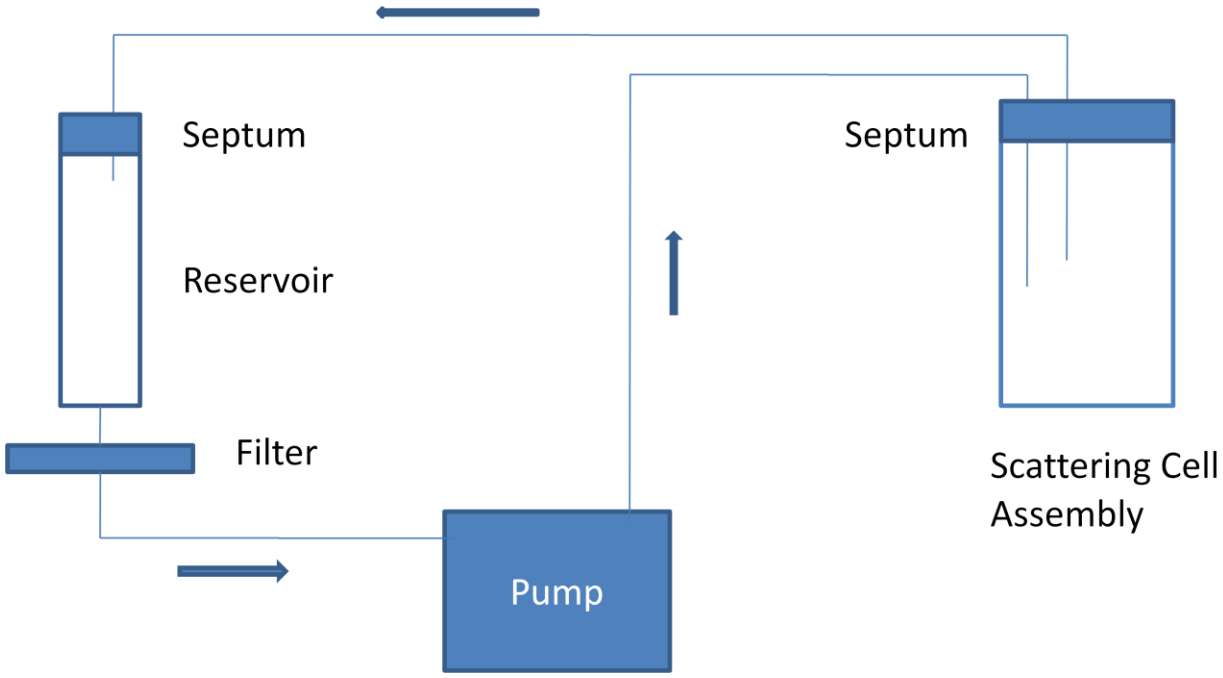



**Figure 8: Closed-Loop Filtration Schematic**

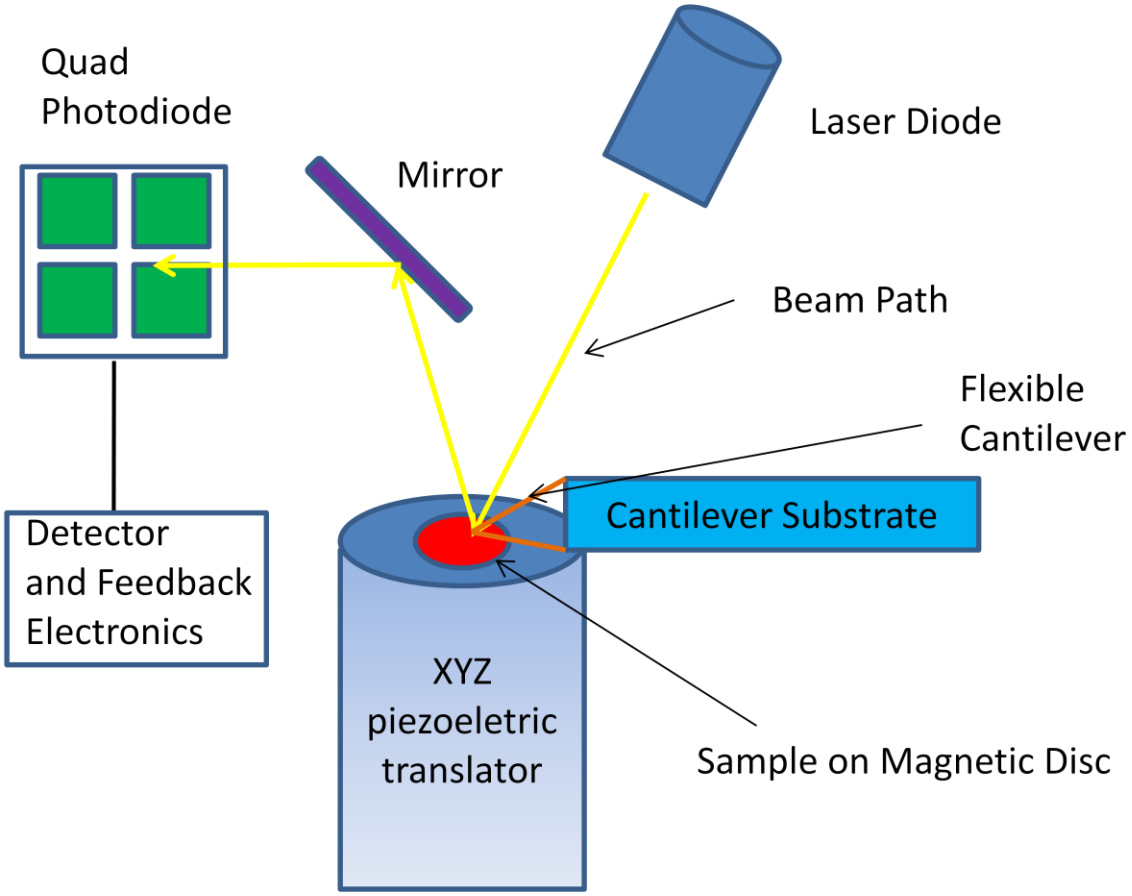



**Figure 9: Atomic Force Microscopy Schematic**

# References

(1) Chiefari, J.; Chong, Y. K.; Ercole, F.; Krstina, J.; Jeffery, J.; Le, T. P. T.; Mayadunne, R. T. A.; Meijs, G. F.; Moad, C. L.; Moad, G.; Rizzardo, E.; Thang, S. H. *Macromolecules* **1998**, *31*, 5559-5562.

(2) Keoshkerian, B.; Georges, M. K.; Boils-Boissier, D. *Macromolecules* **1995**, *28*, 6381-6382.

(3) Lowe, A. B.; McCormick, C. L. *Progress in Polymer Science* **2007**, *32*, 283-351.

(4) Hsieh, H. L.; Quirk, R. P. *Anionic Polymerization*; Marcel Dekker, Inc.: New York, NY, 1996.

(5) Szwarc, M. *Joural of the American Chemical Society* **1956**, *78*, 2656.

(6) Szwarc, M. *Nature (London)* **1956**, *178*, 1168.

(7) Szwarc, M. *Carbanions, living polymers, and electron transfer process*; Wiley Interscience: New York, 1968.

(8) Wakefield, B. J. *Organolithium Methods*; Academic Press: New York, 1988.

(9) Fernyhough, C. M.; Young, R. N.; Ryan, A. J.; Hutchings, L. R. *Polymer* **2006**, *47*, 3455-3463.

(10) Bauer, B. J.; Fetters, L. J. *Rubber Chemistry and Technology* **1978**, *51*, 406-436.

(11) Young, R. N.; Fetters, L. J. *Macromolecules* **1978**, *11*, 899-904.

(12) Kuccaronera, F.; Janccaron, J. *Polymer Engineering & Science* **1998**, *38*, 783-792.

(13) Makowski United States, 1975; Vol. 3,870841.

(14) Baigl, D.; Seery, T. A. P.; Williams, C. E. *Macromolecules* **2002**, *35*, 2318-2326.

(15) Vink, H. *Die Makromolekulare Chemie* **1981**, *182*, 279-281.

(16) Smisek, D. L.; Hoagland, D. A. *Macromolecules* **1989**, *22*, 2270-2277.

(17) Muller, G.; Yonnet, C. *Die Makromolekulare Chemie, Rapid Communications* **1984**, *5*, 197-201.

(18) Heimenz, P. C. *Polymer Chemistry: The Basic Concepts*; Marcel Dekker, Inc.: New York, 1984.

(19) Berry, G. C. *The Journal of Chemical Physics* **1966**, *44*, 4550-4564.

(20) Andersson, M.; Wittgren, B.; Wahlund, K.-G. *Analytical Chemistry* **2003**, *75*, 4279-4291.

(21) Farmer, B. S., University of Tennessee, 2006.

# Part 3: Synthesis and Characterization of Star-Branched Polyelectrolytes

## *Abstract*

In this thesis, we examined the effect of branching on the solution characteristics of polyelectrolytes using a set of star-branched NaPSS. The polystyrene precursors to these polyelectrolytes were synthesized using anionic polymerization, employing a novel method of dividing the solution containing the reactive anionic chain ends and subsequently linking them together using DVB. This method of synthesis allowed for the production of three distinct groups of star-branched polystyrenes, with each group consisting of three samples that had the same degree of polymerization of each arm, but different numbers of arms in each sample. We used SEC-TALS to establish that the precursor polymers were relatively monodisperse and to determine *f* and the degree of polymerization of each arm. To complete the synthesis, the precursors were sulfonated using conditions that were modified from the original Vink procedure.

Due to the rather open question as to what extent the degree of sulfonation changes the solution characteristics of NaPSS, we sought to quantify this parameter for the star-branched NaPSS samples using several methods commonly employed in the literature. All methods used indicated that the sulfonation degree was above 90% for every sample. TGA was also demonstrated to allow for quantitative determination of the water content and qualitative estimations of the amount of residual low molecular weight salt in the sample as well as qualitative indications of the relative amount of monomers in sulfonic acid and sodium salt form and the sulfonation degree.

We used aqueous SEC coupled with a multiple angle light scattering detector to determine the $M_w$, $R_g$, and polydispersity of the star-branched NaPSS samples. Linear NaPSS synthesized via radical polymerization and polymer-analogous sulfonation of

polystyrene were also characterized using this method and important differences between NaPSS synthesized by the two methods were established, mainly indicating the presence of crosslinking and hydrophobic interactions for NaPSS synthesized by the polymer-analogous sulfonation route. Scaling relationships between $R_g$ and $M_w$ of both branched and linear species were established. Also, dynamic light scattering experiments established a qualitative link between the presence of a slow diffusive mode and the degree of sulfonation. The branching parameter *g* was determined for the star-branched NaPSS samples and compared to theoretical predictions of *g*, verifying the type and extent of branching and the retention of the molecular structure after polymer-analogous sulfonation.

## *Introduction*

Sodium poly(styrenesulfonate) (NaPSS) is a material that has enjoyed a long history as a model system for the study of polyelectrolyte behavior. With relatively few exceptions, research has focused on the properties of the linear polymer.[1-6] However, there is a great deal of interest from theoreticians in the properties of branched polyelectrolytes, in particular those with a star-branched architecture. This is largely because this particular molecular architecture is seen as a model to examine the effects of branching in general.[7-9] The literature currently available on the subject from both the experimental and theoretical standpoints has been examined in detail in the Introduction, so only a couple of points will be reviewed here.

Until recently, researchers have primarily utilized NaPSS synthesized via the polymer analogous sulfonation of anionically polymerized polystyrene as model compounds. Recently, due to concerns about possible cross-linking side reactions, as

well as difficulty obtaining and verifying high degrees of sulfonation, some researchers have used NaPSS synthesized by radical polymerization of the sodium styrenesulfonate monomer.[4,10] While this method of polymerization avoids the aforementioned problems, it has a couple of significant drawbacks. The first is that radically polymerized NaPSS must be fractionated in order to obtain the narrow molecular weight distribution necessary for use as a model polyelectrolyte. The second is that this method of polymerization is limited to the synthesis of the linear polymers of a relatively low molecular weight, not allowing the synthesis of high molecular weight or branched architectures.

Perhaps because well defined structures are hard to obtain, studies of the solution properties of NaPSS with a branched architecture are rare. Mays provided the earliest report of star-branched polystyrenesulfonate when he synthesized star-branched KPSS of varying functionality and reported the $R_h$ of the stars as a function of the KCl concentration.[11] This value was normalized relative to the $R_h$ at high ionic strength (0.5M KCl) and compared to the viscosimetric radius ($R_v$) for the analogous linear material. It was found that the size of a highly branched polyelectrolyte is much less sensitive to added electrolyte concentration than that of the linear material. There is no other example of a comparison between linear and branched NaPSS reported in the literature.

Recently, Fernyhough and coworkers synthesized a series of NaPSS materials with a comb architecture in the interest of using it as a model for proteoglycan, an important component of cartilage.[12] They reported an increase in polydispersity after sulfonation, indicative of crosslinking, and incomplete sulfonation. To avoid these problems, Lienkamp and coworkers synthesized similar structures via the polymer

analogous hydrolysis of polystyrenesulfonate ethyl and dodecyl ester combs.[13] Unfortunately, hydrolysis of these structures ranged from 10% to 90%, with a significant degree of crosslinking if the extent of hydrolysis exceeded 66%. Even a small percentage of hydrophobic patches or crosslinking could have significant effects on the solution properties of these polymers, as has been recently verified by Akhil in studies comparing the properties of linear NaPSS synthesized by polymer analogous sulfonation of polystyrene and NaPSS synthesized by radical polymerization of the sodium styrenesulfonate monomer. [14] In this work, the osmotic coefficient of the free radically polymerized NaPSS was found to be 20% higher than NaPSS obtained from polymer analogous sulfonation. Since both species were fully sulfonated, this difference must be due to structural differences between the two polymers. The authors postulated that this gives strong evidence for the presence of a small number of intramolecular sulfone linkages in the NaPSS synthesized by polymer analogous sulfonation, since sulfone formation is not likely for the free radically polymerized NaPSS. The authors argued that sulfone linkages in the NaPSS obtained by polymer analogous sulfonation would bring anionically charged segments of the NaPSS chain closer together, thereby bringing about an increase in the condensation of counterions onto the polymer chain to mediate the electrostatic repulsion between segments. Since the osmotic coefficient has a direct relationship to the fraction of uncondensed counterions, the authors thereby concluded that the NaPSS synthesized by polymer analogous sulfonation possessed sulfone linkages, unlike the free radically polymerized NaPSS.

Due to the concerns outlined above, there is still significant interest in quantifying the degree of sulfonation and detecting the presence of inter- and intramolecular sulfone

linkage resulting from polymer analogous sulfonation in the interest of maximizing the former while minimizing the latter. The literature reviewed above also indicated a need for a thorough examination of the solution properties of star-branched NaPSS. To this end, we have synthesized a series of star-branched NaPSS polymers of varying arm length and functionality for the purpose of examining the degree of sulfonation and the procedures commonly used to determine it. Additionally, examination of the nonionic precursors (star-branched PS) as well as the sulfonated material (NaPSS) using SEC coupled with light scattering detection will allow for a comparison of the solution properties of the ionic and nonionic forms of the star-branched polymers and to linear analogues, as well as the properties calculated from theory.

## *Experimental*

### *Synthesis*

All chemicals used in the synthesis were purchased from Aldrich or Fisher, and those used for anionic synthesis of the polystyrene parent materials were purified according to the procedures described in detail in Part 2. All other chemicals were used as received. The anionic synthesis, workup, sulfonation, neutralization, dialysis, and lyophilization required to obtain the desired NaPSS star-branched polymers have also been described previously.

Radically polymerized NaPSS was synthesized via a method identical to that recently used by Cong.[10] The following conditions were used: 50 mL of a 50/50 by volume solution of methanol/distilled water was added to a round-bottom flask containing 5 g of sodium styrenesulfonate and 10 mg of azobisisobutyronitrile and the flask was capped with a rubber septum. Dry nitrogen was bubbled through the flask for

~2 hrs to purge the solution, and the flask was slowly heated to 75 °C with stirring under nitrogen. After ~24 h, after which the reaction was quenched by cooling the flask to room temperature and exposing it to air. The polymer was recovered through dialysis and lyophilization of the samples following the procedure described in Chapter 2.

*Elemental Analysis*

Elemental analyses for the weight percent of C, O, S, Na and H were performed by Galbraith Labs, Knoxville, TN.

*$^{1}$H NMR*

All $^{1}$H NMR spectra of the samples were measured on a Bruker 250 MHz NMR spectrometer. The samples were dissolved in deuterium oxide ($D_2O$, ~0.6 mL) and the experiments were performed at room temperature.

*Titration*

For the purpose of titration, NaPSS samples (~100 mg) were typically dissolved in water (20 mL) in screw-top polypropylene vials to which an excess of carefully washed Amberlite IR-120-H exchange resin (Aldrich) was added. The vial was tightly closed and shaken for ~48 hours on a laboratory shaker to ensure the conversion to the sulfonic acid form of the polymer. Measured volumes of the resulting solutions were injected into a large volume (~50 mL) of water and titrated with ~0.005M NaOH. pH measurements were conducted using a Fisher Scientific AR15 pH meter with an AccuTupH electrode.

*Thermogravimetric Analysis*

A TA Instruments TGAQ50 was used to conduct thermogravimetric analysis of the samples, using a sample size of ~5-10 mg with a ceramic pan. The samples were heated at a heating rate of 10°C/min from room temperature to 900°C, in the presence of air. The experiments were found to be reproducible within ± 3 °C and ± 3 % in the measurements of $T_{onset}$ and $T_{max}$, and percentage water and residue respectively.

*Size-Exclusion Chromatography*

The size-exclusion chromatography (SEC) experiments were performed with two different setups, designated as SEC-TALS and as ASEC-MALLS. SEC-TALS consisted of a Polymer Labs GPC-120 setup equipped with two 10μm and one 500 angstrom PLgel Mixed-B columns, a PD 2000DLS dynamic light scattering detector, a Viscotek 220 differential viscometer, and a PD2040 static light scattering detector, which detects scattered light at 15° and 90°. The eluent was tetrahydrofuran (THF) flowing at 1mL/min at 40°C.

ASEC-MALLS is an aqueous system consisting of a Knauer K-501 HPLC pump with an Optilab DSP interferometric refractometer and DAWN EOS static light scattering detector. A set of three 10 μm PSS Suprema columns, with sizes 3000, 1000, and 100 and a guard column were used in this system. The mobile phase was an 80/20 solution of 0.1M $NaNO_3$/acetonitrile. Polymer solutions were injected into the sample loop with a plastic syringe fitted with a 0.45 μm PTFE filter. The concentration of the injected solutions ranged from 0.4-0.8 mg/mL, and a flow rate of 0.5 mL/minute was used for all samples.

*Dynamic Light Scattering*

The instrument used for dynamic light scattering of the aqueous solutions was a Precision Detectors PD Expert Multiangle Light Scattering Platform. All measurements were performed at 95°. Solution concentrations ranging from 0.4-0.7 mg/mL were used, and no extrapolation to infinite dilution was performed. CONTIN software was used for analysis of the correlation functions.

*Measurement of Refractive Index Increment*

The *dn/dc* of the polystyrene samples was determined on a Brice-Pheonix interferometric refractometer and was determined to be 0.186 ml/g at 670 nm in THF. For the NaPSS samples, the *dn/dc* at fixed chemical potential ($\mu$) of diffusible components $(dn/dc)_\mu$ was needed, so samples 54s and NaPSSrad1 were dialyzed against the 0.1M $NaNO_3$/acetonitrile solution as described in Part 2. A Wyatt Optilab interferometric refractometer was used to determine the $(dn/dc)_\mu$ of the polymers, which was 0.200 ml/g in both cases. This value was used for analysis of all of the NaPSS samples.

## *Results and Discussion*

### *Synthesis and Characterization of Precursor Polystyrenes*

Anionic polymerization under high vacuum was used to synthesize the polystyrene precursors, as has been previously described. The synthetic procedure outlined in Part 2 was followed three times to produce three sets of star polymers, with each set consisting of three star polymers that have arms of the same $M_w$ but different star functionality (*f*). SEC-TALS coupled with SLS, DLS, and RI detectors was used to characterize the resulting star-branched samples, as well as the linear star arms. SEC

chromatograms of the 40 series of stars are displayed in Figure 10, showing monomodal peaks and a decrease in elution volume with molecular weight. Table 1 displays the characteristics of the polystyrene stars as determined by SEC-TALS. As expected, both the $M_w$ and *f* of the stars increase with the increasing molar ratio of DVB/Li, though it is difficult to establish a quantitative correlation between these parameters, as has been reported previously.[15] The values of $M_{w,arm}$ were obtained from separate SEC analysis of the terminated unlinked arms, and showed a polydispersity less than 1.04. The values of %DVB range from 0.21 to 5.6, although it is noted that only the samples in the 40 series contain more than 1 % DVB. The values of $M_w/M_n$ are all close to 1.1, indicating fairly monodisperse samples.

Table 2 lists the radii of the samples determined by SEC-TALS. As anticipated, both $R_g$ and $R_h$ increase in each series of polymers as both the $M_w$ and *f* increase. For the 4 series of polymers, the $R_g$ of each polymer is below the accessible range of dependable light scattering data so these values were omitted. The ratio of $R_g/R_h$ is sensitive to the conformation of macromolecules in solution. Typically, a value of 1.2-1.5 is found for polymers that achieve a random coil conformation in solution, and a value of 0.775 is found for those that adopt a hard spherical conformation. All of the star-branched polystyrenes have values of $R_g/R_h$ of less than one which is indicative of branched structures. It is important to note that the values of Rg/Rh of the polystyrene stars are slightly higher ($0.790 < R_g/R_h < 0.875$), than the theoretically predicted value of hard sphere conformation which is 0.775, irrespective of their functionality. However, the ratio is also observed to decrease as *f* increases for each series of stars, indicating a more compact structure with increased *f*.

One powerful aspect of SEC coupled with TALS and differential refractive index detectors is the ability to examine different "slices" of the elution profile of injected polymer samples. Generally, it is assumed that gel-permeation chromatography separates polymer samples based on the hydrodynamic radius of species. When this separation is combined with TALS, the $R_g$ and $M_w$ of small, nearly monodisperse portions of the sample can be determined, leading to the ability to observe trends in the separation of individual samples. Figure 11 shows the elution profile of 54p, depicting the evolution of $M_w$ and concentration with elution volume, with a generally linear correlation indicating the efficient separation of the sample on the basis of molecular weight. A small plateau at the high molecular weight end of the elugram indicates that separation may not be as efficient in this regime, though it is noted that the concentration in this regime is very low and the $M_w$ determination is subject to considerably more error here than in other portions of the elugram. These trends in the elution profile are the same for all of the samples examined, hence it is concluded that the characterization of the samples using SEC-TALS was successful.

***Sulfonation Degree Characterization***

After the thorough characterization described above, the parent polymers were sulfonated using the modified Vink method described in detail in Chapter 2. After neutralization, dialysis and lyophilization, numerous experimental methods were used to determine the degree of sulfonation of the resulting polymers. A description of each method, as well as the conclusions drawn from it and a comparison of results obtained from different methods follows.

*Titration*

One important aspect of the determination of sulfonation degree using titration is the accurate determination of the concentration of NaPSS in the titrated solutions. A recent publication pointed to the possibility that some of the variation in the sulfonation degree of NaPSS synthesized by polymer analogous sulfonation reported in the literature is due to the inaccurate determination of the concentration of NaPSS.[14] This difficulty is caused by the extreme hydrophilicity of the "dry" polymer samples, often leading researchers to overestimate the concentration of NaPSS in solutions used for titration. With these observations in mind, thermogravimetric analysis was performed on all of the NaPSS materials examined in this thesis in order to determine the percentage of water in the solid samples (%$H_2O$), which is shown in Table 4 and ranges from 7.7 to 16%, and is around 14% for most samples, a percentage that indicates the presence of about two water molecules per monomer unit. These values were used to determine the mass extinction coefficient of the materials (1.764 mL/mg at 262nm) using the sample NaPSSrad2, which is close to the values determined by other researchers.[10] This allowed for accurate determination of the concentration of polymer after the titration, enabling the calculation of the degree of sulfonation by the following equation:

$$\text{Degree of Sulfonation} = \frac{\text{Concentration Measured by Titration}}{\text{Concentration Measured by UV}} \quad (20)$$

The titration curve of 54s is shown in Figure 11, revealing the sharp transition expected for a strong acid/ base titration. The sulfonation degree obtained using titration showed sulfonation degrees ~90 % for 4 series stars and 97-100 % for 5 and 6 series stars (Table

3). This difference could be attributed to the relatively higher levels of DVB at the core of the stars in the 4 series, which may not be sulfonated.

*$^1$H NMR*

Another commonly used method of determining the degree of sulfonation is $^1$H NMR. One problem we encountered using this technique was that the NMR spectra obtained displayed poor resolution due to the relatively large amount of residual water in the samples. In an effort to remove the water, a number of samples with reported degrees of sulfonation ranging from 85-98% were placed into vials containing DMSO-$d_6$ and activated molecular sieves to remove the residual water from both the NaPSS sample and the solvent. Unfortunately, the samples did not dissolve in the dry DMSO-$d_6$ solvent and it was necessary to use $D_2O$ instead. It appears that DMSO is not a good solvent for NaPSS at room temperature, and requires at least a small percentage of absorbed water that is commonly present in the samples to act as a co-solvent to solubulize the polymer, an observation that has not previously been reported.

The $^1$H NMR spectrum of 54s in $D_2O$ is shown in Figure 13. The inset shows the peak assignment of the protons in the sample, with the aliphatic $H_C$ protons being assigned to the broad peak in the region between 0.8 and 2.2 ppm, the ortho $H_A$ protons being assigned to the peak between 6-7.2 ppm with a maximum at 6.8 ppm, and the meta $H_B$ protons assigned to the peak between 7.2-8.2 ppm with a maximum at 7.7 ppm. The peak at 4.76 ppm is assigned to incomplete deuteration of the solvent, $D_2O$, and residual water. No peak can be discerned in this sample at 7.45 ppm, which would be indicative of unsulfonated polystyrene units in the polymer and would be assigned to the meta and para aromatic protons of those units, hereafter designated as $H_U$. The values of

integration for the previously described areas of the spectrum are presented at the bottom of the figure. The value for the integration of the $H_C$ protons is assigned as 3, and the other integrations are normalized to this number. It is noted that none of the values for the integrations have the expected values for fully sulfonated NaPSS: the $H_A$ to $H_B$ ratio should be equal to 1, and the ratio of the aromatic region to the aliphatic should be 4/3. This trend is observed throughout all of the examined samples, including the radically polymerized NaPSS1, which must be 100% sulfonated. These trends have been noted before by Baigl in a detailed study of NaPSS with widely varying degrees of sulfonation, and hence the analysis proposed in that study is used in this thesis.[2] Briefly, this method of analysis, called the modified peak heights ratio, consists of the following relationship:

$$\text{Degree of Sulfonation} = 0.91\ \frac{\text{Height of peak } H_B}{\text{Height of peak } H_U} \tag{21}$$

It is noted that the estimate of the height of the peak at $H_U$ is subject to a large amount of uncertainty, due to the large amount of noise in the spectrum as well as the relatively high sulfonation degree of the NaPSS examined. However, the results obtained showed quantitative sulfonation for several stars with an exception that a few samples in star series 4 exhibited less than 96 % sulfonation.

*Elemental Analysis*

Analysis of the results from elemental analysis consisted of the following three ratios of the mole percentages of the components in NaPSS: %S/%C, %Na/%C. Results of the different analyzes are displayed in Table 3 for comparison. First it is noted that all methods of analysis give sulfonation degrees >94%, for the star NaPSS samples, with the exception of the titration results for the 4 series of stars. This can be partially explained by the relatively large percentage of DVB present in these materials (1.9-5.6 wt %),

which is apparently not sulfonated in this case. Assuming this, the effective sulfonation degree for the arms of this series of stars is in the >94% range reported for the other star materials, all of which have significantly smaller percentages of DVB (≤ 1%). Another trend to note is the S/C and Na/C columns, which consistently give degrees of sulfonation above 100% for the star NaPSS samples, particularly for samples 54s, 56s, 64s which have an excess of S, and for 66s which has an excess of Na. It should be noted that elemental analysis is affected by the presence of the second most common impurity in NaPSS samples next to water: $Na_2SO_4$. Since titration would be more sensitive to small percentages of $Na_2SO_4$ in the bulk sample (which is converted to sulfuric acid under the conditions used to convert NaPSS to its acidic form) than elemental analysis, we conclude that these star samples do not contain significant amounts of $Na_2SO_4$. Conversely, the titration results for the non-dialyzed commercially available linear NaPSS (denoted by std) are all well above 100% (with the exception of 2.2M std) indicating that these samples are contaminated by a significant amount of $Na_2SO_4$, even though the company literature for elemental analysis of these samples indicate sulfonation degrees ranging from 85-97%.

*Thermogravimetric Analysis*

In an attempt to further characterize the NaPSS stars, thermogravimetric analysis was performed. A typical TGA graph is shown in Figure 14, with the green line representing the change in weight percent vs. temperature and the blue line representing the derivative weight percent as a function of temperature. The first transition, occurring from 100-300 °C, is attributed to the loss of tightly bound water in the sample and is equal to about 15% for this sample. At 395 °C decomposition of the polymer begins, and

a complex series of transitions occurs until 650 °C, at which point the weight maintains a constant value and a residue of 22.3% by weight of the dried sample remains. Table 4 lists the weight loss values obtained from TGA for all of the polymers analyzed, along with the percentage molar ratio of S/Na included and the results for titration reprinted for reference. A few trends related to the characteristic temperatures $T_{onset}$ and $T_{max}$ are noted. $T_{onset}$, which is the temperature at which the sample begins to lose weight after the residual water has evaporated, is observed to be significantly higher for the linear standard NaPSS samples( ~401°C on average) than for the star-branched NaPSS (~388°C on average). The radically polymerized sample, NaPSSrad1 has a $T_{onset}$ of 392°C, much closer to the average value of the star-branched NaPSS than the linear standards. $T_{max}$ is the peak in the first derivative of the plot of weight percent vs. temperature indicating the point at which the sample is losing weight at the fastest rate, and follows some of the same trends as $T_{onset.}$ It is observed that the $T_{max}$ of the star-branched NaPSS materials does not deviate much from an average of ~519°C (with the exception of 46s), very close to the value obtained for NaPSSrad1 (518°C). On the other hand, the linear standards have a much higher average $T_{max}$ (531°C). These observations on $T_{max}$ and $T_{onset}$ could be interpreted as evidence for the presence of sulfone linkages in the linear standard. Such linkages could increase the thermal and oxidative stability of the materials, though the complexity of the system makes it difficult to establish a quantitative relationship.

Analysis of the percent residue in the samples also provides evidence of contamination of the bulk polymer sample with $Na_2SO_4$. Although it is acknowledged that the identity of the decomposition products is not known, if we assume that the only decomposition product remaining in the residue is $Na_2SO_4$, assuming full sulfonation and

the absence of low molecular weight salt, then the % residue would be equal to 34.5%. In this respect, sample NaPSSrad1 is a good reference point for the other samples. This sample has a 100% sulfonation degree and could not contain any $Na_2SO_4$ contaminant, thus the 32.7% residue that is obtained from its decomposition originates solely from the fully sulfonated polymer in the sodium salt form. The reasonably good agreement between the theoretical % residue and the experimental % residue for this sample provides some support for the theory that the main residue constituent is $Na_2SO_4$. For samples 64s, 54s, and 52s, a low percent residue and a high molar ratio of S/Na indicates that these samples have relatively high percentages of monomers in sulfonic acid form rather than sodium salt form, as the sodium salt form leaves a larger residue than the sulfonic acid form, which would decompose into various volatile sulfur oxides. With this in mind, any sample with a residue above 32.7% most likely contains some percentage of $Na_2SO_4$. This conclusion is reinforced by examination of the percent residue for the undialyzed std samples, which all contain residues above 32.7% and titration values above 100%, both of which are indicative of significant percentages of $Na_2SO_4$ in the bulk sample. It is noted that, in spite of extensive dialysis, 44s and 66s also contain more than the theoretical percent residue.

***Aqueous SEC Results***

*Linear NaPSS*

For the purpose of comparison to the star-branched materials, linear NaPSS commercial standards and radically polymerized samples were analyzed using aqueous SEC-MALLS. The elugrams of the highest molecular weight commercial NaPSS samples (1.18Mstd, 2.2Mstd, 2.69Mstd) exhibited a multimodal peak similar to the one

shown in Figure 15. The middle peak at highest concentration is attributed to the main product of the sulfonation and, for polymers 1.18Mstd and 2.2Mstd, closely corresponds to the molecular weight reported in the company literature. A smaller peak observed at lower elution volume is close to double the molecular weight of the middle peak and displays a significantly different $R_g$ vs. $M_w$ relationship. This peak is attributed to dimer formed from crosslinking of the sulfonated polymer. Finally a shoulder is observed at the higher elution volume side of the middle peak, at longer elution times. This shoulder could be due to some compositional heterogeneity of the sulfonation level of portions of the sample, but it is unclear from the data if this is the case. The elugram of 505kstd exhibited a relatively sharp peak with a small high molecular weight shoulder again attributed to dimer and 57kstd exhibited a single sharp peak.

Due to the complexity exhibited by the elugrams of the commercial linear NaPSS, two NaPSS samples were prepared from the sodium styrenesulfonate monomer by free radical polymerization. While these materials have a high polydispersity, they are free from the crosslinking and compositional heterogeneity of the commercial samples. An elugram of the free radically polymerized NaPSSrad2 is shown in Figure 16, and shows the expected broad, monomodal peak. The evolution of $M_w$ with elution volume is also shown on the graph and is linear throughout the evolution of the peak, suggesting that the polymer is structurally and chemically homogeneous.

Table 7 lists the characteristics of the linear NaPSS samples as determined by ASEC-MALLS. It is seen that the $M_w$ determined is close to both the theoretical and experimental values reported by the manufacturer for all of the commercial samples except for 2.69Mstd. A possible explanation for this is that this polymer has the lowest

degree of sulfonation of all of the samples tested (85% as calculated by theoretical percent of sulfur content), and this probably results in a different *dn/dc* value than the other polymers. A relatively high unsulfonated content can also lead to different retention behavior, affecting the elution profile and resulting in a high measured polydispersity (1.59), a result similar to that reported by Baigl using the same analyte/eluent system.[2] As expected, the radically synthesized NaPSS samples have significantly higher polydispersities than the commercial standards, with the exception of 2.69Mstd.

In order to establish the scaling relationship between $R_g$ and $M_w$ for linear NaPSS, we combined data from the slice tables of the following polymers: NaPSSrad1, NaPSSrad2, 1.18Mstd, and 2.2Mstd. There were several criteria for the selection of samples and slices used for fitting the curve:

1. The radically polymerized samples were chosen because they cover a wide range of molecular weight, and are assumed to be chemically and structurally homogeneous.
2. The commercial standards were chosen on the basis of a close match between their experimentally determined and theoretical molecular weights and sufficient coverage of molecular weight in the range of interest.
3. The slices of all samples were chosen based on a sufficient concentration to reduce error in the measurement, close to the maximum in the concentration detector peak.

4. Slices of the commercial samples were selected with the additional criterion that they are located in a linear region of the $R_g$ vs. $M_w$ plot, indicating at least structural homogeneity within this region.

Using these criteria, the following relationship was determined for $M_w$ ranging from 200k to 2.75 million g/mol in the mobile phase used for ASEC:

$$R_g = 0.00944 M_w^{0.625}$$

For comparison, the scaling relationship for polystyrene in THF was previously found to be $R_g = 0.01118 M_w^{0.600}$. The 0.625 exponent indicates that NaPSS is slightly less flexible under these conditions than styrene, because $M_w$ is directly proportional to the degree of polymerization of the polymer, and a less flexible chain will assume a more extended conformation in solution than a less flexible one.

*Star-branched NaPSS*

To verify that the structure of the star-polymers was retained after sulfonation, and to compare the solution properties of the star-branched NaPSS with linear NaPSS, aqueous SEC was performed on the NaPSS star-branched polymers. With the exception of polymers 44s, 46s, and 66s, the elugrams are monomodal and relatively sharp with somewhat curved evolution of molecular weight with elution volume, similar to the one of 52s shown in Figure 17. The elugram of 66s shows a shoulder at high molecular weight that is about double the molecular weight of the highest concentration species in the sample. Since this highest molecular weight sample would be the most likely to be close to the overlap concentration under the sulfonation conditions, it is reasonable to expect that this shoulder is due to a small concentration of crosslinked material in the sample. The elugram of 46s shown in Figure 18 is more difficult to interpret. Although

the signal from RI is symmetrical, the broad light scattering signal indicates the presence of a low concentration of high molecular weight species. Crosslinking due to sulfone formation during the sulfonation reaction is much less likely in this case, due to the relatively small dimensions of the unsulfonated polymer. Since this polymer contains the largest percentage of DVB and has one of the lower degrees of sulfonation of the star-branched NaPSS samples, the origin of this high molecular weight portion may be aggregates formed due to hydrophobic interactions originating from both unsulfonated patches on the arms of the star and the relatively large DVB core. Sample 44s shows the same behavior to a lesser degree, possibly due to a smaller percentage of DVB and hence fewer hydrophobic interactions.

Shown in Table 6 are the aqueous SEC results for the star-branched NaPSS samples. It is noted that the $M_w$ determined is within 15% of the theoretical value, with the exception of sample 44s, and 46s, due to the aggregation phenomenon mentioned earlier. $R_g$ values follow the same pattern of a direct relationship between *f* and $R_g$ as in the precursor polymers, although $R_g$ increases more rapidly with *f* in the case of the polyelectrolytes, as shown in Figure 19. This behavior can be attributed to an increase in the excluded volume of the polyelectrolyte relative to the precursor, due to electrostatic repulsion between arms of the star. The measured polydispersities are close to the values obtained for the precursor polymers with the exceptions of samples 44s and 46s.

Figure 20 shows the $R_g$ vs $M_w$ plot for the 6 series of stars. At the low molecular weight section of the plot of each sample, there is a curved portion, which seems to indicate that two slices with the same $M_w$ have different values of $R_g$. A similar profile was described by Frater in a work on polystyrene stars with mixed arm lengths, and was

attributed to an inefficient separation of the polymer at relatively high flow rates, causing the elution of a very polydisperse mixture of high and low $M_w$ species at the tail of the elution.[16] Since the measured $R_g$ is a z-average property, the relationship between $R_g$ and $M_w$ in this portion of the elugram is not the same as in the other portions where separation is more efficient, as the larger molecules will affect the measured Rg proportionally more than the smaller ones. Portions of the $R_g$ vs. $M_w$ plots are linear for each polymer, allowing for the calculation of power law relationships between $R_g$ and $M_w$ for the 50s and 60s series of stars. These are:

$$50s \qquad R_g = 0.02959 M_w^{0.494}$$

$$60s \qquad R_g = 0.0074 M_w^{0.594}$$

The values of the exponents are significantly less than that determined for linear NaPSS, which can partially be attributed to the increase in the functionality of the stars with molecular weight, but also to the reduced sensitivity of $R_g$ to $M_w$ expected in highly branched systems such as stars, where the addition of an additional arm increases the $M_w$ more than the $R_g$. Unfortunately, a similar calculation could not be performed for the 40s series of stars due to the aforementioned aggregation phenomenon affecting the elution of samples 44s and 46s.

*Dynamic Light Scattering*

Further characterization of both the linear and star NaPSS samples was performed using dynamic light scattering in the same solvent that was used for ASEC-MALLS (80% 0.1M$NaNO_3$/20% acetonitrile). The data obtained are listed in Table 7. The apparent hydrodynamic radii ($R_h$) for the star polymers show the same general pattern as the $R_g$ determined from ASEC-MALLS: an increase with degree of branching within

each series. The variance in the distribution measured here qualitatively corresponds to the polydispersities measured using ASEC-MALLS, with two of the samples with the highest polydispersities, 46s and 66s, having a variance above 0.5. The modest polydispersities measured for the 60s series do not closely match the variances measured for the samples, an observation that is attributed to the previously observed imperfect separation of these species by ASEC. For the other star-branched polymers the dispersities range from 0.11-0.22, indicative of moderately disperse samples and matching the polydispersities measured from ASEC-MALLS well. The next column in Table 6, headed % Fast Mode, refers to the portion of the scattered intensity that originates from species with a higher value of $D(c)_{(app)}$ in the bimodal distribution observed for these samples. Typically the contribution from the slow mode is insignificantly small, but for samples 42s and 44s there is a signficant contribution from this mode. Notably, these samples are measured as having the lowest degree of sulfonation among the star-branched NaPSS samples, with the exception of 46s which has a very high variance. The $R_g/R_h$ ratios generally follows the pattern seen in the polystyrene precursors, with the ratio generally decreasing as *f* increases, and are in the range of 0.868-1.16, indicating a branched structure that most likely behaves as a soft sphere. Again, samples 46s and 66s display behavior that is significantly different from the other samples, exhibiting ratios that are below the uniform non-draining sphere limit of 0.775.

For the linear NaPSS samples, $R_h$ increases with $M_w$, as expected. The dispersities again qualitatively match the polydispersities measured from ASEC, with the most polydisperse sample, 2.69Mstd, having a dispersity of 0.49. The % Unimer values

again correspond qualitatively to the sulfonation degree of the polymers analyzed. The fully sulfonated NaPSSrad1 shows essentially no contribution from a slower relaxation mode, while the sample with the lowest sulfonation degree, 2.69Mstd, has a significant contribution. Samples 1.18Mstd and 505kstd with sulfonation degrees between those extremes, have intermediate contributions from a slow relaxation mode. Sample 2.2Mstd is anomalous in this respect, with the largest contribution from a slow mode (25%) in spite of a sulfonation degree above 90% according to elemental analysis. This could be rationalized by considering the unusually high $T_{onset}$ (~408°C), which may signal increased sulfone linkages in this sample, and hence lower solubility and increasing aggregation, which results in increased contribution from a slow mode in this sample. The $R_g/R_h$ ratios for the linear samples are close to the ratio of 2.13 calculated for a polydisperse linear polymer with significant excluded volume, with the exception of sample 505kstd.

*Branching Parameter $g$*

As a simple parameter to describe the branching in polymers, the following ratio is defined for molecules of the same molecular weight and composition:

$$g = \frac{\langle S^2 \rangle_{branched}}{\langle S^2 \rangle_{linear}} \tag{22}$$

where $g$ is known as the branching factor, $\langle S^2 \rangle_{branched}$ is the mean squared radius of gyration of the branched polymer, and $\langle S^2 \rangle_{linear}$ is the mean squared radius of gyration of the analogous linear polymer.[17] The dependence of $g$ on several molecular parameters has been calculated for a number of different molecular architectures, including star-branched polymers with arms of equal length. According to Zimm and Stockmayer, the relationship between $g$ and $f$ can be described by

$$g = (3f - 2)/f^2 \quad (23)$$

with the assumption that the star arms assume the conformation of Gaussian chains in a theta solvent, though the theoretical values often lie close to experimental ones usually determined in good solvents.[18] The values calculated using this equation are listed in Table 8, along with the experimentally determined values for both the NaPSS stars in the ASEC mobile phase and their corresponding polystyrene precursors in THF. The values of $g_{(pre)}$ are somewhat below the values for $g_{(zimm)}$, as expected for branched samples analyzed in a good solvent, due to the higher expansion parameter for branched versus linear polymers. The $g_{(sulf)}$values are significantly higher than the $g_{(pre)}$values, in many cases close to or even slightly above the theoretical $g_{(zimm)}$values. This seems to provide further proof that the structure of the polymers does not change upon polymer analogous sulfonation, as a significant degree of crosslinking or incomplete sulfonation would change the conformation of the stars in solution, resulting in values that do not follow the same trend as the predicted ones. It is interesting that the theory described by Zimm and Stockmayer describes the behavior of the star NaPSS rather well, considering all of the complications that could be caused by electrostatic interactions in these polyelectrolytes. It seems that under the experimental conditions, these interactions are effectively screened, leading to nearly ideal behavior. Muthukumar predicted that the $g$ values obtained for unperturbed polyelectrolyte stars would match those obtained for neutral stars It is interesting to compare $g_{(sulf)}$ measured for samples 42, 54 and 64, for which $g_{(zimm)}$ is nearly the same. The values for 54 and 64 are nearly identical and close to $g_{(zimm)}$, whereas the value for 42 is significantly lower. This can be attributed to the relatively short arms of 42, which adopt a rod like conformation on the length scale of the

arm. In other words, the small contour length of the arms of this polymer does not contain the minimum number of statistical segment lengths required for Gaussian behavior, and hence the predictions of Zimm-Stockmayer would not be applicable in this case. According to Huber, the $g_{(theo)}$ calculated for rodlike arms similar to those in 42 is lower than those calculated for Gaussian arms by nearly an order of magnitude.[19]

## *Summary and Conclusions*

A series of star-branched polystyrenes were synthesized with arms of varying length and $f$ using anionic polymerization. Characterization of their solution properties using SEC-TALS verified that the stars were relatively monodisperse and that the synthesis was successful in producing the desired star architecture. Analysis of the $R_g/R_h$ ratio confirmed the branched structure of the polymers.

Following sulfonation of the precursor polymers, extensive characterization of the sulfonation degree was performed. A sulfonation degree above 90% was confirmed for all star-branched NaPSS samples by the methods of NMR, titration, and elemental analysis, with most samples showing near quantitative sulfonation. Linear NaPSS was also examined for comparison. TGA measurements were qualitatively correlated to some properties of the bulk sample, including confirmation of the presence of low molecular weight salt and determination of the weight percent of water.

ASEC-MALLS was used to characterize the solution properties of both the linear and star-branched NaPSS samples, allowing for the determination of the $M_w$, $R_g$, and polydispersity. The elution profiles of a star-branched NaPSS, a radically polymerized NaPSS, and a commercial NaPSS standard were compared and revealed information about ASEC separation efficiency, crosslinking, and molecular architecture of the

samples. Scaling relationships between $R_g$ and $M_w$ were established for both branched and linear species. DLS measurements indicated a correlation between sulfonation degree and the presence of a slow mode, and the $R_g/R_h$ ratio confirmed the branched structure of the NaPSS stars and the relatively extended conformation of the linear NaPSS samples.

Finally, a comparison between the $g$ parameters determined experimentally for the star- branched NaPSS and the polystyrene precursors and the values calculated from a theoretical model provide further verification of type and extent of branching in the samples and indicate that the star-branched structure of the polymers is retained after polymer analogous sulfonation.

# *Appendix*

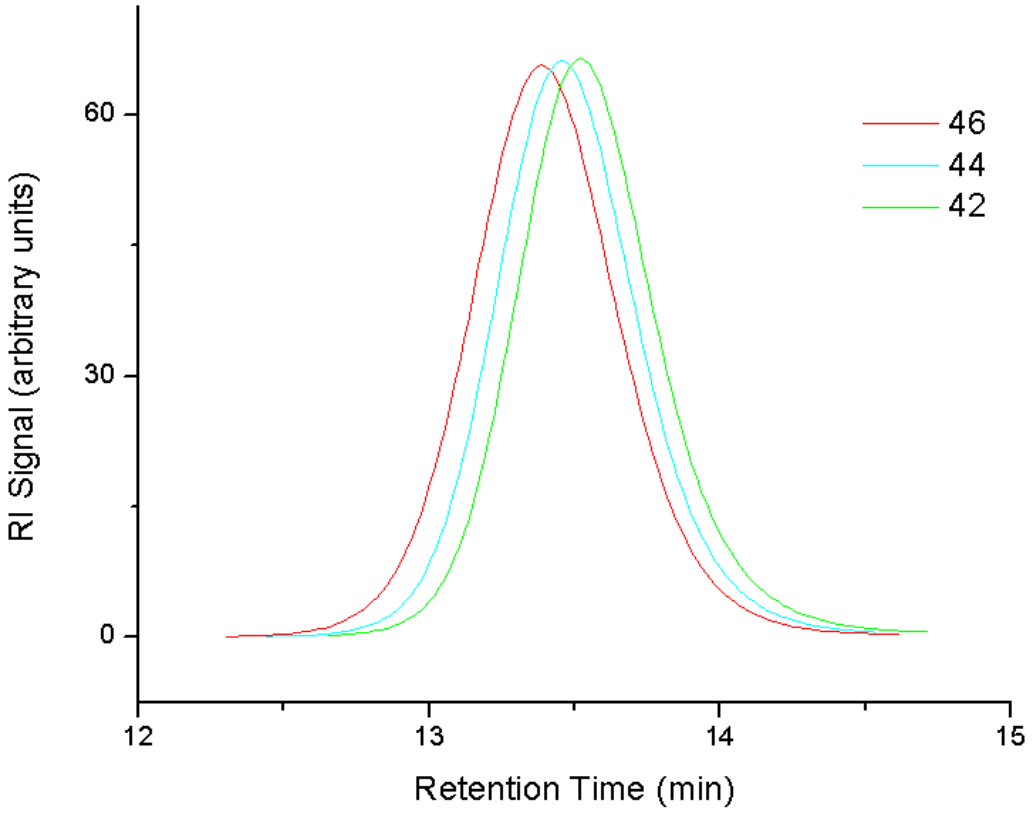



**Figure 10: SEC elugrams of 40 star series in THF, showing the decrease in Retention Time with an increase in both molecular weight and *f*.**

**Table 1: Molecular Characteristics of Star Polystyrenes**

| Sample | $M_w$ ($\times 10^{-6}$ g mol$^{-1}$) | $M_{w,arm}$ ($\times 10^{-4}$ g mol$^{-1}$) | $f$ [a] | % DVB | $M_w/M_n$ | DVB/Li |
|---|---|---|---|---|---|---|
| 42p | 0.128 | 1.15 | 10.9 | 1.9 | 1.10 | 2 |
| 44p | 0.154 | 1.15 | 12.9 | 3.8 | 1.10 | 4 |
| 46p | 0.192 | 1.15 | 15.8 | 5.6 | 1.11 | 6 |
| 52p | 0.479 | 6.93 | 6.9 | 0.34 | 1.14 | 2 |
| 54p | 0.691 | 6.93 | 10.0 | 0.67 | 1.13 | 4 |
| 56p | 0.745 | 6.93 | 10.8 | 1.0 | 1.14 | 6 |
| 62p | 0.964 | 11.5 | 8.4 | 0.21 | 1.15 | 2 |
| 64p | 1.190 | 11.5 | 10.3 | 0.42 | 1.13 | 4 |
| 66p | 1.385 | 11.5 | 12.0 | 0.62 | 1.12 | 6 |

[a] Determined as $f = M_w\,(100-(\%DVB)/100)/M_{w,arm}$.

## Table 2: Radii of Star Polystyrenes

| Sample | $R_{gz}$ (nm) | $R_h$ (nm) | $R_g / R_h$ |
|---|---|---|---|
| 42p | - | 9.0 | - |
| 44p | - | 9.5 | - |
| 46p | - | 10.0 | - |
| 52p | 16.7 | 19.7 | 0.85 |
| 54p | 17.7 | 21.5 | 0.82 |
| 56p | 17.7 | 22.4 | 0.79 |
| 62p | 24.2 | 27.9 | 0.87 |
| 64p | 25.1 | 28.7 | 0.88 |
| 66p | 25.9 | 30.4 | 0.85 |

[a] values at limit of light scattering detection.

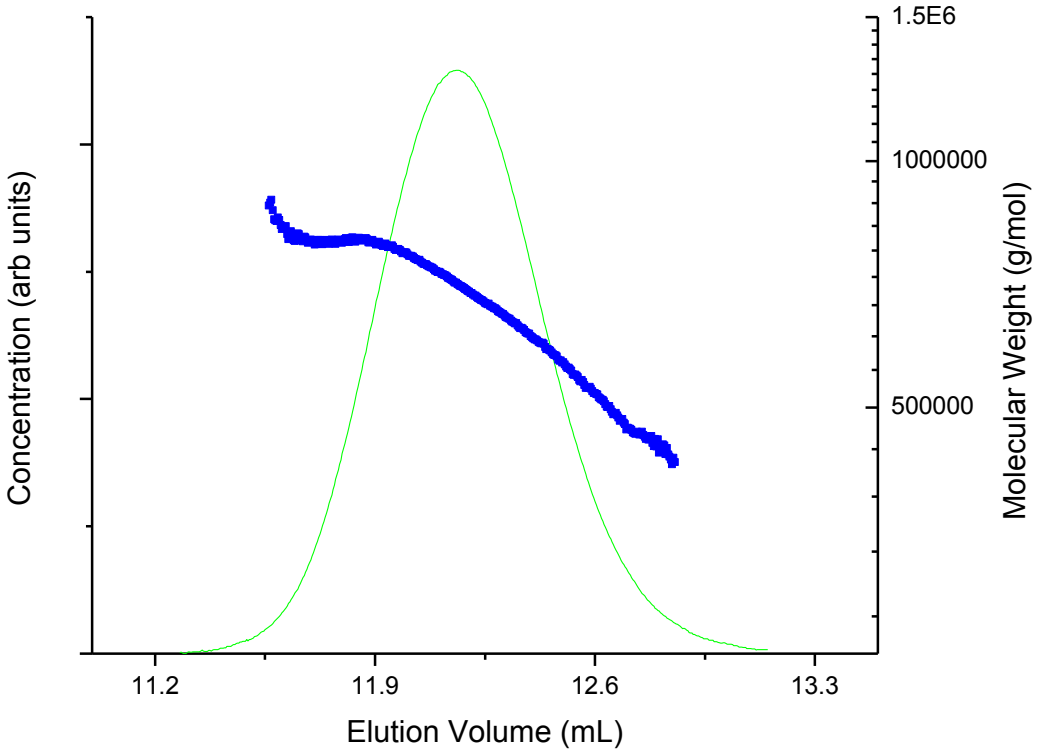



**Figure 11: Elution Profile of 54p, showing an efficient separation of the portions of the sample on the basis of molecular weight.**

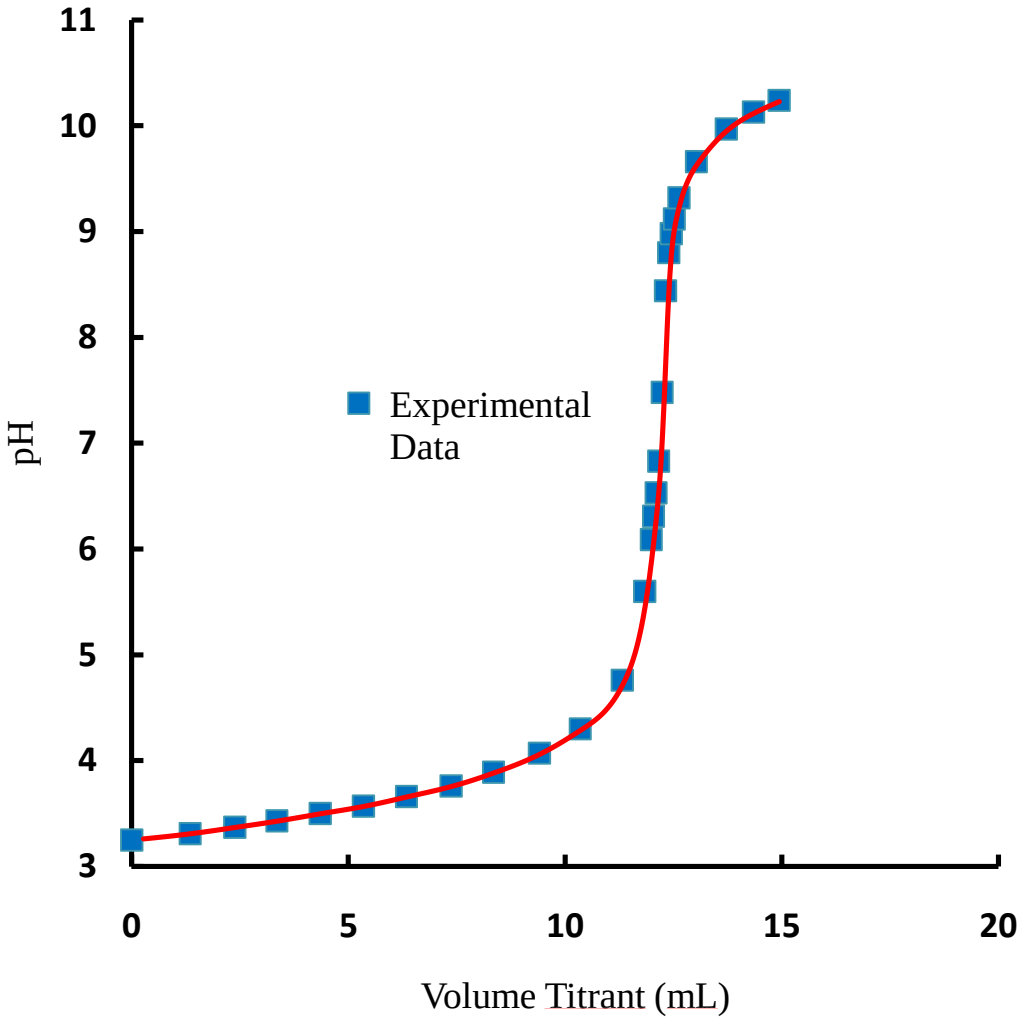



**Figure 12: Titration of 54s, showing a sharp transition expected for titration of a strong acid by a strong base.**

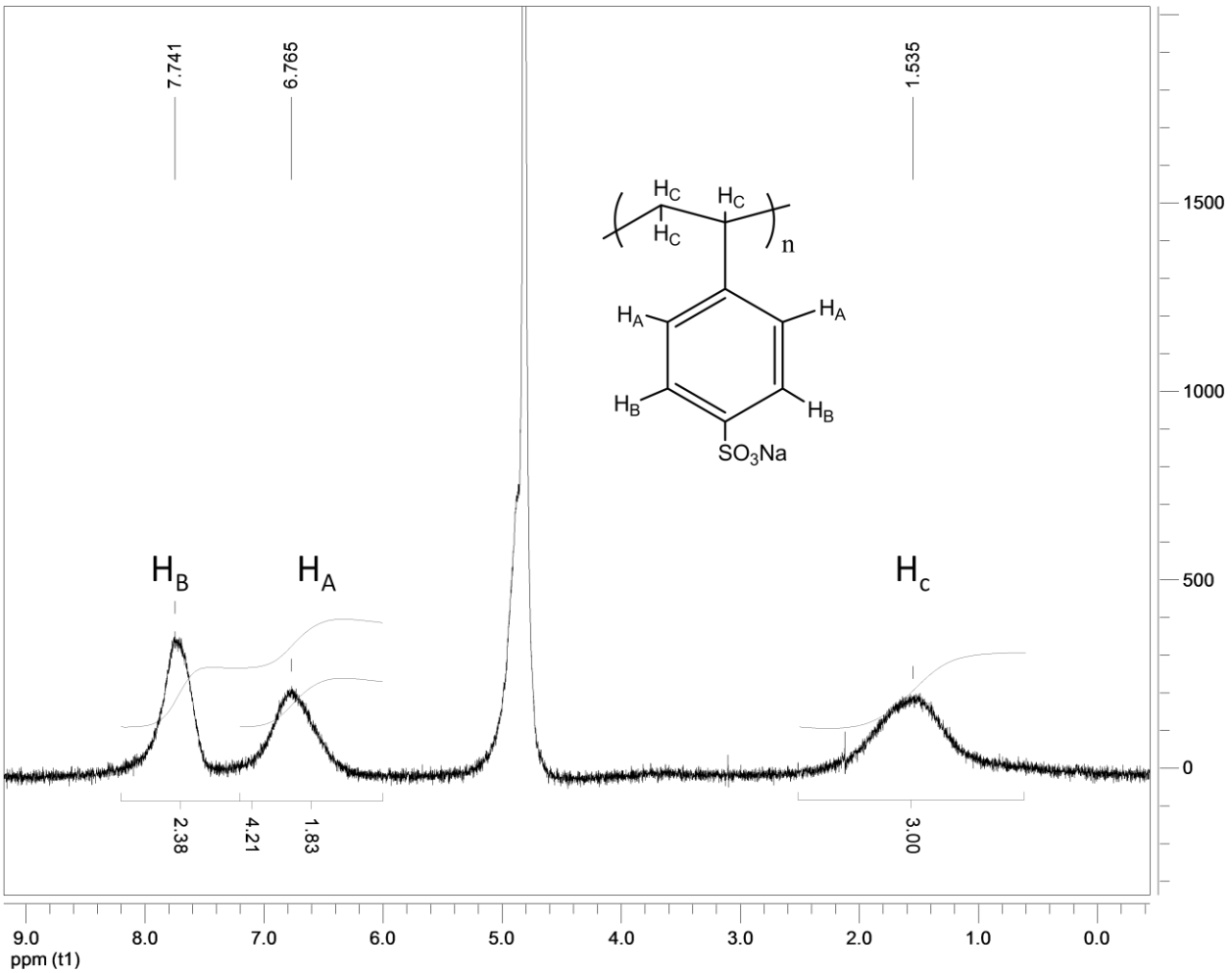



**Figure 13: $^{1}$H NMR of 54s in $D_2O$, showing peak assignments and integrations relative to the 3 $H_c$ protons on the polymer backbone.**

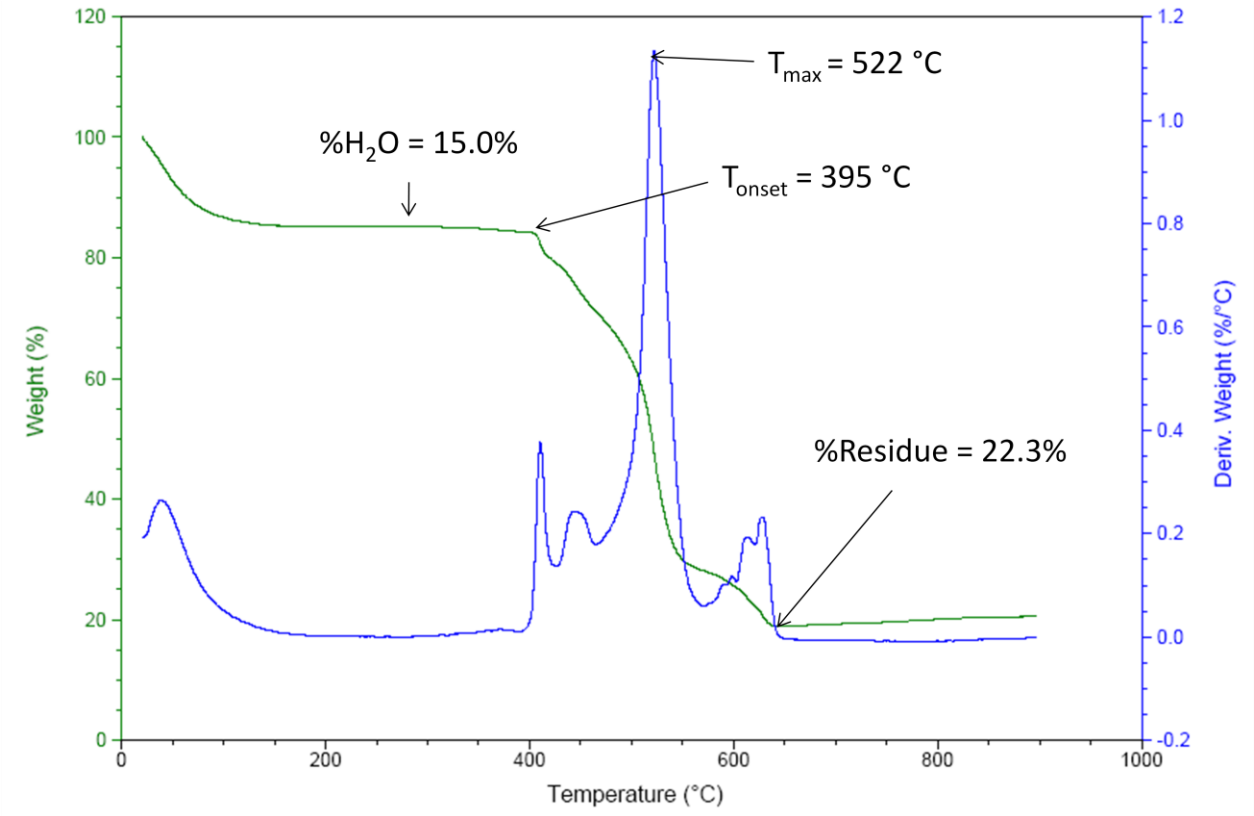



**Figure 14: Thermogravimetric Analysis of 54s, displaying the parameters discussed in the text.**

**Table 3: Characterization of Sulfonation Degree for Star-branched and Linear NaPSS**

| Sample | Elemental Analysis | | NMR | Titration |
|---|---|---|---|---|
| | S/C | Na/C | | |
| 42s | 103 | 98 | 95 | 92 |
| 44s | 103 | 103 | 94 | 90 |
| 46s | 103 | 102 | 100 | 90 |
| 52s | 105 | 98 | 100 | 97 |
| 54s | 111 | 98 | 100 | 97 |
| 56s | 110 | 103 | 100 | 95 |
| 62s | 103 | 103 | 100 | 95 |
| 64s | 107 | 103 | 96 | 97 |
| 66s | 103 | 107 | 97 | 99 |
| NaPSSrad | - | - | 97 | 100 |
| 1.18M std | 96[a] | - | 96 | 224[b] |
| 505k std | 94[a] | - | 100 | 146[b] |
| 2.69M std | 85[a] | - | 100 | 154[b] |
| 2.26M std | >90[a] | - | 100 | 105[b] |
| 57.5k std | 92[a] | - | - | 129[b] |

[a] % of theoretical sulfur content, from company literature. [b] samples not dialized prior to titration.

**Table 4: TGA Results for Star-branched and Linear NaPSS**

| Sample | $EA_{S/Na}$ | Titration (% Sulf) | $T_{onset}$ (°C) | $T_{max}$ (°C) | % $H_2O$[b] | % Residue[c] |
|---|---|---|---|---|---|---|
| 42s | 1.05 | 92 | 398 | 513 | 13.8 | 31.3 |
| 44s | 1.00 | 90 | 380 | 517 | 12.2 | 36.9 |
| 46s | 1.01 | 90 | 374 | 627 | 14.5 | 30.1 |
| 52s | 1.07 | 97 | 393 | 519 | 13.5 | 27.8 |
| 54s | 112 | 97 | 395 | 522 | 14.9 | 22.3 |
| 56s | 1.07 | 95 | 388 | 521 | 13.1 | 33.9 |
| 62s | 1.00 | 95 | 386 | 518 | 13.6 | 32.7 |
| 64s | 1.04 | 97 | 391 | 517 | 14.6 | 23.4 |
| 66s | 1.00 | 99 | 384 | 520 | 10.5 | 39.3 |
| NaPSrad1 | - | 100 | 392 | 518 | 7.7 | 32.7 |
| 1.18M std | - | 224[a] | 399 | 527 | 13.6 | 42.4 |
| 505k std | - | 146[a] | 399 | 542 | 12.5 | 51.4 |
| 2.69M std | - | 154[a] | 399 | 534 | 16.0 | 36.3 |
| 2.2M std | - | 105[a] | 408 | 529 | 12.0 | 35.1 |
| 57.5k std | - | 129[a] | 402 | 524 | 14.6 | 39.3 |

[a] undialyzed samples. [b] weight percent at 300°C. [c] weight percent at 650°C.

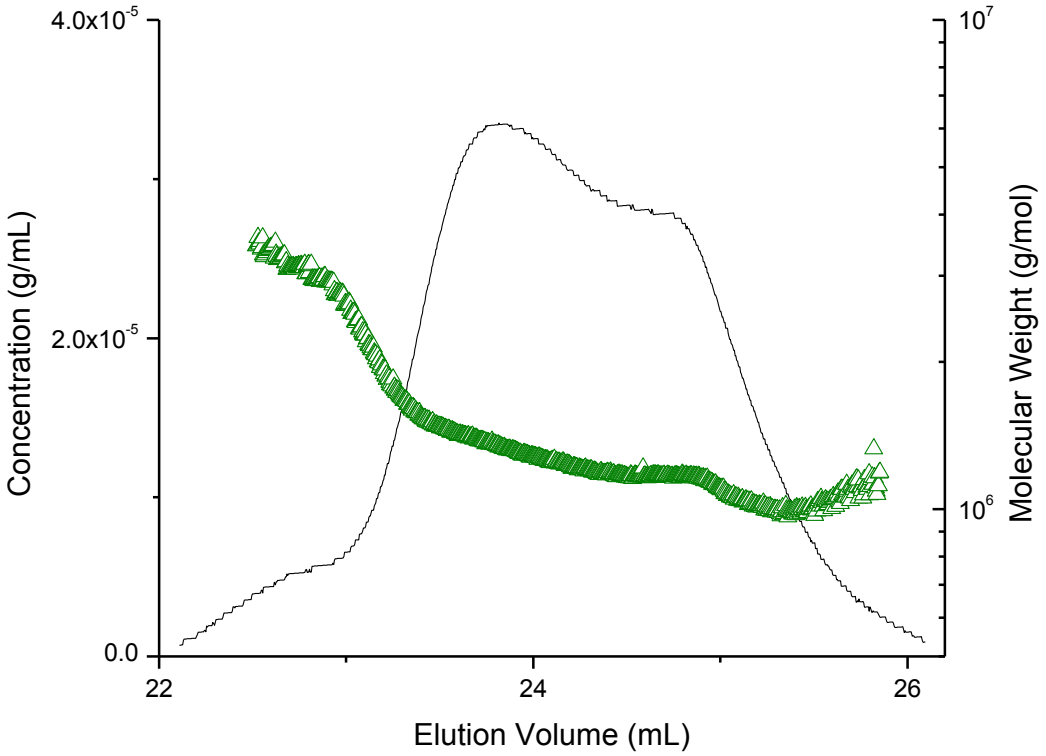



**Figure 15: ASEC-MALLS elugram of 1.18Mstd, displaying a multimodal peak and nonlinear evolution of molecular weight with elution volume.**

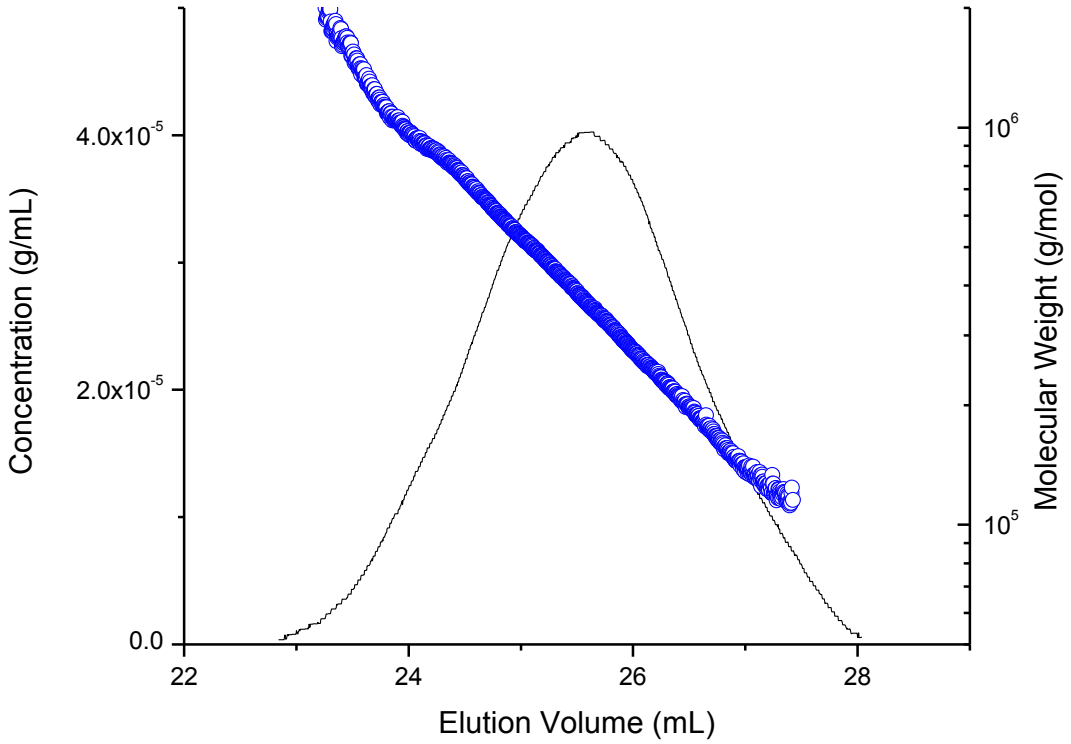



**Figure 16: ASEC-MALLS elugram of NaPSSrad2, showing a linear evolution of molecular weight with elution volume, indicative of homogeneity.**

**Table 5: Aqueous SEC Results for Linear NaPSS**

| Sample | $M_w$ ($x10^{-6}$g/mole) | $M_n$ ($x10^{-6}$g/mole) | $M_w/M_n$ | $R_g$ (nm) | $M_{w(theo)}$[a] ($x10^{-6}$g/mole) | $M_{w,rep}$[a] ($x10^{-6}$g/mole) |
|---|---|---|---|---|---|---|
| 57.5kstd | 0.0460 | 0.0458 | 1.01 | - | 0.058 | 0.058 |
| 505kstd | 0.383 | 0.367 | 1.04 | 28.4 | 0.442 | 0.505 |
| 1.18Mstd | 1.390 | 1.307 | 1.06 | 67.4 | 1.256 | 1.19 |
| 2.2Mstd | 2.339 | 1.909 | 1.23 | 98.6 | 2.376 | 2.26 |
| 2.69Mstd | 1.714 | 1.081 | 1.59 | 87.8 | 2.356 | 2.69 |
| NaPSSrad1 | 0.256 | 0.176 | 1.45 | 30.9 | - | - |
| NaPSSrad2 | 0.455 | 0.314 | 1.45 | 40.6 | - | - |

[a] Values as reported from company literature.

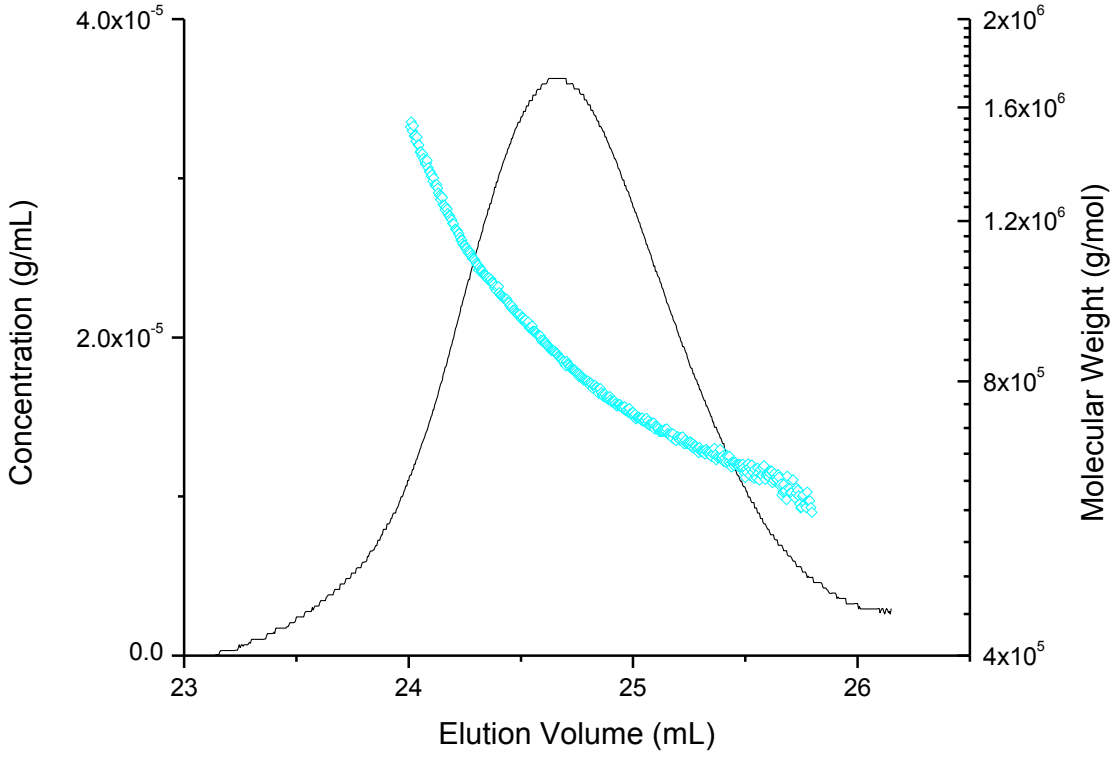



**Figure 17: ASEC-MALLS Elugram of 52s, showing an almost linear evolution of molecular weight with elution volume.**

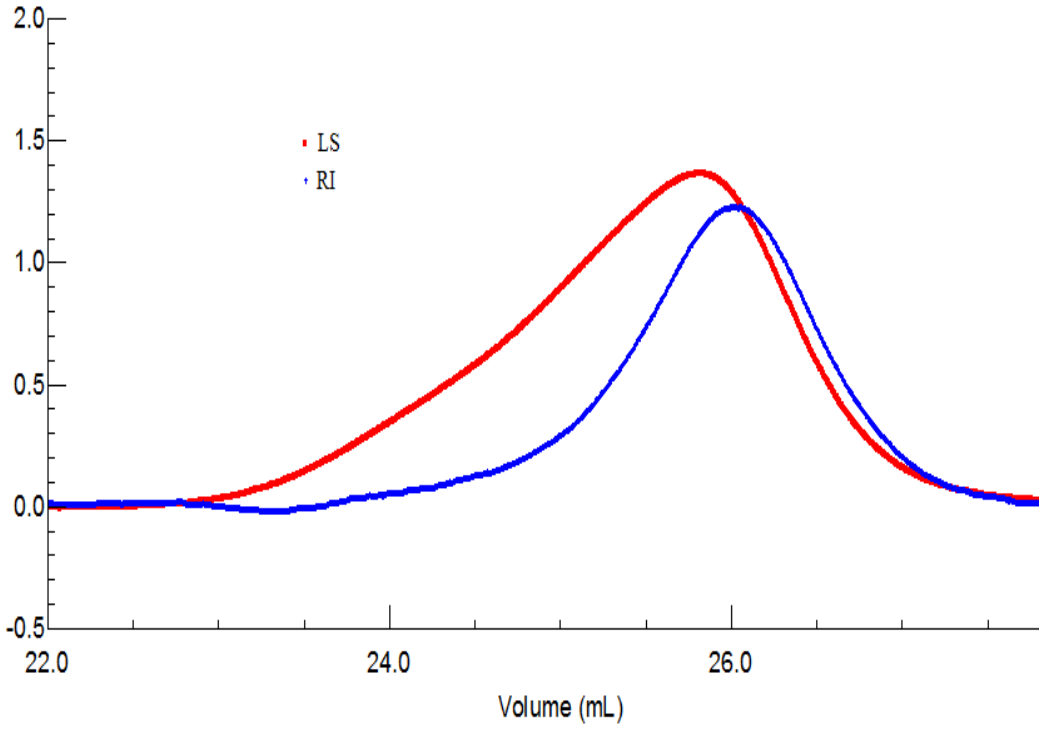



**Figure 18: ASEC-MALLS of 46s, showing 90° light scattering and refractive index signals.**

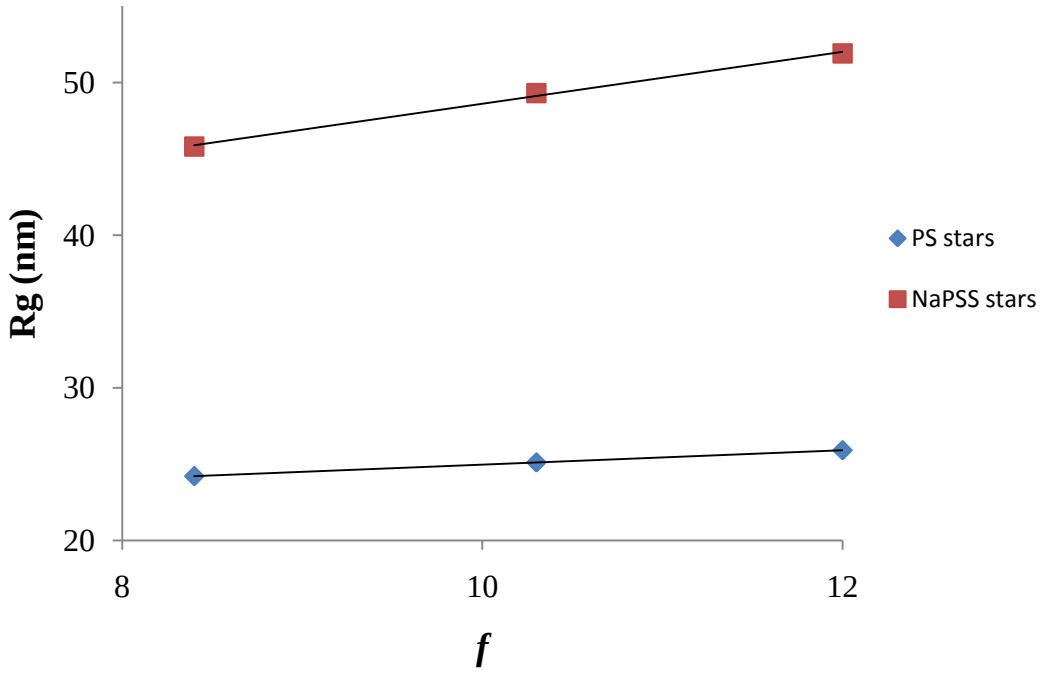



**Figure 19: Comparison of $R_g$ vs. *f* between polystyrene (PS) precursors and NaPSS stars for 6 series of star polymers, showing a slightly larger increase of $R_g$ with *f* for the NaPSS series of stars.**

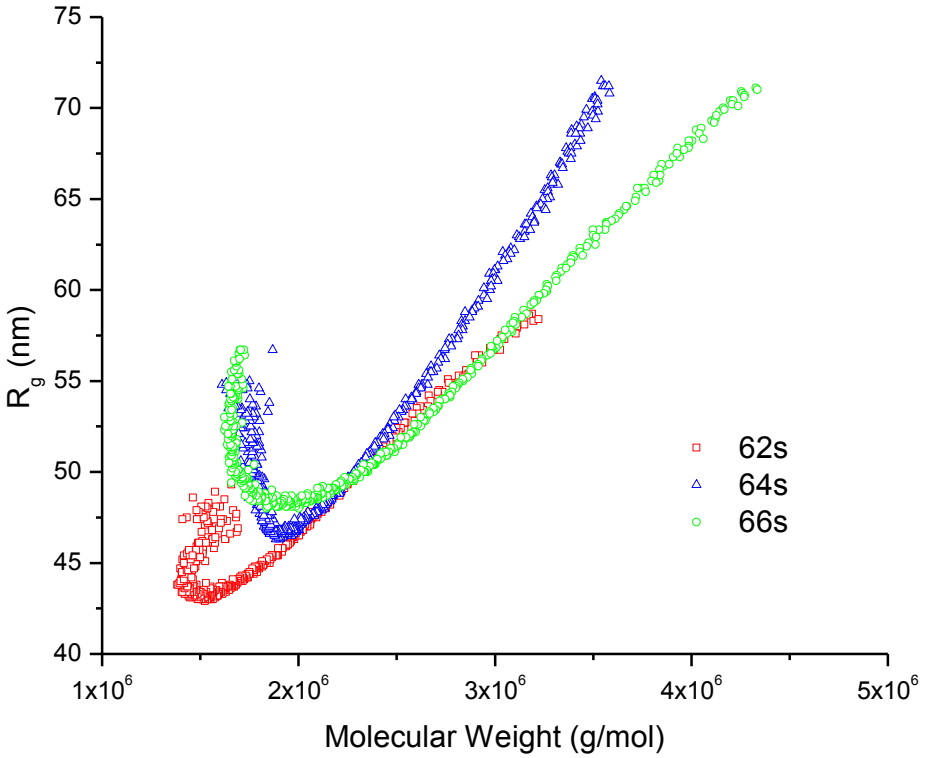



**Figure 20: $R_g$ vs. $M_w$ for the 6 series.**

**Table 6: Aqueous SEC Results for Star-branched NaPSS**

| Sample | $M_n$ ($x10^{-6}$g/mol) | $M_w$ ($x10^{-6}$g/mol) | $M_{w,theo}$[a] ($x10^{-6}$g/mol) | $R_{g,z}$ (nm) | $M_w/M_n$ |
|---|---|---|---|---|---|
| 42s | 0.251 | 0.269 | 0.253 | 9.9 | 1.07 |
| 44s | 0.316 | 0.370 | 0.305 | 14.0 | 1.17 |
| 46s | 0.658 | 0.880 | 0.380 | 21.7 | 1.34 |
| 52s | 0.869 | 0.963 | 0.948 | 31.0 | 1.11 |
| 54s | 1.268 | 1.382 | 1.368 | 34.0 | 1.09 |
| 56s | 1.439 | 1.652 | 1.475 | 35.5 | 1.13 |
| 62s | 1.880 | 2.080 | 1.909 | 45.8 | 1.11 |
| 64s | 2.512 | 2.380 | 2.356 | 49.3 | 1.05 |
| 66s | 2.466 | 2.766 | 2.742 | 51.9 | 1.12 |

[a] $M_{w,theo}$ is reported as 1.98 times $M_w$ of the parent polystyrene material, based on 100% monosulfonation.

**Table 7: Dynamic Light Scattering of Linear and Star-branched NaPSS**

| Sample | $R_{h(app)}$ (nm) | $D(c)_{(app)}$ ($x10^{8}$ cm2/sec) | Variance | % fast mode | Sulfonation Degree | $R_g/R_h$ |
|---|---|---|---|---|---|---|
| 42s | 11.4 | 18.2 | 0.11 | 91 | 92[a] | 0.87 |
| 44s | 14.0 | 15.1 | 0.17 | 91 | 90[a] | 1.00 |
| 46s | 29.7 | 10.0 | 0.54 | 99 | 90[a] | 0.73 |
| 52s | 26.8 | 7.92 | 0.18 | 97 | 97[a] | 1.16 |
| 54s | 34.8 | 6.05 | 0.19 | 99 | 97[a] | 0.98 |
| 56s | 36.2 | 5.94 | 0.22 | 98 | 95[a] | 0.98 |
| 62s | 42.1 | 5.30 | 0.28 | 95 | 95[a] | 1.09 |
| 64s | 48.2 | 4.42 | 0.31 | 98 | 97[a] | 1.02 |
| 66s | 69.3 | 3.82 | 0.52 | 95 | 99[a] | 0.75 |
| 505kstd | 18.7 | 11.1 | 0.10 | 91 | 94[b] | 1.52 |
| 1.18Mstd | 34.0 | 6.28 | 0.20 | 90 | 96[b] | 1.90 |
| 2.2Mstd | 42.8 | 6.36 | 0.50 | 75 | >90[b] | 2.14 |
| 2.69Mstd | 37.8 | 6.80 | 0.49 | 85 | 85[b] | 2.32 |
| NaPSSrad1 | 14.4 | 16.1 | 0.38 | 99 | 100 | 2.14 |

[a] Values from titration. [b] % theoretical sulfur content, from company literature.

## Table 8: g Values for Star-branched NaPSS and Polystyrene Precursors

| Sample | $g_{(sulf)}$ [a] | $g_{(precursor)}$ [b] | $g_{(zimm)}$ [c] |
|---|---|---|---|
| 42 | 0.19 | - | 0.26 |
| 44 | 0.30 | - | 0.22 |
| 46 | 0.56 | - | 0.18 |
| 52 | 0.37 | 0.34 | 0.39 |
| 54 | 0.28 | 0.25 | 0.28 |
| 56 | 0.27 | 0.23 | 0.26 |
| 62 | 0.33 | 0.31 | 0.33 |
| 64 | 0.30 | 0.26 | 0.27 |
| 66 | 0.27 | 0.23 | 0.24 |

[a] calculated from NaPSS samples. [b] calculated from polystyrene precursors. [c] calculated from Zimm-Stockmayer theory.

*References*

(1) Baigl, D.; Ober, R.; Qu, D.; Fery, A.; Williams, C. E. *EPL (Europhysics Letters)* **2003**, 588.

(2) Baigl, D.; Seery, T. A. P.; Williams, C. E. *Macromolecules* **2002**, *35*, 2318-2326.

(3) Foerster, S.; Schmidt, M.; Antonietti, M. *J. Phys. Chem.* **1992**, *96*, 4008-4014.

(4) Hirose, E.; Iwamoto, Y.; Norisuye, T. *Macromolecules* **1999**, *32*, 8629-8634.

(5) Lin, K.; Cheng, H.; Cheng, Y. *Polymer* **2004**, *45*, 2387-2392.

(6) Reed, W. F.; Ghosh, S.; Medjahdi, G.; Francois, J. *Macromolecules* **1991**, *24*, 6189-6198.

(7) Hoffmann, N.; Likos, C. N.; Lowen, H. *The Journal of Chemical Physics* **2004**, *121*, 7009-7021.

(8) Misra, S.; Mattice, W. L.; Napper, D. H. *Macromolecules* **1994**, *27*, 7090-7098.

(9) Shusharina, N. P.; Rubinstein, M. *Macromolecules* **2008**, *41*, 203-217.

(10) Cong, R.; Temyanko, E.; Russo, P. S.; Edwin, N.; Uppu, R. M. *Macromolecules* **2006**, *39*, 731-739.

(11) Mays, J. W. *Polymer Communications* **1990**, *31*, 170-172.

(12) Fernyhough, C. M.; Young, R. N.; Ryan, A. J.; Hutchings, L. R. *Polymer* **2006**, *47*, 3455-3463.

(13) Lienkamp, K.; Noe, L.; Breniaux, M. H.; Lieberwirth, I.; Groehn, F.; Wegner, G. *Macromolecules* **2007**, *40*, 2486-2502.

(14) Akhil, K. S.; Sandip, R.; Juvekar, V. A. *Polymer International* **2007**, *56*, 167-174.

(15) Hsieh, H. L.; Quirk, R. P. *Anionic Polymerization*; Marcel Dekker, Inc.: New York, NY, 1996.

(16) Frater, D. J.; Mays, J. W.; Jackson, C. *Journal of Polymer Science Part B: Polymer Physics* **1997**, *35*, 141-151.

(17) Barth, H. G.; Mays, J. W. *Modern Methods of Polymer Characterization*; John Wiley and Sons: New York, 1991; Vol. 113.

(18) Zimm, B. H.; Stockmayer, W. H. *The Journal of Chemical Physics* **1949**, *17*, 1301-1314.

(19) Huber, K.; Burchard, W. *Macromolecules* **1989**, *22*, 3332-3336.

# Part 4: Static Light Scattering Study of Star-branched NaPSS in Aqueous Solutions of Varying Ionic Strength

## *Abstract*

Static light scattering experiments were performed to elucidate the effect of varying ionic strength on the $R_g$, where it was determined that $R_g \sim C_s^{-0.11}$ for the whole range of samples. The apparent persistence length was determined using the combinatorial wormlike star theory, and relations were established for its variation as a function of $C_s$, *f* and degree of arm polymerization. Additionally, no agreement was found between theoretical predictions of *g* and experimentally determined ones. No slow diffusive mode was observed for very dilute solutions of the samples in solutions with $C_s$. A novel method was developed that enabled the determination of molecular dimensions of star-branched NaPSS using AFM with a high degree of agreement with the radii established using scattering methods on solutions of the polyelectrolytes. The method was found to be applicable over a wide range of $C_s$.

## *Introduction*

Much of the rationale for examining the solution properties of branched polyelectrolytes in aqueous solutions of varying ionic strength was presented in the Introduction, along with descriptions of much of the available literature related to the subject. However, a number of publications in which the solution properties of branched polyelectrolytes, such as the apparent persistence length ($l_{app}$) and the branching ratio *g* were determined from scattering measurements will be reviewed in detail here. The term $l_{app}$ is an apparent value because it is determined by substituting the perturbed, or good solvent values, for the unperturbed, or theta solvent values, of the mean-square radius of gyration in the wormlike chain model.

In a recent publication, Moinard and collaborators examined the solution properties of four- and six-arm sodium, cesium, and rubidium polyacrylate star systems in comparison to their linear analogues.[1] The authors established that the $l_{app}$ of the star systems was slightly higher than that of comparable linear polymers and also increased with *f*, which they attributed to comparably fewer degrees of freedom for the arms of the star as compared to linear chains. The authors also examined the viscosity of the star solutions and established that the *g*' of star polymer solutions at high $C_s$ (0.5M NaCl) could be described by predictions established by Zimm-Kilb and Fixman-Stockmayer for neutral star systems. To the author's knowledge this is the only publication comparing the solution properties of polyelectrolyte stars to linear analogues, other than the work by Mays mentioned in Part 3.

Recently, two works examining the scattering characterization of branched NaPSS with a comb-like architecture have been published. The first is a study by Kanemaru and coworkers in which a series of NaPSS "macromonomers" consisting of a backbone with short side chains (DP=15) were characterized.[2] They determined the Kuhn segment length through fitting of the parameters of the cylindrical wormlike chain model to the $R_g$ and $M_w$ and intrinsic viscosity ($[\eta]$) data obtained from static light scattering (SLS), small-angle X-ray scattering, and viscometry. The authors established that the estimated Kuhn length, which is double the $l_{app}$, was much larger in the case of the NaPSS (120 nm) than the value determined for the polystyrene precursor (16 nm), which was attributed to a high degree of electrostatic repulsion significantly stiffening the main chain of the polymer. The second work concerns a small angle neutron, SLS and small angle X-ray scattering study of comb-branched NaPSS with much longer side

chains (DP ~ 300 or 670) reported by Papagiannopoulos and coworkers.[3] In this study, the authors fit a modified cylindrical form factor to the scattering data of the polyelectrolytes in both 1M CsCl and pure water, and found that the combs adopted an extended cylindrical conformation in dilute solution. Interestingly, a fitting parameter directly related to the persistence length was found to be slightly larger in 1M CsCl than in pure water, an effect the authors state may be attributed to increasing excluded volume effects as the backbone of the comb polymer contracts in higher ionic strength solutions.

In addition to the works examined above, a study by Li and Reed of proteoglycan monomers, which are branched biological polyelectrolytes, is of particular interest for the purposes of the current chapter.[4] The authors performed light scattering measurements on proteoglycan over a large range of ion strengths and polymer concentrations, establishing that the $l_{app}$ varies approximately as the -0.50 power of ionic strength and observing the appearance of a bimodal distribution of relaxation times in DLS at low ionic strength that could be removed by filtering.

In contrast to the dearth of publications dealing with the experimental aspects of aqueous solutions of well-defined branched polyelectrolytes, there are a large number of publications focusing on the theoretical aspects of this system.[5-9] The most recent and thorough among these is the publication by Shusharina and Rubinstein that was described in some detail in the Introduction. For the sake of clarity, the scaling relationships described in that publication will be presented in the relevant sections of the following text.

As both the reviews of experimental works on well-defined branched polyelectrolytes and the large number of publications dealing with the theoretical aspects

make clear, a detailed examination of the scattering of well-defined star-branched NaPSS in dilute aqueous solutions is novel and relevant. To this end, the star-branched NaPSS characterized extensively in Part 3 will be examined by SLS, DLS, and AFM in dilute aqueous solutions of 0.01M, 0.1M, and 1M NaCl in this chapter. These experiments will allow for the determination of $M_w$, $R_g$, $A_2$, and $R_h$, as well as $l_{app}$ and $g$ for the polymers in each solvent, and allow for an examination of the changes in these parameters with regard to $C_s$.

## *Experimental*

### *Materials*

The materials characterized in this section are the same materials examined in detail in the previous section. The solutions used in all experiments were prepared by dissolving the dried sample in stock solutions of 0.01M, 0.1M, and 1M NaCl. The NaCl used to prepare the solutions was Fischer Scientific NaCl (99.8% purity) that was extensively dried by heating in a vacuum oven at 100 °C for ~2 days. The water used for the stock solutions was obtained from a Barnstead Nanopure system.

### *Static Light Scattering*

Details of both the closed loop filtration setup used for static light scattering and the SLS experimental procedure were described previously in Chapter 2. For analysis of the scattering function obtained, a Berry plot was used to extrapolate to infinite dilution and zero angle, as described previously in Part 2. Linear fits of the angular data plotted in this manner were very good, with the Wyatt ASTRA software estimating less than 2 nm variance for the determination of $R_g$ for all of the samples examined. To determine $(dn/dc)_\mu$ at 690 nm the procedure described in Part 2 was used on a selection of samples

in each solvent used, utilizing a Wyatt Optilab interferometric refractometer. Within the error inherent in the procedure, no variation was observed between samples in each solvent. An average value of 0.221 mL/g, 0.202 mL/g, and 0.196 mL/g was determined for the 0.01M, 0.1M, and 1M NaCl solutions respectively.

*Dynamic Light Scattering*

The instrument used for dynamic light scattering of the aqueous solutions was a Precision Detectors PD Expert Multiangle Light Scattering Platform. All measurements were performed at 95°. For determining the $R_h$ of the solutions used for light scattering, the sample from SLS was conserved in a screw-top plastic vial and the dilute solutions were analyzed with no extrapolation to infinite dilution. In all other DLS experiments, the concentration of the solutions is specified. CONTIN was used for analysis of the obtained correlation functions.

*Atomic Force Microscopy*

A Veeco Nanoscope IIIA was the instrument used for AFM measurements, with silicon nitride tips. Freshly cleaved mica was used as the substrate for all samples. Due to the desire that the method used for sample preparation not disturb the solution conformation of the polyelectrolyte, it was not trivial to establish a method to accomplish this. Thus, sample preparation involved the following steps:

1) A steel sample holder to which a freshly cleaved disk of mica was attached was dipped into a dilute solution of the sample to be analyzed. The length of time allowed for dipping (from 5s to 30s), the $C_p$($10^{-6}$ g/mL-$10^{-5}$ g/mL), and the ionic strength of the solution ( 0.01M, 0.1M, and 1M NaCl) were all variables that affected the amount of adsorbed material on the mica surface.

2) After the required time elapsed, the sample disk was removed from the solution and immediately dried by blowing it with compressed air. In this step, the $C_p$ was an important factor in obtaining well resolved single polyelectrolytes: if the $C_p$ was too high, the viscous solutions often gathered on the surface before drying, causing an inhomogeneous distribution of polyelectrolyte on the surface and disturbing the conformation from solution.
3) At this point the sample is prepared for scanning with the AFM. Due to the hydrophilicity of the adsorbed NaPSS, it was found that the experiment be performed immediately after drying to avoid conformation changes brought about by the subsequent adsorption of water to the surface.

Tapping mode was used for all samples, and a variety of scan sizes and scanning speeds were used to obtain the images shown, and are indicated with each image caption.

## *Results and Discussion*

### *Static Light Scattering-$R_g$, $R_h$, $A_2$*

The scattering intensity data obtained from SLS was interpreted using a Berry plot analysis, a typical example of which is shown in Figure 21. Most plots were fit well by a linear extrapolation of $(Kc/R\theta)^{1/2}$ to infinite dilution and zero angle over the range of angles and concentrations studied, though some samples did show a slight downturn at higher angles. None of the plots exhibited the slight upturn at higher angles predicted for a monodisperse sample of star-branched polymers [10,11], though some samples did show a small downturn, particularly at the lowest Cs (0.01M NaCl). Whether this observation can be attributed to polydispersity or a high degree of chain stiffness cannot be determined unambiguously. The plots of sample 46s showed large downward curvature

in all solvents, $M_w$ that were several times the theoretical value and $A_2$ values that were relatively small or negative, characteristics consistent with the phenomenon of aggregation, as shown recently by Lienkamp et al. on a similar system.[12] A similar scattering profile and resulting molecular characteristics are exhibited to a lesser extent by sample 44s. As previous aqueous SEC characterization indicated that these samples are most likely significantly crosslinked or show a remarkable tendency to aggregate, the data obtained from these samples is left out of the following discussion, which focuses on the solution properties of single molecules.

Tables 9, 10, and 11 list the results from SLS of all of the star-branched NaPSS samples and an additional linear NaPSS sample (denoted 2.69Mstd in the table) in the 1M, 0.1M, and 0.01M NaCl solvents, respectively. The values of $M_w$ determined experimentally are within 15% of the $M_{w,theo}$ for all polymers in all solvents, with the exception of the polymers listed in the previous paragraph. These values match closely with the values previously determined using aqueous SEC, even for samples 46s and 44s, which are suspected to aggregate.

The, $R_{g\,z}$ values are observed to increase within each series of stars as *f* increases and to decrease steadily with an increase of $C_s$. A different response was observed for the star-branched and linear NaPSS. The star polymers decreased on average as 75% and 60% of the $R_g$ in 0.01M NaCl for the 0.1M NaCl and 1M NaCl solvents, respectively. By contrast, the linear NaPSS sample (2.69Mstd), decreased to 67% and 54% of the $R_{g,z}$ measured at 0.01M NaCl. The average power law dependence of $R_{g,z}$ on $C_s$ is $R_{g,z} \sim C_s^{-0.11}$. This is closer to the $R_g \sim C_s^{-0.15}$ relationship measured by many others for linear NaPSS than to the dependence predicted by Shusharina and Rubinstein and observed by

Muller for this regime ($R_{g,z} \sim C_s^{-0.2}$)[9,13]. The 2.69Mstd linear NaPSS sample measured here displayed a $C_s^{-0.13}$ dependence, which matches fairly well with the relationship established in the literature. Sample 42s shows a very limited sensitivity to $C_s$, with the $R_{g,z}$ at 1M NaCl being ~ 78% of the size at 0.01M NaCl, a finding consistent with the small arm length and relatively large *f* associated with this sample leading to an open structure with highly stretched arms.

The $R_h$ values obtained from DLS of the same solutions used for SLS are also displayed in Tables 9, 10 and 11. For the star polyelectrolytes, they display the same tendencies as the $R_g$ values, decreasing with increasing $C_s$ and increasing with *f*. The values of the $R_g/R_h$ ratio show only slight variation for the polyelectrolyte stars 52s-66s, ranging from 1.02-1.13 and displaying no discernible trends with regard to changes in *f* or $C_s$. The $R_g/R_h$ values obtained for sample 42s show little variation upon changing $C_s$, ranging only from 1.38 to 1.45 upon changing $C_s$ from 0.01M NaCl to 1M NaCl. The $R_g/R_h$ ratio values obtained for these branched polyelectrolytes are reasonable, coming between the values of 0.775 theoretically predicted for hard spheres and 1.25-1.45 predicted and observed for Gaussian chains in good solvents. The higher value obtained for 42s may reflect the relatively open conformation of this star due to highly stretched arms. In contrast to the behavior observed for the star polyelectrolytes, the $R_h$ measured for the linear 2.69Mstd NaPSS sample does not vary greatly with $C_s$, increasing only about 10% from 1M NaCl to 0.01M NaCl. The corresponding $R_g/R_h$ ratio varies from 1.51 to 2.54, indicating an extended coil conformation even in the 1M NaCl solution, ranging to rodlike ($R_g/R_h > 2$) at 0.01M NaCl. This gradual extension of the chain is commonly observed with NaPSS as the $C_s$ is lowered, and is attributed to decreased

screening of anionic charges on the polymer backbone, resulting in electrostatic repulsion that drives the extension of the chain, The vastly different behavior of the linear NaPSS and star-branched samples demonstrates that these samples are branched.

Values of the second virial coefficient ($A_2$) are listed in Tables 9, 10, and 11. Qualitatively, it is observed that $A_2$ decreases with both increasing $C_s$ and *f* as previously observed with linear analogues and predicted by theory, respectively. Experimentally, it has been shown using linear NaPSS that $A_2$ decreases gradually as $C_s$ increases, with the theta solvent ($A_2 = 0$) being 4.17M NaCl.[14] The 2.69Mstd linear NaPSS sample has higher $A_2$ values than the similar molecular weight, branched 64s in all solvents, a trend that has been previously observed in both polyelectrolytes and neutral polymers.[1,6,15] The inverse relation between $A_2$ and *f* is related to the increasing segment density of the polymer as *f* is increased. Burchard [16] has shown that there is a direct relation between $A_2$ and the interpenetration function. This function has an inverse relation with *f* (in other words, more branched stars interpenetrate less than less branched stars) and therefore $A_2$ is observed and predicted to decrease as *f* increases. Likewise, as $A_2$ represents the pairwise interaction between two particles, $A_2$ is expected to decrease as electrostatic interactions between polyelectrolytes are progressively screened has been observed to do so many times.

***Persistence Length***

While much of the current literature on linear NaPSS utilizes the wormlike chain model for analysis of the SLS data to determine average persistence lengths of linear polyelectrolytes at different $C_s$ in aqueous solutions, there has been no model created for the analysis of star-branched polyelectrolytes such as the ones synthesized here.

Considering the success of the wormlike chain model in explaining behavior in the linear case, it seems reasonable to use a theoretical model for the NaPSS star that assumes wormlike behavior for the arms of the star. Such a model, called the combinatorial broken wormlike star model, has been described by Huber and Burchard [17] and modified by Huber [18] to analyze the characteristics of polydisperse dyestuff aggregates in aqueous solutions at various ionic strengths. The equation describing the relationship between $R_g$, the Kuhn length ($l_k$), the contour length of an arm ($L$)and the star functionality ($f$) in the aforementioned model is presented below.

$$R_{g0}^2 = \left[(3f-2)\left(\frac{2L}{3l_k}\right) + 1 - 2f + \frac{l_k}{L} + 2(f-1)\left(1-\exp\left(-\frac{2l_k}{L}\right)\right) - 2\left(\frac{l_k}{2L}\right)^2\left(1-\exp\left(-\frac{2l_k}{L}\right)\right)\right]\left(\frac{{l_k}^2}{4f}\right) \quad (24)$$

This equation was developed for neutral, monodisperse star polymer solutions and hence is obviously not ideal for the current system, but is the best model available to the our knowledge. As outlined in detail in Part 3, the star polyeletrolytes characterized herein are relatively monodisperse ($M_w/M_n < 1.2$) and are extensively characterized in regards to parameters $L$ and $f$. Also, as AFM images described later will demonstrate, these samples possess a star-branched architecture. In light of these observations, and the ability of the combinatorial wormlike star model to fit arm conformations ranging from random coil to rodlike, we propose the use of equation (24) for calculation of the apparent persistence length ($l_{app}= \frac{l_k}{2}$ ) with no modification. Table 12 lists the parameters used in equation (2) to calculate the $l_{app}$ for the samples listed along with the values of $l_{app}$ calculated at each ionic strength, as well as the value obtained from a linear extrapolation to 'infinite ionic

strength' commonly used in the literature [1,19], denoted ($l_{inf}$). In addition, the values of $l_{app}$ calculated for the polystyrene stars, using the $R_{g,z}$ values obtained from SEC in THF, denoted as $l_{ps}$ are listed. Unfortunately, $l_{app,0.01}$ could not be calculated for sample 42s, probably due to its stiff, short arms at this $C_s$ being outside of the applicable range of the theory.

As expected, $l_{app}$ displays an inverse dependence on $C_s$ for all of the samples listed, and also increases with *f* in each series of stars, an effect attributed by Huber to a higher segment density in the center portions of the star with increasing *f*, even in the case of neutral polystyrene stars.[17] For linear NaPSS, it is often assumed [4,19-21] that there are intrinsic ($l_{int}$) and electrostatic ($l_{el}$) components to the $l_{app}$ calculated for polyelectrolytes through use of the Koyama approximation for linear wormlike chains, as in the following equation:

$$l_{app} = l_{\mathrm{int}} + l_{\mathrm{el}} \qquad (25)$$

It has been asserted that $l_{inf}$ should correspond to $l_{int}$, since electrostatic interactions are screened out at infinite ionic strength, and the resulting $l_{app}$ should correspond to that of uncharged polymer in a good solvent.[19,20] Examination of the values of $l_{inf}$ and $l_{ps}$ in Table 12 reveals large differences, though THF can be considered a good solvent for the polystyrene parent polymers. The values determined for $l_{ps}$ are close to those determined by Burchard using the same model for polystyrene 12-arm stars in a θ solvent (2.8-3.4 nm).[17] The values of $l_{inf}$ increase with *f* in each series of stars, perhaps indicating an increasing contribution from excluded volume as the degree of branching increases.

Quantitatively, the variation of $l_{app}$ with $C_s$ was fitted with the following equation:

$$l_{\text{app}} = l_{inf} + bC_s^{-\gamma} \quad (26)$$

where $b$ and $\gamma$ are listed in Table 12. In this equation, $l_{inf}$ and the second term correspond to $l_{int}$ and $l_{el}$ in Equation (25), respectively, by analogy with the work done by Reed on several different polyelectrolyte systems.[4,19,20,22] With the exception of 62s, $b$ increases with $f$ in each series of stars. More notable is the variation of $\gamma$ in relation to $L$ and $f$. Generally, $\gamma$ increases with $f$ within each series, indicating that the $l_{app}$ of highly branched stars are more sensitive to changes in ionic strength than stars of lower $f$. The samples in the 60 series exhibit a smaller sensitivity to $C_s$ than the samples in the 50 series, probably due to their longer arms retaining the behavior of linear NaPSS. Indeed, for sample 62s, with the lowest $f$ of samples in the 60 series $l_{el} \sim C_s^{-0.46}$, very similar to the $l_{el} \sim C_s^{-0.5}$ relationship established by several researchers for several different linear polyelectrolytes.[20,22-25]

***Branching ratio g***

As described in Part 3, the branching ratio $g$ is often used to describe the branching that is present in a polymer sample. Muthukumar proposed detailed descriptions of how $g$ should vary with $f$ for star-branched polyelectrolytes, finding as the main conclusion that the value of $g$ calculated for star polyelectrolytes with strongly screened electrostatic interaction and no excluded volume effects was the same as that for star polymers in good solvents with no electrostatic interaction present (but accounting for excluded volume).[26] In order to calculate $g$ for the star-branched NaPSS examined here, the $R_g$ of linear NaPSS of the same $M_w$ under the same solvent conditions must be

determined. The following equation describing the wormlike chain is often fitted to experimentally determined $R_g$ to determine the $l_{app}$ of linear NaPSS in the literature:

$$R_g^2 = \left(l_{\text{app}}\right)^2 \left[\frac{\text{b}}{3} - 1 + \frac{2}{\text{b}^2}\left(\text{b} - 1 + \exp^{-\text{b}}\right)\right] \quad (27)$$

where $b = L_t/l_{app}$, with $L_t$ being the total contour length of the linear chain.[19,22,24,27] $R_g^2$ denotes the perturbed squared radius of gyration that is obtained in this case because $l_{app}$ is a perturbed value. For the variation of $l_{app}$ with ionic strength, the following empirical relationship determined by Reed for NaPSS in solutions of widely varying $C_s$ is used:

$$l_{app} = 3.13 + 47.21\text{C}_\text{s}^{-0.5} \quad (28)$$

and the quantities $l_{app}$ and $C_s$ are in units of nm and mmol respectively.[24] Using the result of Equation (28) in Equation (27), the $R_g^2$ of linear NaPSS in the pertinent aqueous solvents can be estimated. To ascertain the accuracy of the resulting calculations, the values calculated using equations 27 and 28 for the linear NaPSS 2.69Mstd sample are compared to the experimental values. The calculated $R_g$ results for the 1, 0.1 and 0.01M NaCl solvents are 65.2, 84.6, and 127 nm respectively, whereas the experimental results for the same solvents are 65.7, 80.9, and 121 nm, respectively. This is a high level of agreement, with the theoretical results within 5% of the experimental results, and as such, the results of equations 26 and 27 were used without further modification. The resulting *g* values are tabulated in Table 13, along with the experimental g for the polystyrene precursors in THF ($g_{ps}$), the values of *g* calculated according to Muthukumar for the limits of strong electrostatic screening ($g_{ss}$), weak electrostatic screening ($g_{ws}$), and excluded volume with no electrostatic interactions ($g_{ev}$). A couple of trends are noted for the experimentally determined data. The first is that the experimentally determined *g* has a direct relationship with $C_s$, indicating that the dimensions of the branched NaPSS

become closer to those of the analogous linear NaPSS as the electrostatic screening increases. Another trend relates to the direct relationship observed between $g$ and $f$, counter to the inverse relationship predicted by theory. Again, sample 42s shows a relative insensitivity to $C_s$, approaching the same dimensions as the linear analogue in both 0.1M and 1M solvents. Sample 52s is also an interesting case, as it comes very close to matching the theoretical values at $g_{0.01}$, perhaps because this is the sample with the lowest $f$, thereby being less influenced by excluded volume effects than the other polymers with higher $f$. It is interesting that $g_{1M}$ does not closely match $g_{ss}$ or $g_{ev}$ though electrostatic interactions must be strongly screened at this ionic strength, and in fact $g_{0.01M}$ at the lowest ionic strength comes closest to matching $g_{ss}$. Clearly, there is significant disagreement between the theoretical calculations and experimental results for the $g$ of star-branched NaPSS, perhaps indicating that both excluded volume and electrostatic interactions play different roles than predicted in the dimensions of star-branched NaPSS.

***Dynamic Light Scattering***

In the star NaPSS solutions examined in this Part, the phenomenon of multimodal relaxation was found to be related to both $C_s$ and $C_p$. The extensively filtered, dilute solutions obtained from SLS displayed no contribution from a slow relaxation mode in the case of the 1M and 0.1M NaCl solvents, and very minimal contributions in the 0.01M NaCl aqueous solutions, with the amplitude of the slow mode reaching less than ~8% of the total amplitude at the maximum. A long standing debate is whether the slow mode can be removed by extensive filtration of polyelectrolyte solutions [4,19,21,24,28]. These results on extensively filtered solutions seem to run counter to that hypothesis, though it

is noted that these solutions were filtered through 0.45 μm pore size filters, whereas those publications where the slow mode was successfully removed were 0.1 μm or smaller.

***Atomic Force Microscopy***

For further verification of properties determined using SLS, the solutions retained from SLS were examined using atomic force microscopy. The method described in detail in the experimental section was used to cast the solutions onto mica. This methodology enabled the casting of solutions over a wide range of $C_s$, as illustrated in Figure 22, where sample 54s is cast from both pure water and 1M NaCl solution. Encouraged by the initial results, we attempted to establish a simple method to estimate the size of the polymers adsorbed onto the mica for comparison to the dimensions measured in solution. The methodology is illustrated in Figure 23, and essentially consists of measuring the diameter of the molecule straight from one edge to the other through core of the molecule, which can be conveniently and easily identified in all cases as a region that is higher off the surface than the rest of the molecule. The measured diameters are then averaged and halved to give an apparent radius, denoted $R_{afm}$ , with the average set of measurements consisting of at least 30 separate molecules. The results are tabulated in Table 14, where it is seen that there is very good agreement between the respective radii, with $R_{afm}$ sometimes falling between $R_h$ and $R_g$, but most often matching up very closely with $R_h$. The standard deviation of the measurements used for calculation of $R_{afm}$ are also listed next to the values determined, and average ~13% of the $R_{afm}$ values. The results indicate that this method of measurement gives reasonable estimates of the molecular radius and is applicable across a wide range of $C_s$ for dilute solutions of star-branched NaPSS.

Though it is certainly counterintuitive that the anionic polyelectrolytes described here would readily adsorb on an anionically charged surface such as mica, there are some predictions that indicate why this may be possible. In simulations on the adsorption of branched homopolymers onto surfaces with varying degrees of attractive interaction, it was found that compact polymers such as stars and dendrimers adsorb more readily to a surface with a weak attractive force than linear polymers of the same material.[29]

An example of the adsorption profile is shown in Figure 24, in which the 54s sample cast from 1M NaCl solution is shown, with a height profile measured for the three molecules shown in the scanning image. As can be seen from part (b) of the figure, there is a consistent size and maximum height for each of the three molecules shown, with a higher central "core" of the molecule surrounded by a region of progressively lower height as distance from the core is increased. The consistency of the measurements of the peak height at the core to the periphery of the molecule is some indication that there is homogeneity with regards to adsorption mechanism and size, at least within a sample.

Using a freeware program developed by Minko called 2D Single Molecules, which has been used to estimate the persistence length and other properties of many different adsorbed polymers using AFM images [30-32], it was possible to determine an estimate of $l_{app}$ for samples 64s and 66s. An example of the measurement is illustrated in Figure 25, which shows the manually drawn lines used to estimate $l_{app}$ using the software. The results are 36 nm for sample 66s and 51 nm for sample 64s, compared to the estimates of 45.4 nm and 35.4 nm from SLS. Though these estimates are taken from relatively small sample sizes (< 30 points), they do give some indication that the $l_{app}$ determined from SLS is reasonable, even if quantitative agreement is obviously lacking.

Due to the high segment density near the core of stars with shorter or less extended arms, this calculation was not possible on the other samples.

## *Summary and Conclusions*

In this Chapter, the solution properties of a diverse set of star-branched NaPSS were examined in aqueous solutions of varying ionic strength using SLS, DLS, and AFM. Contrary to predictions and experimental observations on micelles, the $R_g$ was found to vary with $C_s$ as $R_g \sim C_s^{-0.11}$. The $l_{app}$ of the various star-branched samples was estimated using relationships from the combinatorial wormlike star theory and was determined to vary as $l_{\mathrm{app}} = l_{inf} + bC_s^{-\gamma}$. Parameters $l_{inf}$, $b$, and $\gamma$ were found to vary with $L$ and $f$, with $l_{inf}$ and $\gamma$ approaching the values determine for linear NaPSS as $L$ increases and $f$ decreases. Using a previously established relationship to determine the $R_g$ of linear NaPSS at various molecular weights and $C_s$, the values of the branching parameter $g$ was determined for the star-branched NaPSS samples at each $C_s$. A significant difference was observed between the experimentally determined and theoretically predicted values of $g$, especially those samples with higher $f$. DLS experiments revealed the absence of a slow mode in the dilute solutions used for SLS, with the exception of a small contribution to the total scattered intensity at the lowest ionic strength solution. A method was developed that allowed for the casting of star-branched NaPSS onto mica with retention of solution dimensions. The applicability of this casting method in solutions of widely varying ionic strength was verified by measurement of the approximated radius using AFM and comparison of this measurement to the radii determined using SLS and DLS. This finding points the way to using this method of measurement for solutions at lower ionic strengths, where interpretation of the scattering data is more difficult or impossible.

# *Appendix*

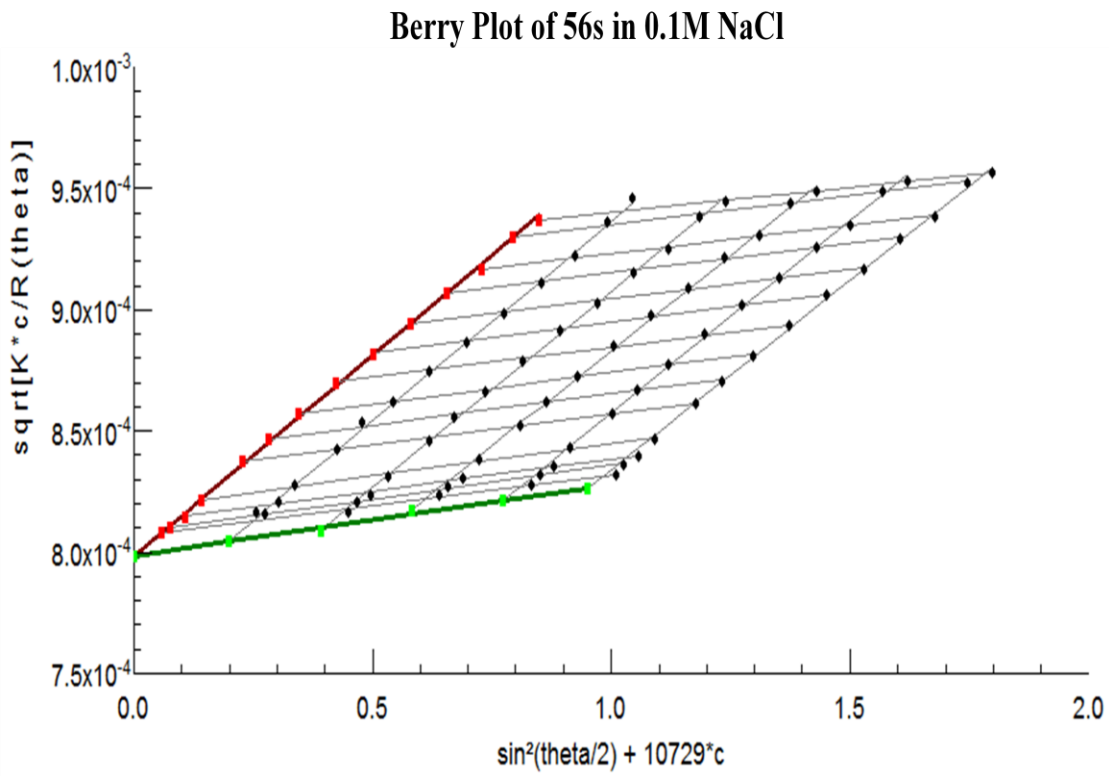



**Figure 21: Berry Plot of 56s in 0.1M NaCl.**

**Table 9: Static Light Scattering of Star-branched NaPSS in Aqueous 1M NaCl**

| Sample | $M_w$ ($\times 10^{-6}$ g mol$^{-1}$) | $M_{w,theo}$ ($\times 10^{-6}$ g mol$^{-1}$) | $R_{g,z}$ (nm) | $R_h$ (nm) | $A_2$ ($\times 10^4$ mol*mL/g) | $R_g/R_h$ |
|---|---|---|---|---|---|---|
| 42s | 0.251 | 0.253 | 19.0 | 13.1 | 2.32 | 1.45 |
| 44s | 0.378 | 0.305 | 24.9 | 18.2 | 1.03 | 1.37 |
| 46s | 0.654 | 0.380 | 26.6 | 19.6 | -4.76 | 1.36 |
| 52s | 0.980 | 0.948 | 29.8 | 27.0 | 1.14 | 1.10 |
| 54s | 1.48 | 1.37 | 33.0 | 29.6 | 1.49 | 1.11 |
| 56s | 1.60 | 1.48 | 35.2 | 33.7 | 0.391 | 1.04 |
| 62s | 1.77 | 1.91 | 42.5 | 40.5 | 0.199 | 1.05 |
| 64s | 2.55 | 2.36 | 49.9 | 48.5 | 0.394 | 1.03 |
| 66s | 3.07 | 2.74 | 57.2 | 54.4 | 0.285 | 1.05 |
| 2.69Mstd | 2.23 | 2.54 | 65.7 | 43.4 | 1.247 | 1.51 |

**Table 10: Static Light Scattering of Star-branched NaPSS in Aqueous 0.1 M NaCl**

| Sample | $M_w$ ($\times 10^{-6}$ g mol$^{-1}$) | $M_{w,theo}$ ($\times 10^{-6}$ g mol$^{-1}$) | $R_{g,z}$ (nm) | $R_h$ (nm) | $A_2$ ($\times 10^4$ mol*mL/g) | $R_g/R_h$ |
|---|---|---|---|---|---|---|
| 42s | 0.267 | 0.253 | 22.7 | 15.7 | 2.91 | 1.45 |
| 44s | 0.438 | 0.305 | 29.6 | 19.9 | 3.38 | 1.49 |
| 46s | 1.16 | 0.380 | 64.5 | 26.6 | 0.853 | 2.42 |
| 52s | 0.871 | 0.948 | 37.4 | 34.1 | 3.70 | 1.10 |
| 54s | 1.43 | 1.37 | 42.8 | 38.9 | 2.03 | 1.10 |
| 56s | 1.57 | 1.48 | 47.1 | 46.3 | 2.32 | 1.02 |
| 62s | 1.78 | 1.91 | 49.8 | 47.4 | 0.357 | 1.05 |
| 64s | 2.52 | 2.36 | 62.3 | 57.1 | 1.33 | 1.09 |
| 66s | 3.07 | 2.74 | 70.9 | 63.1 | 1.32 | 1.12 |
| 2.69Mstd | 2.24 | 2.54 | 80.9 | 48.5 | 2.83 | 1.67 |

**Table 11: Static Light Scattering of Star-branched NaPSS in 0.01 M NaCl**

| Sample | $M_w$ ($\times 10^{-6}$ g mol$^{-1}$) | $M_{w,theo}$ ($\times 10^{-6}$ g mol$^{-1}$) | $R_{g,z}$ (nm) | $R_h$ (nm) | $A_2$ ($\times 10^4$ mol*mL/g) | $R_g/R_h$ |
|---|---|---|---|---|---|---|
| 42s | 0.245 | 0.253 | 24.5 | 17.7 | 11.2 | 1.38 |
| 44s | 0.385 | 0.305 | 40.5 | 21.7 | 4.68 | 1.87 |
| 46s | 1.050 | 0.380 | 70.7 | 27.2 | -0.373 | 2.60 |
| 52s | 0.866 | 0.948 | 48.3 | 44.4 | 14.5 | 1.09 |
| 54s | 1.27 | 1.37 | 55.5 | 47.7 | 9.25 | 1.16 |
| 56s | 1.53 | 1.48 | 61.8 | 57.6 | 8.35 | 1.07 |
| 62s | 1.67 | 1.91 | 72.3 | 64.0 | 5.60 | 1.13 |
| 64s | 2.17 | 2.36 | 80.4 | 71.9 | 5.49 | 1.12 |
| 66s | 2.98 | 2.74 | 91.9 | 84.6 | 3.32 | 1.09 |
| 2.69Mstd | 2.14 | 2.54 | 121.0 | 47.7 | 7.90 | 2.54 |

**Table 12: Combinatorial Wormlike Chain Parameters**

| Sample | $L$ (nm) | $f$ | $l_{app,0.01M}$ (nm) | $l_{app,0.1M}$ (nm) | $l_{app,1M}$ (nm) | $l_{inf}$ (nm) | $l_{ps}$ (nm) | $b$ | $\gamma$ |
|---|---|---|---|---|---|---|---|---|---|
| 42s | 24.1 | 10.9 | - | 27.2 | 18.0 | 13.7 | - | - | - |
| 52s | 145.3 | 6.9 | 21.5 | 12.2 | 7.4 | 6.6 | 2.2 | 0.993 | 0.62 |
| 54s | 145.3 | 10 | 27.9 | 15.8 | 8.9 | 8.0 | 2.4 | 1.15 | 0.66 |
| 56s | 145.3 | 10.8 | 34.7 | 19.4 | 10.2 | 9.1 | 2.4 | 1.32 | 0.69 |
| 62s | 241.1 | 8.4 | 27.7 | 12.2 | 8.7 | 6.1 | 2.7 | 2.47 | 0.46 |
| 64s | 241.1 | 10.3 | 34.4 | 19.6 | 12.1 | 10.6 | 2.9 | 1.63 | 0.61 |
| 66s | 241.1 | 12 | 45.4 | 25.8 | 16.0 | 14.1 | 3.0 | 2.21 | 0.61 |

**Table 13: Experimental and Theoretical $g$ values for NaPSS star polymers in aqueous solvents of varying ionic strength**

| Sample | $g_{0.01M}$ | $g_{0.1M}$ | $g_{1M}$ | $g_{ps}$ | $g_{ss}$ | $g_{ws}$ | $g_{ev}$ |
|---|---|---|---|---|---|---|---|
| 42s | 0.62 | 0.91 | 0.99 | - | 0.29 | 0.31 | 0.29 |
| 52s | 0.43 | 0.56 | 0.59 | 0.34 | 0.42 | 0.42 | 0.42 |
| 54s | 0.38 | 0.50 | 0.50 | 0.25 | 0.31 | 0.32 | 0.31 |
| 56s | 0.43 | 0.56 | 0.52 | 0.23 | 0.29 | 0.31 | 0.29 |
| 62s | 0.45 | 0.48 | 0.59 | 0.31 | 0.36 | 0.37 | 0.36 |
| 64s | 0.45 | 0.61 | 0.66 | 0.26 | 0.30 | 0.32 | 0.30 |
| 66s | 0.50 | 0.67 | 0.74 | 0.23 | 0.27 | 0.29 | 0.27 |

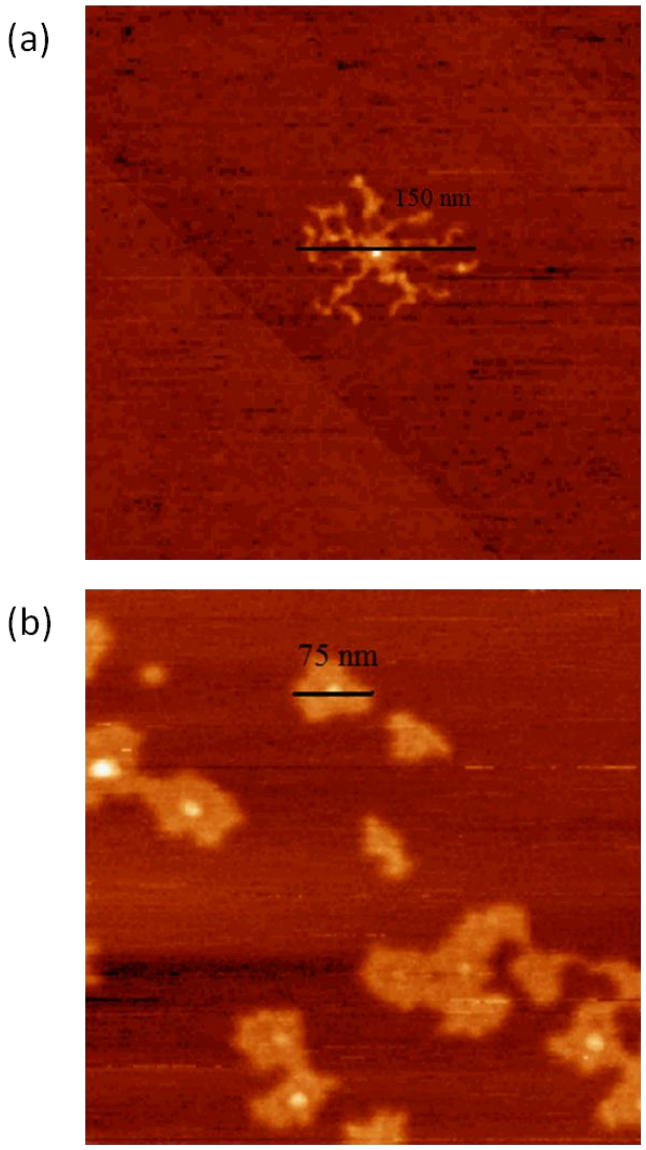



**Figure 22: Sample 54s in (a) water and (b) 1M NaCl aqueous solution, showing change with change in $C_s$.**

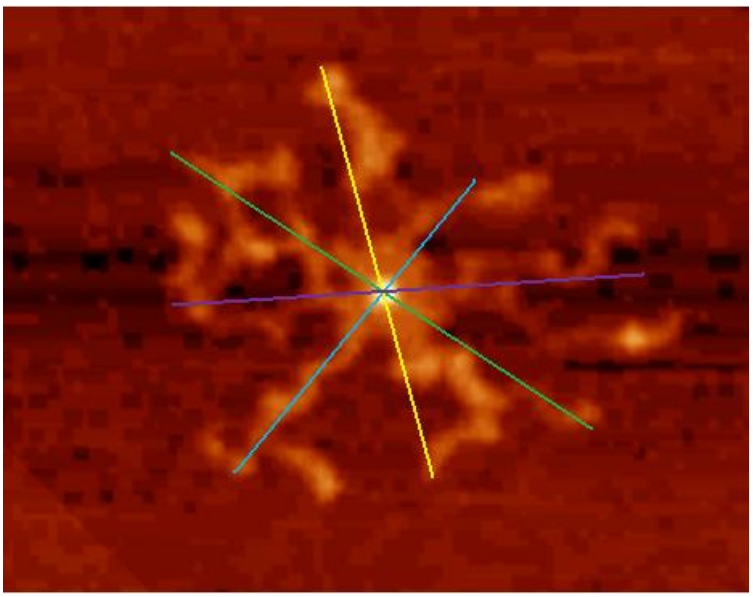


**Figure 23: Sample 54s cast on mica from water. The colored lines illustrate the method of measuring $R_{afm}$ described in detail in the text.**

## Table 14: $R_{afm}$ Averages in Solutions of Varying $C_s$

| Sample[a] | $R_{g,z}$ (nm) | $R_h$ (nm) | $R_{afm}$ (nm) |
|---|---|---|---|
| 42s | 24.5 | 17.7 | 21.3 ± 2.8 |
| 44s | 40.5 | 21.7 | 20.5 ± 3.4 |
| 46s | 70.7 | 27.2 | 22.6 ± 3.5 |
| 52s | 48.3 | 44.4 | 43.8 ± 5.7 |
| 54s | 55.5 | 47.7 | 51.1 ± 10.8 |
| 56s | 61.8 | 57.6 | 52.2 ± 4.1 |
| 62s | 72.3 | 64.0 | 63.4 ± 10.4 |
| 64s | 80.4 | 71.9 | 74.1 ± 6.6 |
| 66s | 91.9 | 84.6 | 82.2 ± 7.8 |
| 52s,0.1 | 37.4 | 34.1 | 31.5 ± 4.5 |
| 62s,0.1 | 49.8 | 47.4 | 48.2 ± 3.1 |
| 54s,1 | 33.0 | 29.6 | 36.3 ± 3.5 |
| 52s,1 | 29.8 | 27.0 | 24.1 ± 5.3 |

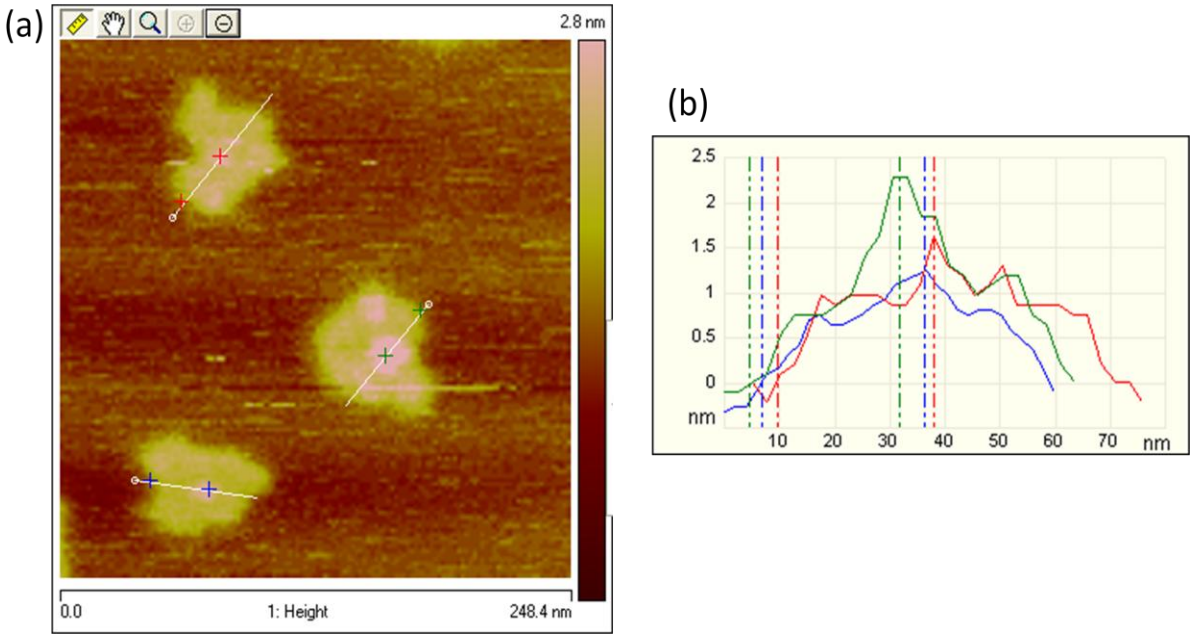



**Figure 24: (a) AFM image of the sample 54s cast on mica from 1M NaCl solution showing the raised core region surrounded by a "sombrero" rim. (b) Graph corresponding to lines and crosshairs, with dotted lines corresponding to position of crosshairs on image. The distances measured between crosshairs placed at periphery and the core are 29 nm, 28 nm, and 26 nm for the blue, red, and green markers respectively.**

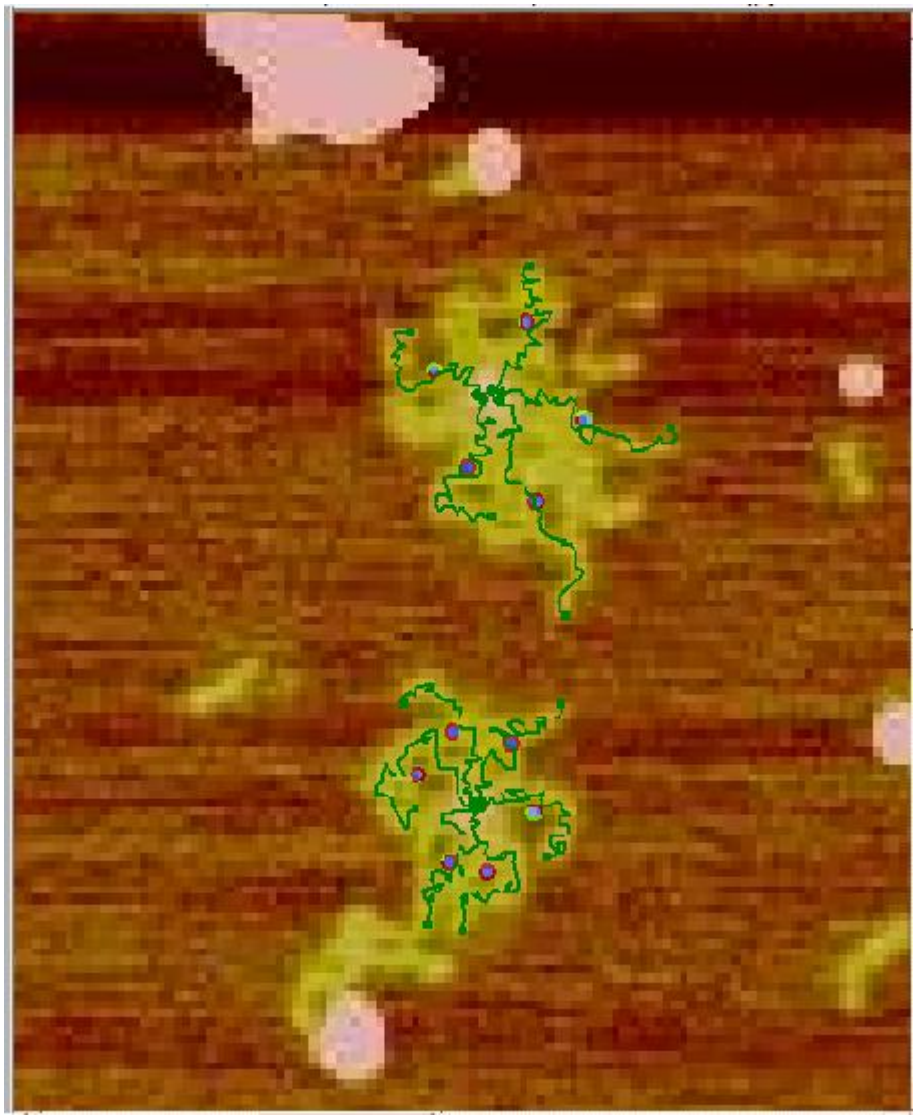


**Figure 25: AFM image of sample 66s cast from 0.01M NaCl aqueous solvent onto mica, copied from 2D Single Molecules program. The green lines tracing the star arms are manually drawn.**

***References***

(1) Moinard, D.; Borsali, R.; Taton, D.; Gnanou, Y. *Macromolecules* **2005**, *38*, 7105-7120.

(2) Kanemaru, E.; Terao, K.; Nakamura, Y.; Norisuye, T. *Polymer* **2008**, *49*, 4174-4179.

(3) Papagiannopoulos, A.; Fernyhough, C. M.; Waigh, T. A.; Radulescu, A. *Macromolecular Chemistry and Physics* **2008**, *209*, 2475-2486.

(4) Li, X.; Reed, W. F. *The Journal of Chemical Physics* **1991**, *94*, 4568-4580.

(5) Denton, A. R. *Physical Review E* **2003**, *67*, 011804.

(6) Hoffmann, N.; Likos, C. N.; Lowen, H. *The Journal of Chemical Physics* **2004**, *121*, 7009-7021.

(7) Jusufi, A.; Likos, C. N.; Lowen, H. *The Journal of Chemical Physics* **2002**, *116*, 11011-11027.

(8) Misra, S.; Mattice, W. L.; Napper, D. H. *Macromolecules* **1994**, *27*, 7090-7098.

(9) Shusharina, N. P.; Rubinstein, M. *Macromolecules* **2008**, *41*, 203-217.

(10) Burchard, W. In *Light Scattering from Polymers* 1983, p 1-124.

(11) H. Benoit *Journal of Polymer Science* **1953**, *11*, 507-510.

(12) Lienkamp, K.; Noe, L.; Breniaux, M. H.; Lieberwirth, I.; Groehn, F.; Wegner, G. *Macromolecules* **2007**, *40*, 2486-2502.

(13) Muller, F.; Delsanti, M.; Auvray, L.; Yang, J.; Chen, Y. J.; Mays, J. W.; Demé, B.; Tirrell, M.; Guenoun, P. *The European Physical Journal E - Soft Matter* **2000**, *3*, 45-53.

(14) Hirose, E.; Iwamoto, Y.; Norisuye, T. *Macromolecules* **1999**, *32*, 8629-8634.

(15) Adam, M.; Fetters, L. J.; Graessley, W. W.; Witten, T. A. *Macromolecules* **1991**, *24*, 2434-2440.

(16) Burchard, W. In *Branched Polymers II* 1999, p 113-194.

(17) Huber, K.; Burchard, W. *Macromolecules* **1989**, *22*, 3332-3336.

(18) Katzenstein, A.; Huber, K. *Langmuir* **2002**, *18*, 7049-7056.

(19) Reed, W. F.; Ghosh, S.; Medjahdi, G.; Francois, J. *Macromolecules* **1991**, *24*, 6189-6198.

(20) Reed, C. E.; Reed, W. F. *The Journal of Chemical Physics* **1991**, *94*, 8479-8486.

(21) Ghosh, S.; Peitzsch, R. M.; Reed, W. F. *Biopolymers* **1992**, *32*, 1105-1122.

(22) Ghosh, S.; Li, X.; Reed, C. E.; Reed, W. F. *Biopolymers* **1990**, *30*, 1101-1112.

(23) Foerster, S.; Schmidt, M.; Antonietti, M. *J. Phys. Chem.* **1992**, *96*, 4008-4014.

(24) Peitzsch, R. M.; Burt, M. J.; Reed, W. F. *Macromolecules* **1992**, *25*, 806-815.

(25) Reed, W. F. *The Journal of Chemical Physics* **1994**, *101*, 2515-2521.

(26) Muthukumar, M. *Macromolecules* **1993**, *26*, 3904-3907.

(27) Sedlak, M. In *Physical Chemistry of Polyelectrolytes*; Radeva, T., Ed.; Marcel Dekker: New York, NY, 2001; Vol. 99.

(28) Norwood, D. P.; Benmouna, M.; Reed, W. F. *Macromolecules* **1996**, *29*, 4293-4304.

(29) Striolo, A.; Prausnitz, J. M. *The Journal of Chemical Physics* **2001**, *114*, 8565-8572.

(30) Minko, S.; Roiter, Y. *Current Opinion in Colloid & Interface Science* **2005**, *10*, 9-15.

(31) Roiter, Y.; Jaeger, W.; Minko, S. *Polymer* **2006**, *47*, 2493-2498.

(32) Roiter, Y.; Minko, S. *The Journal of Physical Chemistry B* **2007**, *111*, 8597-8604.

# Part 5: Viscometric Properties of Star-branched NaPSS in Solutions of Varying Ionic Strength

## *Abstract*

We examined the viscometric behavior of star-branched NaPSS in a range of aqueous solutions of varying ionic strength. The intrinsic viscosity could reliably be determined in solutions with $C_s$ using either a Huggins equation or a Wolf equation. For aqueous solutions with no $C_s$, the Huggins equation over the linear portion of the data at low $C_p$ provided a better fit, as confirmed by AFM measurements of the dimensions of the polyelectrolyte and comparisons to the viscometric radii determined from the intrinsic viscosities calculated using the two equations. A very close fit between the $R_{afm}$ and the $R_v$ calculated from intrinsic viscosities determined by the Huggins equation led to the conclusion that this method of analysis can be used in the regime of $C_p$ significantly below the maximum known as the viscosity polyelectrolyte effect. The observation that the $R_v$ of the 50s and 60s series of stars did not vary significantly with *f* in dilute aqueous solutions with no $C_s$ was correlated to predictions put forward by Shusharina for the dilute osmotic regime with counterion condensation. Several observations support the hypothesis that small, densely branched NaPSS stars display viscosity behavior distinctly different from stars with longer arms, displaying aggregation phenomenon on AFM images and unusual increases in viscosity at very low $C_p$. The values of g' were calculated for solutions of the NaPSS stars in water, where it was observed that sets of stars with shorter arms had much smaller values of g' than that calculated by theory, but the set of stars with the longest arms showed good agreement with the theoretical g' values predicted by Fixman. The maximum in the $[\eta]_{red}$ vs. $C_p$ relation known in the literature as the viscosity polyelectrolyte effect was observed for all star branched NaPSS samples studied.

## *Introduction*

One area of ongoing debate within the polyelectrolyte field concerns the viscosity behavior of polyelectrolyte solutions at low ionic strength. Though extensively studied, a dependable method of determining the intrinsic viscosity ([η]) of these solutions, and often the interpretation of the quantity in any case, is currently lacking. One difficulty concerns the interpretation of experimental data. Unlike the typical case of nonionic polymers in organic solvents, which show a linear relation between reduced viscosity ($\eta_{red}$) and concentration, the extrapolation of the nonlinear relation of $\eta_{red}$ vs. $C_p$ typically found for polyelectrolytes to the limit of infinite dilution is nontrivial. Numerous methods of extrapolation were proposed and utilized to deal with this nonlinearity, most notably by Fuoss [1,2], Martin [3], and Rao [4], though the interpretation of the values obtained from these extrapolations is not clear.

Compared to the large volume of literature concerning the viscometry of linear polyelectrolytes at low ionic strength, studies of the viscometry of solutions of synthetic branched polyelectrolytes at any ionic strength are uncommon. Antonietti provided one of the earliest reports in this area when he studied the viscometry of "critically cross-linked" NaPSS and found that the densely cross-linked spherical polyelectrolytes exhibited the same peak in $\eta_{red}$ as linear NaPSS. This was counter to the common interpretation of the peak as resulting from a gradual increase in the dimensions of the polymers due to chain expansion resulting from reduced screening of electrostatic effects at low $C_p$, as the crosslinked particles Antonietti used could not undergo this expansion, and therefore the peak was attributed solely to electrostatic effects. Similar results were demonstrated by Ise on weakly charged colloidal particles[5], leaving the debate open as to

the role that interparticle electrostatics and intraparticle chain expansion play in the observed peak in $\eta_{red}$.

Recently, a series of publications have utilized an alternative method of determining [η] that was proposed by Wolf.[6] This method was used to examine the dilute solution viscosity of linear NaPSS [7], dextran [8], peripherally charged, dendronized PMMA [9], and carboxymethyl guar [10] in aqueous solutions with and without added salt. The successful application of this method of analysis to systems of natural and synthetic polyelectrolytes displaying varying types of branching and degrees of charge demonstrates its versatility.

In light of the above discussion, we propose the study of the viscometric behavior of a series of model, star-branched NaPSS in solutions of varying ionic strength, ranging from pure water to 1M NaCl. A study of this sort will allow for comparisons between the viscosity of the uncharged analogues of the polymers and linear NaPSS of analogous molecular weight with the viscosity of star-branched NaPSS, revealing the effects of branching on solution viscosity. Further, we propose the use of AFM measurements to determine the relative dimensions of star-branched NaPSS as a function of $C_p$ giving insight into the role of chain expansion in the observed peak in $\eta_{red}$, as well as the dimensions at very low $C_p$, which should correspond to [η] in some manner.

## *Experimental*

Solution preparation involved dissolving the dried sample in salt or pure water solutions until homogeneity was reached, usually overnight. The 1M, 0.1M and 0.01M NaCl solvents were prepared as described in Chapter 4, and pure water was obtained from the Barnstead Nanopure system described in Chapter 3.

For the dilute solution viscosity measurements utilizing a viscometer, a Cannon Ubbehlode capillary viscometer of the dilution type of size 0A was used. A water bath with a Fisher thermostated temperature control with an accuracy better than 0.1 °C, was used to maintain the temperature at 23°C for the measurements. The experimental procedure involved the following steps:

1. First, a measured mass of solvent is injected into the viscometer through a 0.2 μm PTFE filter. After a suitable equilibration time (~5 minutes) the flow time of the solvent in the viscometer is measured using the normal methods. The precision of the repeated measurement and comparison to past measurements of the same solvent gives indication of the relative cleanliness of the viscometer. If the flow times are significantly different from past measurements, the viscometer is cleaned using a hot sulfuric acid/chromic acid solution overnight and then thoroughly rinsed with deionized water followed by acetone and dried in an oven at 40 °C.
2. If measurements of the solvent flow times have verified the cleanliness of the viscometer, a measured mass of the concentrated stock solution of the sample to be measured is injected into the viscometer using a syringe fitted with a 0.45 μm PTFE filter. The solution is mixed by drawing the solution up using a pipette bulb and allowed to equilibrate. After equilibration the flow time of the solution is measured and recorded in the normal fashion. Accuracy of the flow times was within 0.1s, and measurements were repeated until they were reproduced three times within this range.

3. After the measurements at a given $C_p$ were completed, the solution was diluted with a measured mass of solvent and allowed to equilibrate. Measurement of the flow times was conducted as in the previous case, and this process was repeated until the flow time of the solution was within ~5% of the flow time of the solvent.

For the viscosities measured with a rheometer, a TA Instruments AR-50 rheometer was used. A cone and plate setup with a titanium plate was used for the measurements, all of which were performed at 23 °C with a steady shear of 100 $s^{-1}$, unless otherwise noted in the text. Approximately 2 mL of the solutions at various $C_p$ were injected using a syringe with a 0.45 μm PTFE filter.

AFM measurements were conducted using the same Veeco IIIa AFM and method of sample preparation described in Chapter 3.

## *Theory*

The intrinsic viscosity is defined as the specific hydrodynamic volume of a polymer in a given solvent under conditions of constant temperature and pressure at infinite dilution in the absence of shear. For the case of neutral polymers, the familiar Huggins equation (Equation 1) has been used successfully for the extrapolation of $\eta_{red}$ to zero concentration. The success of this method of extrapolation in this case is due to the relatively static nature of the conformation of neutral polymers within the dilute range of concentrations typically analyzed. This relation is often not applicable in the case of polyelectrolytes in solvents of low ionic strength, due to the fact that the conformation of these polymers often changes upon dilution, with reduced screening of the electrostatic repulsion causing gradual chain extension. These effects result in a non-linear relation

between $C_p$ and $\eta_{red}$ at very low concentrations where the small difference in viscosity between the pure solvent and that of the solution becomes difficult to determine reliably. These considerations led Wolf to propose an alternative method of determining [η] based on the application of phenomenological thermodynamics to the viscosity of polymer solutions. Following the original derivation [6], the viscosity constitutes a function of state, the changes of which can be modeled by the following expression:

$$d\ln\eta = \left(\frac{\delta\ln\eta}{\delta C_p}\right)_{T,p,\gamma} dC_p + \left(\frac{\delta\ln\eta}{\delta T}\right)_{C_p,p,\gamma} dT + \left(\frac{\delta\ln\eta}{\delta p}\right)_{C_p,T,\gamma} dp + \left(\frac{\delta\ln\eta}{\delta\gamma}\right)_{C_p,T,p} d\gamma \quad (29)$$

The first partial differential represents the specific hydrodynamic volume of the polymer at a given concentration ($C_p$), with constant values of temperature (T), hydrostatic pressure (p) and shear rate (γ), or essentially a generalization of [η] at a given $C_p$ and is denoted as $\{\eta\}$ in the rest of the text. $\{\eta\}$ becomes $[\eta]$ at infinite dilution and zero shear. The next two partial differentials in Equation (29) denote the activation energy and activation volume of flow. The last differential describes the shear thickening and thinning of polymer solutions, and is zero for Newtonian behavior of the solutions. The calculated dependence of $\{\eta\}$ on $C_p$ for the Huggins relation is

$$\{\eta\} = \frac{[\eta]\left(1 + 2k'[\eta]C_p\right)}{1 + [\eta]C_p\left(1 + k'''[\eta]'C_p\right)''} \quad (30)$$

While [η] and k' are suitable for solutions of neutral polymers, another parameter is obviously needed to describe the viscosity behavior in polyelectrolyte solutions. It is postulated that polyelectrolytes respond to increases in ionic strength brought about by increase in $C_p$ or $C_s$ by decreasing in $\{\eta\}$ from a maximum value of [η] at infinite

dilution, to a constant value of [η]*, and that there is an exponential transition between these two limiting values. This being the case, an integration of the expansion of Equation (30) by adding a quadratic term in $C_p$ to the denominator and incorporating [η]* leads to the following equation to describe experimental data:

$$\ln \eta_{\mathrm{rel}} = \frac{C_p[\eta] + BC_p{}^2[\eta][\eta]^*}{1 + BC_p[\eta]} \tag{31}$$

where B is a system specific constant similar to k', and is sometimes called the hydrodynamic interaction parameter. Another relation commonly used in papers employing Equation (31) is as follows:

$$n_I = \frac{1}{[\eta]M_0} \tag{32}$$

where $n_I$ is the molar concentration of ions within the volume occupied by the polymer coil, and $M_0$ is the molar mass of the monomeric unit. This relation takes as its premise the idea that the volume occupied by isolated polyelectrolyte coils is equal to $[\eta]M_0$, that each monomeric unit bears one charge, and that the number of counterions leaving the coil is negligible.

## *Results and Discussion*

### *Intrinsic Viscosity – Solutions with $C_s$*

Figure 26 shows Huggins representations of the viscosity data for sample 54s at each $C_s$, revealing the expected inverse relationship between [η] and $C_s$ and demonstrating the linearity of this representation of the data in solutions at various $C_s$. For the solutions with added salt, the Huggins and Wolf plots gave nearly identical values of [η] for all samples. This being the case, the results from fitting of Equation (31) to the experimental data are presented in Table 15, along with the [η] values of the polystyrene

precursors in THF determined using multi-detector SEC. Some notable trends in regards to the parameters $[\eta]^*$, B, and $[\eta]$ determined by fitting Equation (31) to the data are related in the following paragraphs.

The parameter $[\eta]^*$ assumes a value of 0 for all of the samples tested. This was also found to be the case for linear NaPSS in 0.9% NaCl solutions [7] and solutions of carboxymethyl guar [10], dextran [8], and peripherally charged and uncharged dendronized PMMA[9] in water. This subject will be touched on again in the next section, but one observes that $[\eta]^* = 0$ in solutions where the charges on the polymer chain should not influence the conformation of the polymer backbone, either because they are screened (NaPSS in 0.9% NaCl), separated from the backbone in space (carboxymethyl guar, peripherally charged dendronized PMMA) or not present at all (uncharged dendronized PMMA, dextran).

Values of the hydrodynamic interaction parameter, B, are almost all slightly negative for all of the sample/solvent combinations examined here, with the exception of the linear sample (2.69Mstd). Two different trends are observed in regards to the relationship between $C_s$ and B. The first is that B for samples 42s, 52s, 54s, 56s increase with $C_s$. For the rest of the star samples, with the exception of 44s, B reaches a maximum at 0.1M NaCl and decreases significantly upon increase of $C_s$ to 1M NaCl. Since the samples in the second group have been previously seen to exhibit anomalous effects (aggregation for samples 44s and 46s) or have the highest molecular weights (62s,64s, 66s), this trend is interpreted as resulting from unfavorable solvent-polymer interactions and the resultant decreased solubility. The reason for the increase in B with $C_s$ observed for the other samples is not clear.

[η] shows an inverse relation with $C_s$ for all samples, decreasing from 0.01M NaCl to the values at 1M NaCl, which are very close to the values obtained for the polystyrene precursors in THF, usually <20% larger. Within the 50s and 60s series of stars, [η] increases with *f* at each $C_s$, with 64s being anomalous in this respect. The 40s series of stars show the expected direct relationship between [η] in 1M NaCl, with [η] increasing with *f*. In the 0.1M and 1M solvents however, this interpretation cannot be used as the values for [η] follow no discernable pattern with $C_s$ in this regime, indicative of the aggregation phenomenon first hinted at by the SLS results of Chapter 4.

***Intrinsic Viscosity – No $C_s$ Solutions***

Figure 27 shows the data obtained from the 50s series of stars in water. Examination of the plot reveals that there is a significant degree of curvature to the data even in this representation, and furthermore, that the fitted curve does not show very good agreement with the data points, particularly at the lowest $C_p$. The relatively linear relation observed for the data points at the lower $C_p$ regime led us to examine this portion of the graph with a Huggins relation, in order to have another method for comparison of the results. Figure 28 is a Huggins representation of the same data as Figure 27, with linear fits to the linear portions of the curve at lower $C_p$. The following paragraphs will discuss the values of the parameters obtained using these two procedures to analyze the viscosity data obtained from solutions in water.

First it is notable that, once again, a best fit of Equation (18) establishes that the parameter $[\eta]^* = 0$ for all solutions except for the linear 2.69Mstd sample. In fact, the viscosity data from sample 2.69Mstd was fit very well using Equation (18), as illustrated by Figure 29. Fitting results in $[\eta]^* = 2.75$ $dLg^{-1}$ for this sample, on the order of the

values determined by Eckelt for higher molecular weight samples of linear NaPSS in water.[7] $[\eta]^*$ was also found to be zero for peripherally charged dendronized PMMA[9] and for carboxymethyl guar [10] in water, though the explanation given in those publications that this relates to the large distance of the charged portion of the macromolecule from the polymer backbone does not seem to work for the samples examined here, as the charges lie on the backbone for NaPSS.

The values of the parameter B continue the trend observed for the solutions with $C_s$, decreasing with the ionic strength of the solution, with the notable exception of the linear NaPSS sample 2.69Mstd. This is indicative of the extreme upward curvature of $[\eta]_{rel}$ with $C_p$ observed in Figure 27, which can be interpreted as the relative increase in the viscosity speeding up as $C_p$ increases, rather than slowing down, as is normal for thermodynamically favorable solvents. This behavior was also observed by the authors of Reference 93 for their peripherally charged dendronized PMMA samples of the third and fourth generation. Essentially, this rapid increase in coil dimensions could be attributed to a high preference of the polymer coil to its own segments, rather than the surrounding solvent, resulting in intramolecular collapse. Certainly this interpretation is reinforced by the values discovered for k', which are much higher than the ones usually obtained for solutions of polymers in organic solvents, again with the exception of the linear NaPSS 2.69Mstd sample. Typically k' increases as solvent quality decreases in solutions of polymers in organic solvents, with a value of 0.33 found for good solvent conditions, increasing to slightly above unity as the solvent quality becomes poorer.[11] The opposite behavior of the linear NaPSS sample in this case seems to indicate that the

solvent quality is actually increasing for that sample as $C_s$ decreases, behavior that is expected for polyelectrolytes.

The values of [η] determined by using the Huggins and Wolf equations, denoted $[\eta]_{Huggins}$ and $[\eta]_{Wolf}$ respectively, are generally in good agreement as to the qualitative trends observed within each set of polymers, though the values determined by the two methods vary significantly. Typically, the values of $[\eta]_{Wolf}$ are ~30-40% larger than those of $[\eta]_{Huggins,}$ though the values found for the linear NaPSS and the 40s series of polymers are in good agreement. The reason for the higher estimations of [η] given by using the Wolf equation is clearly due the poor fit to the viscosity data at low $C_p$. Since there is no valid reason to choose between the values of [η] determined using these two methods of analysis without more detailed knowledge of the conformation that only an independent method of characterization can provide, we would like to defer this discussion of [η] values determined using the two methods until the next section.

***Viscometric Radius ($R_v$)***

The viscometric radius ($R_v$) assuming a hard sphere model can be calculated from [η] using the following equation:

$$R_v = 5.41 \times 10^{-9} ([\eta] M_w)^{1/3} \quad (33)$$

where $M_w$ is the molecular weight of the polymer.[11] The values of $R_v$ calculated in this manner are presented in Table 17 using the [η] values obtained for the star-branched NaPSS in 1M, 0.1M, and 0.01M NaCl ($R_{v,1M}$, $R_{v,0.1M}$, and $R_{v,0.01M}$), in water using the Wolf and Huggins methods ($R_{v,w,W}$, $R_{v,w,H}$) and for the polystyrene precursors in THF ($R_{v,\ THF}$). As expected, the trends in these values follow many of the trends observed for [η] at the given values of $C_s$. The $R_v$ has an inverse relationship with $C_s$, increasing

gradually across the table as $C_s$ is decreased from 1M to 0. It is interesting to note that the values calculated for $R_v$ for samples in the 50s and 60s series of polymers, which vary only in *f*, attain nearly the same value in water, regardless of which method is used to determine [η]. In other words, it appears that $R_v$ is nearly independent of *f* for these samples in water. This interesting behavior was predicted by Shusharina for solutions of polyelectrolyte stars with counterion condensation in the dilute osmotic regime without added salt.[12] By contrast, the samples in the 40s series of stars show a progressively larger influence of *f* as $C_s$ decreases, being nearly identical at the highest $C_s$ 1M solvent, and reaching the greatest differences in $R_v$ in water.

***Atomic Force Microscopy - $R_{afm}$ and $R_v/R_h$***

To test the interesting observations of the previous section, as well as to elucidate the conformation of star-branched NaPSS in the very dilute aqueous regime, the method established in the previous chapter was used for sample preparation and measurement of single molecule dimensions using AFM. The values determined in this manner are listed in Table 17 under the heading $R_{afm,w}$ with the standard deviations of the measurements used to calculate them, and Figure 30 shows a representative scan of sample 62s cast from a dilute aqueous solution. For samples 54s, 62s, 64s, and 66s, the correlation between the values of $R_{v,w,Hugg}$ and $R_{afm,w}$ are remarkable. Though a strong correlation has previously been established between $R_{afm}$ and $R_h$ for several star-branched NaPSS samples in solutions of varying $C_s$, the correlation between $R_{afm}$ and $R_v$ in water has not really been established. As multimodal distributions of relaxation times and weak scattering intensities complicate the interpretation of DLS data in this regime of no $C_s$ and low $C_p$, it was not possible to obtain $R_h$ values for the samples in water. However,

the ratio of $R_v$ to $R_h$ is a commonly determined ratio in polymer solutions, often assuming a value close to unity for a variety of linear and branched polymers.[11] Table 18 lists the values determined for the $R_v/R_h$ ratio for each star-branched NaPSS sample in 0.01M, 0.1M and 1M NaCl aqueous solutions, as well as the values determined for the polystyrene precursors in THF. The ratio for the linear NaPSS sample 2.69Mstd is also listed, and it is observed that it increases gradually from a value close to 1 in 1M NaCl to 1.48 in 0.01M NaCl. This trend is also observed for the star-branched samples, with all samples showing a gradual increase in the $R_v/R_h$ ratio as $C_s$ decreases, with the values at 0.01M NaCl generally approaching unity. This being the case, it might be assumed that $R_v \sim R_h$ for solutions of star-branched NaPSS in water, and furthermore, that the correlation between $R_{v,w,Hugg}$ and $R_{afm,w}$ is not coincidental. This being the case, the values of [η] determined by fitting the Huggins equation are used as the values of [η] for star-branched NaPSS in water for the remainder of this chapter. Notably, the aforementioned radii do not match in the case of samples 42s, 44s, and 46s. Examination of the AFM images for sample 46s reveals the presence of large spherical domains, most of which have radii ~ 0.4 μm. These AFM scans are presented in Figure 31, with part (a) showing a detailed image of the one of the domains, and part (b) showing several of the domains at once on a 10 μm scan. Part (c) of Figure 31 shows an AFM scan from sample 44s, which displays domains similar to those observed for sample 46s. If these domains exist as coherent structures in solution, like the semi-ordered structures observed by Sedlak in aqueous solutions of linear NaPSS[13-16], this may explain the discrepancy between $R_{afm,w}$ and $R_{v,w,\,Hugg}$ for these polymers. Another explanation may be related to the relatively small size of the polymers in the 40s series. As equation (18) indicates,

polyelectrolytes with lower values of [η] (and hence smaller dimensions in solution) have higher charge densities than polymers with higher [η]. This effect could be similar to the one observed by Antonietti in his study of crosslinked NaPSS spheres, where strong electrostatic interactions between polymers resulted in measured [η] significantly above the values that should be possible based on the known dimension of the spheres.[17-19] Other explanations of this phenomenon are possible, but further speculation is beyond the scope of this thesis.

Examination of the curves in Figure 28 reveals that they display dependencies of [η] that are not congruent with the assumption that the viscosity polyelectrolyte effect occurs for these samples. Typically, the observed behavior is an increase of $\eta_{red}$ with decreasing $C_p$, whereas the behavior observed for the samples examined here show the typical direct relation between $\eta_{red}$ and $C_p$ normally observed for solutions of neutral polymers in organic solvents, albeit with an unusually sharp increase at a given $C_{p.}$ To determine whether the samples examined previously by capillary viscometry did indeed display the viscosity polyelectrolyte effect, a rheometer was used to determine the viscosity of samples in a much wider range of $C_p$ than was examined using viscometers. Figures 32 and 33 display the results of the experiments for the 50s and 60s series of samples. Clearly, these samples do exhibit a viscosity polyelectrolyte effect, exhibiting an upturn in $\eta_{red}$ with decreasing $C_p$ and finally decreasing rapidly after reaching a maximum. The range of $C_p$ studied using viscometers falls within this regime of $C_p$ after the maximum ($<0.05 gdL^{-1}$). Though the existence of this maximum has previously been verified by several different authors [20-23], few researchers have studied the viscosity in the regime of $C_p$ lower than the maximum, most likely due to the fact that the lower

molecular weight linear NaPSS samples they examined (generally <1 x $10^{-6}$ g/mol) did not have viscosities high enough to be reliably determined at this low $C_p$. Qualitatively, the curves follow the same patterns previously observed for linear NaPSS samples, with the maximum of the curves shifting to higher $C_p$ and also increasing in height with increases in molecular weight.

The plots of $\eta_{red}$ vs. $C_p$ for 44s and 46s are displayed in Figure 34. Sample 42s was not examined in this manner, as the range of $C_p$ covering the peak in the $\eta_{red}$ vs. $C_p$ plot was covered in the capillary viscometer experiments. The maximum in $\eta_{red}$ vs. $C_p$ for these polymers was also relatively small in magnitude, but can be discerned. The most notable feature of these plots is a very rapid increase in $\eta_{red}$ at the lowest $C_p$ for sample 46s and a somewhat smaller one for 44s. This anomalous behavior reinforces the hypothesis that aggregation phenomena play a more important role in the viscosity of these solutions than the dimensions of individual polymers.

***Branching ratio g'***

The branching ration g' is defined as

$$g' = \frac{[\eta]_{\text{branched}}}{[\eta]_{\text{linear}}} \tag{34}$$

where $[\eta]_{\text{branched}}$ is the intrinsic viscosity of a given branched polymer and $[\eta]_{\text{linear}}$ is the intrinsic viscosity of a linear polymer of the same molecular weight under the same conditions. A number of theoretical calculations of g' are reported in literature, among which two of the most commonly used are the Fixman-Stockmayer model [24], which predicts

$$g' = f^{3/2}\left[2 - f + 2^{1/2}(f-1)\right]^{-3} \tag{35}$$

and the Zimm-Kilb model, which predicts

$$g' = \left(\frac{2}{f}\right)^{3/2} \frac{[0.39(f-1)+0.196]}{0.586} \quad (36)$$

additionaly, Roovers established the following empirical relation:

$$\log g' = 0.36 - 0.80 \log f \quad (37)$$

In order to compare our experimental results with these theoretical predictions, we must determine the [η] of linear polymers of the same molecular weight under the same conditions. The values of K and *a* for the Mark-Houwink relation for polystyrene in THF at 30 °C were obtained from Jackson [25] and were 8.63 x $10^{-5}$ and 0.736 respectively. The relation between [η] and molecular weight for linear NaPSS in water at 25 °C was determined by Eckelt [7], and don't follow a typical Mark-Houwink power law relation. Instead, the data is modeled by means of a Boltzmann equation with the form

$$log[\eta] = \left(\frac{-4.023}{1+\exp\left[\frac{\log M_w - 1.071}{0.415}\right]}\right) + 4.116 \quad (38)$$

Using Equation 38 and the M-H-S parameters mentioned previously to determine the [η] of linear analogues, experimental g' values were calculated for both the polystyrene star precursors and star-branched NaPSS in water. Table 19 lists the experimentally determined g' for polystyrene precursors and for star-branched NaPSS, denoted as $g'_{THF}$ and $g'_{water}$ respectively, as well as the values calculated from Equations 35, 36, and 37 which are denoted as $g'_{Fixman}$, $g'_{Zimm}$ and $g'_{Roovers}$ respectively. Within each series of polymers, the values of $g'_{THF}$ and $g'_{water}$ follow the trend predicted by theory of decreasing g' with increasing *f*, with the exception of $g'_{water}$ for the 40s series. For $g'_{THF}$, the empirical $g'_{Roovers}$ provides the closest agreement, with most values of $g'_{Roovers}$ slightly above the values of $g'_{THF}$. This finding provides further confirmation that the *f* determined for the polystyrene precursors is accurate. The values determined for $g'_{water}$

show several interesting features. The anomalous behavior of the 40s series of stars, where $g'_{water}$ increases with *f*, can probably be traced to the aggregation phenomenon previously discussed, which changes the [η] determined. To some extent, it is difficult to rationalize the rather large difference found between the calculated g' values and the experimental ones. A small difference between the values is anticipated based on the fact that the theoretical g' values are calculated for theta conditions and the experimental conditions should correspond to good solvent conditions, a situation that typically results in experimental g' values lower than theoretically predicted ones. This finding is explained by considering that the expansion coefficient for linear polymers is larger than that for star polymers, or in othe words, linear polymers are able to expand more in good solvent than star polymers, relative to the theta solvent state. Perhaps the most curious pattern that is observed in this table is the very near match between $g'_{water}$ for the polymers in the 60s series and $g'_{Fixman}$. This can be contrasted to the 50s series, where it seems that linear NaPSS of the same molecular weight is much more extended relative to the dimension of star-branched NaPSS than that predicted for uncharged analogues in theta solvents. It is speculated that this difference may relate to a possible change in conformation that occurs at $C_p$ after the peak, such as an intramolecular collapse from the maximum extension of the star observed at the maximum in the viscosity plot. It may be proposed with equal validity that the decrease in reduced viscosity after the maximum is related to the gradual decrease of intermolecular electrostatic interactions with dilution as the polyelectrolyte species become spaced further apart out of the range of expected electrostatic interactions. A combination of these effects constitutes a third possible explanation. In any case, it seems that the relationship between $[\eta]_{lin}$ and $[\eta]_{branched}$ for

NaPSS in aqueous solutions with no $C_s$ is very different from the relationship between these parameters in solutions of uncharged polymers.

## *Summary and Conclusions*

In this chapter, solutions of star-branched NaPSS of varying *f* and arm length in solvents with $C_s$ ranging from 1M NaCl to no $C_s$ were characterized using viscometry and AFM. Solutions with $C_s$ were examined using both Huggins and Wolf methods of analysis, where it was found that the parameter $[\eta]^*$ from the Wolf equation was equal to 0, similar to previously observed systems. In solutions with no $C_s$, both Huggins and Wolf methods were used to examine the data and determine $[\eta]$. k' and B parameters determined from both methods of analysis indicated that the star-branched NaPSS samples were in poor solvent conditions, unlike the linear NaPSS sample examined. $[\eta]$ determined by the two methods showed the same qualitative trends, but poor quantitative agreement, and it was found that the fit of the Wolf viscosity equation (Equation 18) to the data was poor. AFM measurements were conducted to determine the $R_{afm}$ of selected star-branched samples at very low $C_p$, and it was found that $R_{afm}$ matched the $R_v$ calculated from the $[\eta]$ determined using the Huggins equation much more closely than that calculated using the Wolf equation. The observation that the $R_v$ of the 50s and 60s series of stars did not vary significantly with *f* in dilute aqueous solutions with no $C_s$ was correlated to predictions put forward by Shusharina for the dilute osmotic regime with counterion condensation. Large domains consisting of aggregated polymers surrounded by bare surface were observed in the AFM images of samples 44s and 46s, and it was theorized that these structures may be present in solution. The ratio $R_v/R_h$ was determined for the set of samples at each value of $C_s$, and it was established that the ratio

shows an inverse relationship with $C_s$, increasing gradually towards unity as $C_s$ decreases. The maximum in the $[\eta]_{rel}$ vs. $C_p$ relation known as the viscosity polyelectrolyte effect was observed for all samples using a rheometer to determine viscosity over a wide range of $C_p$, and an anomalous increase in $[\eta]_{rel}$ at very low $C_p$ was correlated to the previously observed large domains in AFM images of samples 44s and 46s. The branching parameter g' was determined for both the polystyrene precursors and the star-branched NaPSS in water and compared to theoretically and empirically determined values of g'. The values of g' determined for the polystyrene precursors showed a high level of agreement with g' calculated using an empirical relation established by Roovers. The values of g' determined for the star-branched NaPSS samples in water displayed the qualitatively expected trend of a direct relationship between g' and *f* for the 50s and 60s series of stars. Quantitatively, the values of g' determined for the 40s and 50s are much lower than all theoretical predictions, indicating that the samples in these series are collapsed compared to uncharged polymers in theta solvents relative to their linear analogues. Surprisingly, the values of g' for the 60s series are shown to be in close agreement with the predictions of g' made using the model proposed by Fixman.

*Appendix*

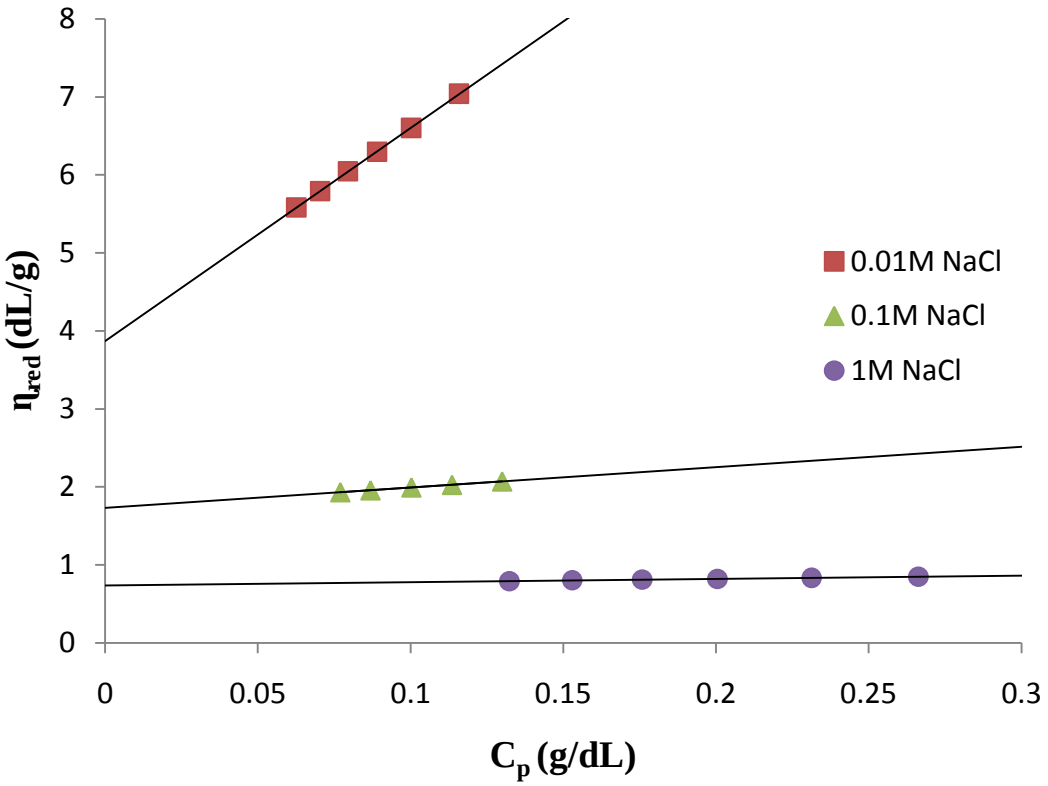



**Figure 26: Typical Huggins plot of the concentration dependence of $\eta_{red}$ for 54s in solutions of varying $C_s$, showing the decrease in [η] with increasing $C_s$.**

## Table 15: Intrinsic Viscosities and Wolf Coefficients for Aqueous Solutions of Star-branched NaPSS at Various $C_s$

| Sample | $B_{0.01}$ | $B_{0.1M}$ | $B_{1M}$ | $[\eta]_{0.01M}$ [a] (dL/g) | $[\eta]_{0.1M}$ [a] (dL/g) | $[\eta]_{1M}$ [a] (dL/g) | $[\eta]_{THF}$ [b] (dL/g) |
|---|---|---|---|---|---|---|---|
| 42s | -1.69 | -0.411 | 0.256 | 0.858 | 0.394 | 0.210 | 0.191 |
| 44s | -1.68 | -1.92 | 0.318 | 0.813 | 0.437 | 0.210 | 0.193 |
| 46s | -1.25 | 0.634 | -0.304 | 0.763 | 0.347 | 0.215 | 0.198 |
| 52s | -0.126 | -0.068 | -0.023 | 4.87 | 1.78 | 0.721 | 0.703 |
| 54s | -0.256 | -0.180 | -0.144 | 5.57 | 1.88 | 0.777 | 0.620 |
| 56s | -0.353 | -0.151 | -0.119 | 5.59 | 1.92 | 0.759 | 0.666 |
| 62s | -0.122 | -0.082 | -0.525 | 7.12 | 2.62 | 1.13 | 1.00 |
| 64s | -0.251 | -0.139 | -1.07 | 8.07 | 2.91 | 1.24 | 0.965 |
| 66s | -0.311 | -0.147 | -0.439 | 7.63 | 2.72 | 1.17 | 0.979 |
| 2.69Mstd | 0.167 | 0.214 | 0.042 | 8.75 | 4.34 | 1.78 | - |

[a] Intrinsic viscosities determined using capillary viscometer in aqueous solutions with $C_s$ at 0.01M, 0.1M, and 1M NaCl, respectively. [b] Determined with online Viscotek viscosity detector using PL-GPC 120 in THF at 40° C.

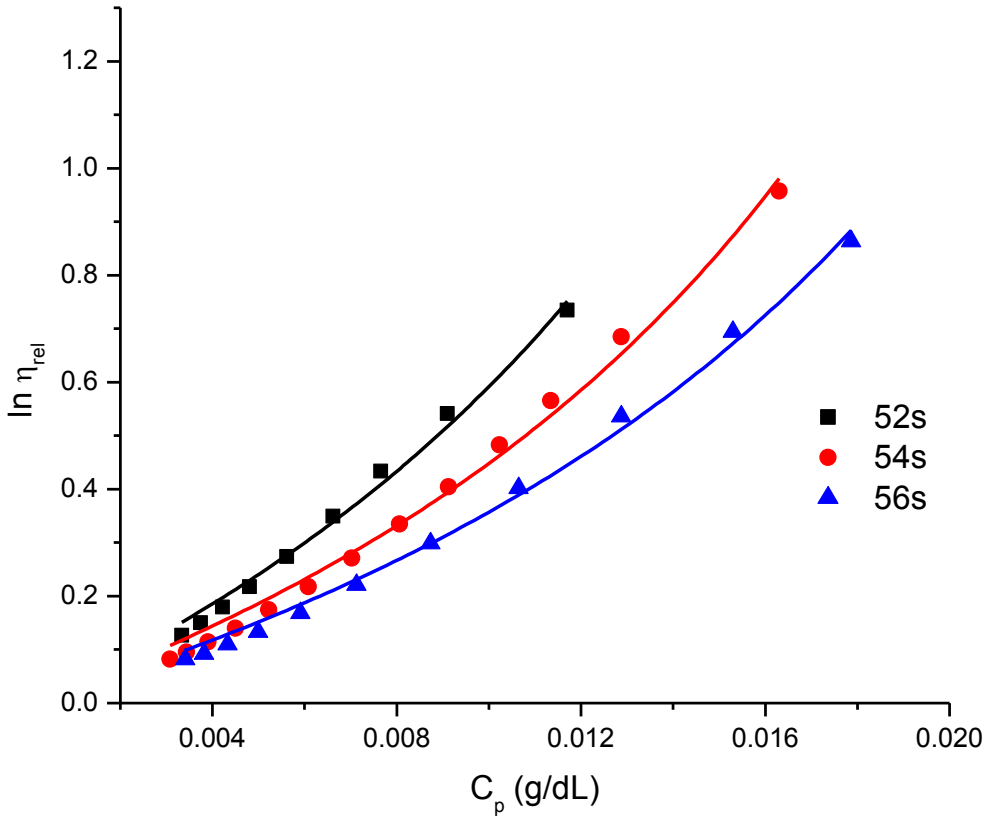



**Figure 27: Plot showing ln $\eta_{rel}$ vs. $C_p$ fitted using Wolf equation (Equation 17).**

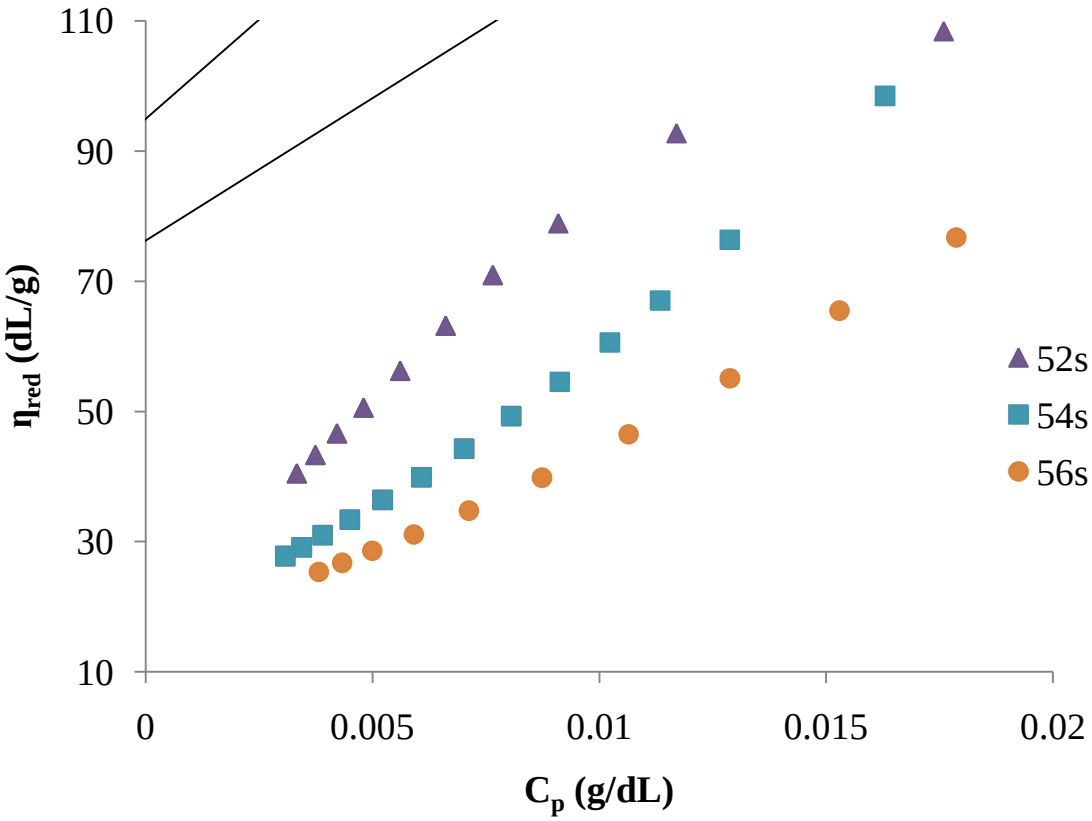



**Figure 28: Huggins plots of the 50s series of polymers in water, showing extrapolation of low concentrations to infinite dilution.**

**Table 16: Intrinsic Viscosities and Coefficients for Aqueous Solutions of Star-branched NaPSS determined by Huggins and Wolf Extrapolations**

| Sample | k' | B | $[\eta]_{Huggins}$ (dL/g) | $[\eta]_{Wolf,\ fit}$ (dL/g) |
|---|---|---|---|---|
| 42s | 1.99 | 0.0150 | 6.92 | 8.00 |
| 44s | 4.83 | -0.251 | 8.91 | 11.8 |
| 46s | 0.487 | 1.11 | 16.1 | 16.4 |
| 52s | 22.6 | -2.39 | 17.5 | 29.6 |
| 54s | 19.0 | -2.96 | 14.8 | 21.8 |
| 56s | 15.0 | -2.22 | 14.0 | 20.6 |
| 62s | 8.54 | -1.29 | 42.4 | 59.6 |
| 64s | 7.93 | -1.26 | 33.8 | 46.7 |
| 66s | 6.10 | -1.14 | 31.7 | 41.1 |
| 2.69Mstd | 0.072 | 0.360 | 64.8 | 62.8 |

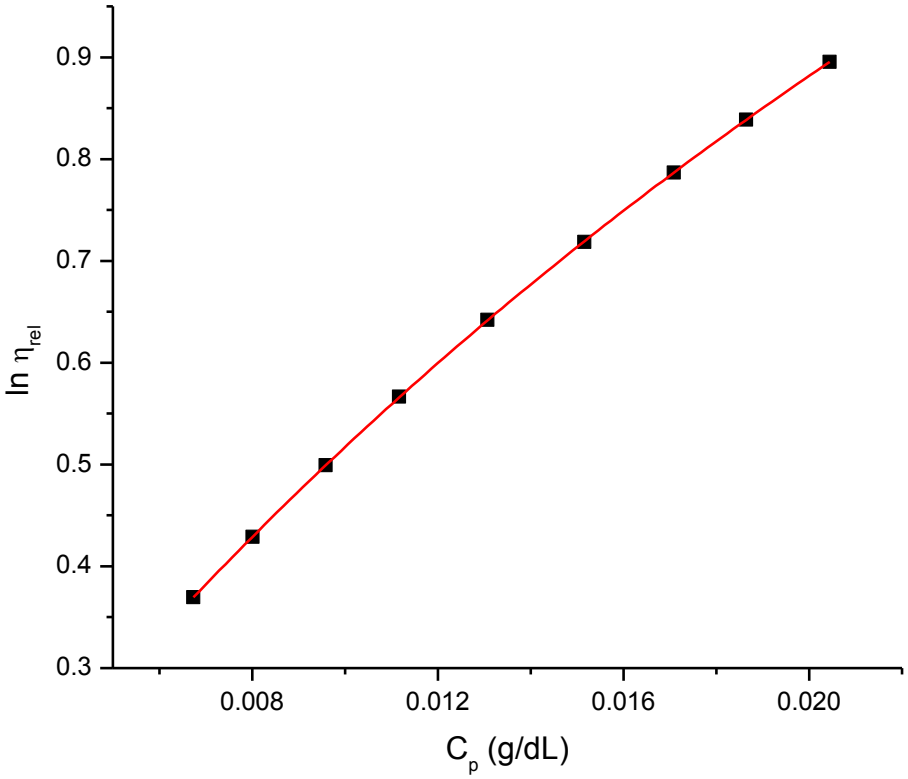



**Figure 29: ln $\eta_{rel}$ vs. $C_p$ for sample 2.69Mstd, fitted using Wolf equation (Equation 17).**

**Table 17: Values of the Viscometric Radius $R_v$ for Solutions of Star-branched NaPSS in Solvents of Varying Ionic Strength with $R_{afm}$**

| Sample | $R_{v,THF}$ (nm) | $R_{v,1M}$ (nm) | $R_{v,0.1M}$ (nm) | $R_{v,0.01M}$ (nm) | $R_{v,w,W}$ [b] (nm) | $R_{v,w,H}$ [c] (nm) | $R_{afm,w}$ (nm) |
|---|---|---|---|---|---|---|---|
| 42s | 7.29 | 9.44 | 11.3 | 15.1 | 68.5 | 30.4 | 16 ± 2.0 |
| 44s | 7.78 | 10.0 | 11.5 | 15.8 | 82.9 | 35.4 | 18[a]± 2.8 |
| 46s | 8.44 | 10.9 | 13.0 | 16.6 | 99.5 | 45.6 | 16[a]± 1.8 |
| 52s | 17.5 | 22.1 | 29.7 | 41.8 | 164 | 70.5 | - |
| 54s | 18.9 | 25.6 | 33.7 | 49.4 | 168 | 72.2 | 73 ± 7.5 |
| 56s | 19.9 | 26.1 | 33.3 | 50.7 | 169 | 72.8 | - |
| 62s | 28.4 | 32.4 | 42.5 | 59.9 | 262 | 114 | 116 ± 15 |
| 64s | 26.3 | 35.9 | 46.8 | 67.0 | 259 | 115 | 116 ± 11 |
| 66s | 27.8 | 37 | 47.8 | 69.2 | 261 | 117 | 120 ± 11 |
| 2.69Mstd | | 41.5 | 55.9 | 70.6 | 293 | 134 | - |

[a] denotes samples that showed significant aggregation on AFM images. [b] $R_v$ calculated using [η] calculated using Huggins equation. [c] $R_v$ calculated using [η] calculated using the Wolf equation.

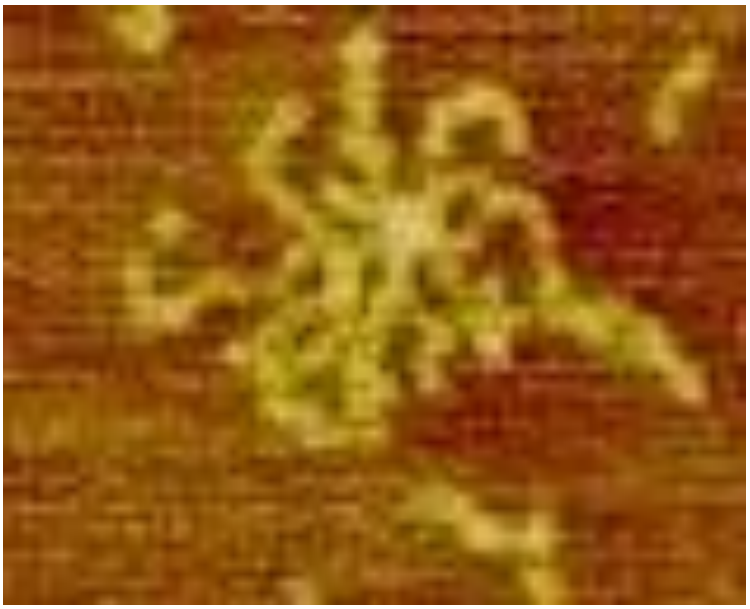


**Figure 30: AFM image of sample 62s, cast from a dilute aqueous solution with no $C_s$.**

**Table 18: $R_v/R_h$ Values for Solutions of Star-branched NaPSS in Aqueous Solvent of Varying Ionic Strength**

| Sample | $R_v/R_{h\ THF}$ | $R_v/R_{h\ 0.01M}$ | $R_v/R_{h\ 0.1M}$ | $R_v/R_{h\ 1M}$ |
|---|---|---|---|---|
| 42s | 0.81 | 0.85 | 0.72 | 0.72 |
| 44s | 0.82 | 0.73 | 0.58 | 0.55 |
| 46s | 0.84 | 0.61 | 0.49 | 0.56 |
| 52s | 0.89 | 0.94 | 0.87 | 0.82 |
| 54s | 0.88 | 1.04 | 0.87 | 0.86 |
| 56s | 0.89 | 0.88 | 0.72 | 0.77 |
| 62s | 1.02 | 0.94 | 0.90 | 0.80 |
| 64s | 0.92 | 0.93 | 0.82 | 0.74 |
| 66s | 0.91 | 0.82 | 0.76 | 0.68 |
| 2.69Mstd | - | 1.48 | 1.15 | 0.96 |

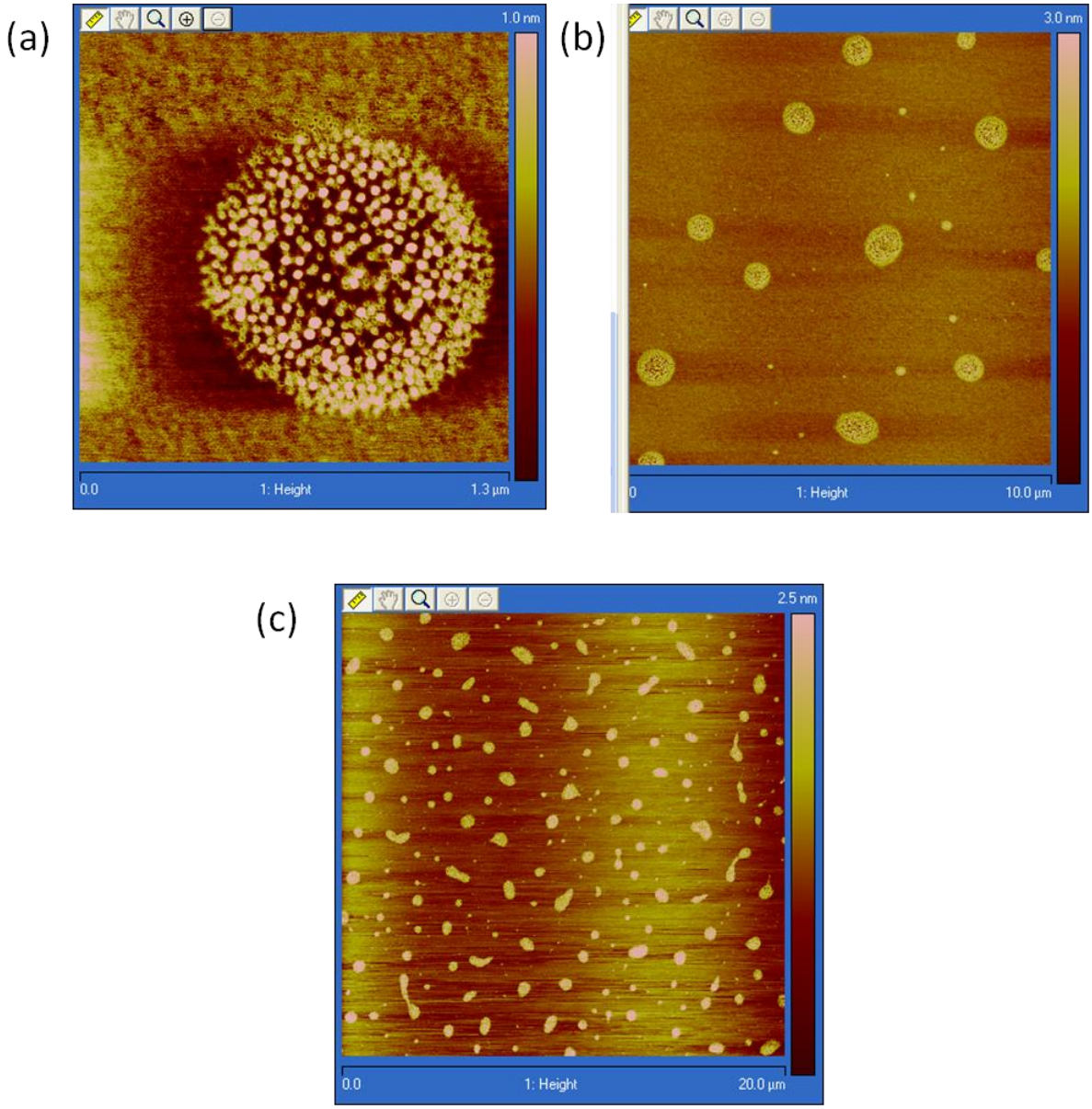



**Figure 31: AFM images of dilute aqueous solutions of star NaPSS, showing possible aggregation at different length scales. (a) shows 46s at a length scale of 1.3 µm, the average lateral diameter of the domains is ~0.7 µm. (b) is an expanded view of the same sample at a length scale of 10 µm, showing domains and individual chains. (c) is an image of a dilute aqueous solution of 44s at a 20 µm length scale.**

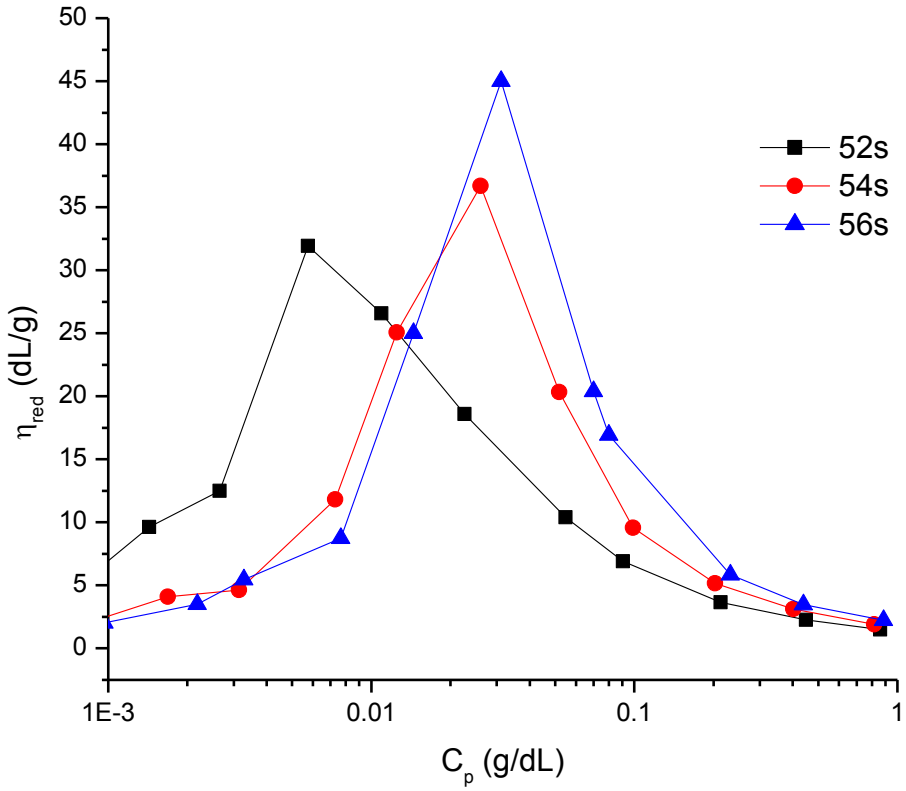



**Figure 32: $\eta_{red}$ vs. $C_p$ for aqueous solutions of 50s series of samples, showing the viscosity polyelectrolyte effect. The lines drawn are guides for the eye only.**

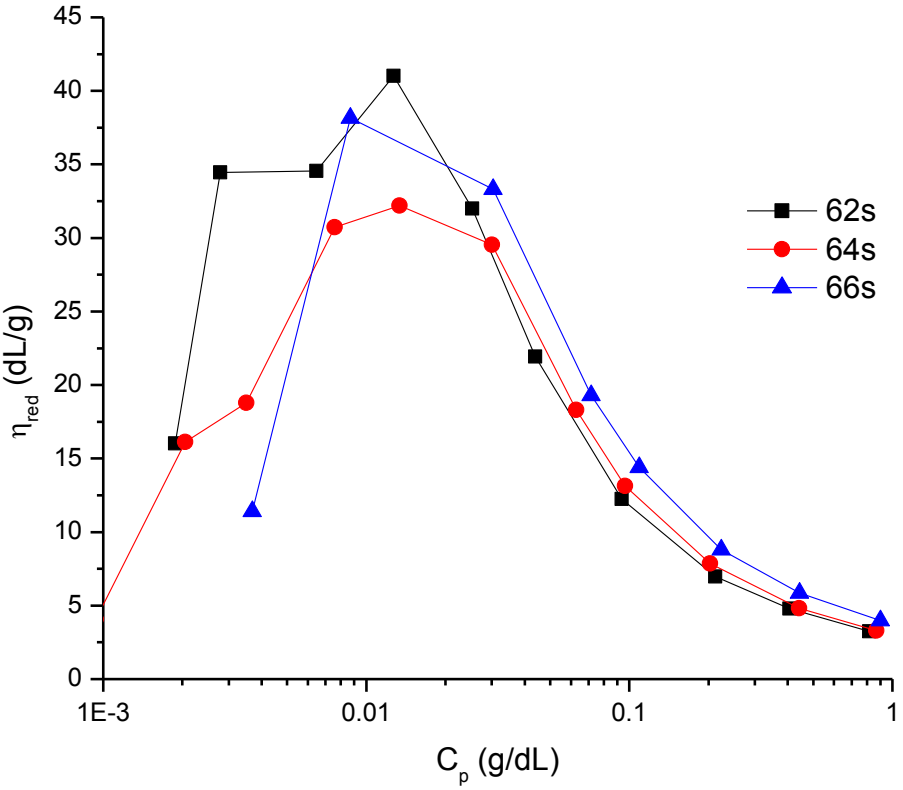



**Figure 33: : $\eta_{red}$ vs. $C_p$ for aqueous solutions of 60s series of samples, showing viscosity polyelectrolyte effect. The lines drawn are guides for the eye only.**

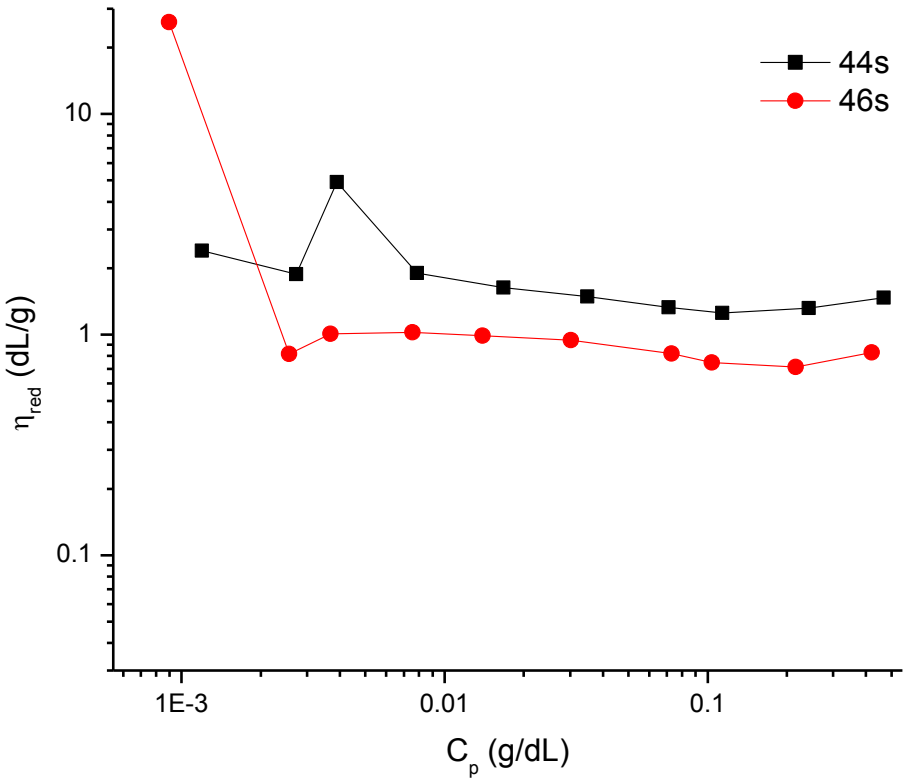



**Figure 34: $\eta_{red}$ vs. $C_p$ plots for 40s series of samples, showing rapid changes in slope at the lowest $C_p$. A log-log scale is employed, and the lines are guides for the eye only.**

**Table 19: Experimental and Theoretical g' values for Solutions of Star-branched NaPSS in Water and Polystyrene Precursors in THF**

| Sample | $g'_{THF}$ | $g'_{water}$ | $g'_{Fixman}$ | $g'_{Zimm}$ | $g'_{Roovers}$ |
|---|---|---|---|---|---|
| 42s | 0.39 | 0.076 | 0.27 | 0.54 | 0.34 |
| 44s | 0.34 | 0.092 | 0.22 | 0.50 | 0.30 |
| 46s | 0.30 | 0.16 | 0.17 | 0.46 | 0.25 |
| 52s | 0.54 | 0.15 | 0.44 | 0.66 | 0.49 |
| 54s | 0.36 | 0.12 | 0.30 | 0.57 | 0.36 |
| 56s | 0.37 | 0.11 | 0.27 | 0.55 | 0.34 |
| 62s | 0.46 | 0.34 | 0.36 | 0.61 | 0.42 |
| 64s | 0.38 | 0.27 | 0.29 | 0.56 | 0.35 |
| 66s | 0.34 | 0.25 | 0.24 | 0.52 | 0.31 |

*References*

(1) Fuoss, R. M.; Strauss, U. P. *Journal of Polymer Science* **1948**, *3*, 246-263.

(2) Strauss, U. P.; Fuoss, R. M. *Journal of Polymer Science* **1949**, *4*, 457-472.

(3) Darskus, R. L.; Jordan, D. O.; Kurucsev, T.; Martin, M. L. *Journal of Polymer Science Part a-General Papers* **1965**, *3*, 1941-&.

(4) Rao, M. V. S. *Polymer* **1993**, *34*, 592-596.

(5) Ise, N. *Proceedings of the Japan Academy Series B-Physical and Biological Sciences* **1998**, *74*, 192-200.

(6) Bernhard A. Wolf *Macromolecular Rapid Communications* **2007**, *28*, 164-170.

(7) Eckelt, J.; Knopf, A.; Wolf, B. A. *Macromolecules* **2008**, *41*, 912-918.

(8) Ghimici, L.; Nichifor, M.; Wolf, B. *The Journal of Physical Chemistry B* **2009**, *113*, 8020-8025.

(9) Samadi, F.; Wolf, B. A.; Guo, Y.; Zhang, A.; Dieter SchluÌˆter, A. *Macromolecules* **2008**, *41*, 8173-8180.

(10) Manohar V. Badiger; Nivika R. Gupta; John Eckelt; Bernhard A. Wolf *Macromolecular Chemistry and Physics* **2008**, *209*, 2087-2093.

(11) Barth, H. G.; Mays, J. W. *Modern Methods of Polymer Characterization*; John Wiley and Sons: New York, 1991; Vol. 113.

(12) Shusharina, N. P.; Rubinstein, M. *Macromolecules* **2008**, *41*, 203-217.

(13) Marian, S. *The Journal of Chemical Physics* **1996**, *105*, 10123-10133.

(14) Sedlak, M. *Langmuir* **1999**, *15*, 4045-4051.

(15) Sedlak, M. In *Physical Chemistry of Polyelectrolytes*; Radeva, T., Ed.; Marcel Dekker: New York, NY, 2001; Vol. 99.

(16) Sedlak, M.; Amis, E. J. *The Journal of Chemical Physics* **1992**, *96*, 826-834.

(17) Antonietti, M.; Briel, A.; Forster, S. *The Journal of Chemical Physics* **1996**, *105*, 7795-7807.

(18) Antonietti, M.; Briel, A.; Grohn, F. *Macromolecules* **2000**, *33*, 5950-5953.

(19) Grohn, F.; Antonietti, M. *Macromolecules* **2000**, *33*, 5938-5949.

(20) Vink, H. *Polymer* **1992**, *33*, 3711-3716.

(21) Cohen, J.; Priel, Z. *Polymer Communications* **1989**, *30*, 223-224.

(22) Cohen, J.; Priel, Z.; Rabin, Y. *The Journal of Chemical Physics* **1988**, *88*, 7111-7116.

(23) Rabin, Y.; Cohen, J.; Priel, Z. *Journal of Polymer Science Part C: Polymer Letters* **1988**, *26*, 397-399.

(24) Stockmayer, W. H.; Fixman, M. *Annals of the New York Academy of Sciences* **1953**, *57*, 334-352.

(25) Jackson, C.; Chen, Y.; Mays, J. W. *Journal of Applied Polymer Science* **1996**, *61*, 865-874.

# Part 6: Final Conclusions and Summary

## *Final Conclusions*

In this thesis, we examined the effect of branching on the solution characteristics of polyelectrolytes using a set of star-branched NaPSS. The polystyrene precursors to these polyelectrolytes were synthesized using anionic polymerization, employing a novel method of dividing the solution containing the reactive anionic chain ends and subsequently linking them together using DVB. This method of synthesis allowed for the production of three distinct groups of star-branched polystyrenes, with each group consisting of three samples that had the same degree of polymerization of each arm, but different numbers of arms in each sample. We used SEC-TALS to establish that the precursor polymers were relatively monodisperse and to determine *f* and the degree of polymerization of each arm. To complete the synthesis, the precursors were sulfonated using conditions that were modified from the original Vink procedure.

Due to the rather open question as to what extent the degree of sulfonation changes the solution characteristics of NaPSS, we sought to quantify this parameter for the star-branched NaPSS samples using several methods commonly employed in the literature. All methods used indicated that the sulfonation degree was above 90% for every sample. By comparing the results using these methods on the set of star-branched NaPSS and an additional set of linear NaPSS of varying degrees of sulfonation to data obtained using TGA, we were able to find qualitative correlations between the sulfonation degree and several characteristics of the decomposition curve obtained from TGA. TGA was also demonstrated to allow for quantitative determination of the water content and qualitative estimations of the amount of residual low molecular weight salt in the sample as well as the percentage of monomers in sulfonic acid and sodium salt form.

We used aqueous SEC coupled with a multiple angle light scattering detector to determine the $M_w$, $R_g$, and polydispersity of the star-branched NaPSS samples. Linear NaPSS synthesized via radical polymerization and polymer-analogous sulfonation of polystyrene were also characterized using this method and important differences between NaPSS synthesized by the two methods were established, mainly indicating the presence of crosslinking and hydrophobic interactions for NaPSS synthesized by the polymer-analogous sulfonation route. Scaling relationships between $R_g$ and $M_w$ of both branched and linear species were established. Also, dynamic light scattering experiments established a qualitative link between the presence of a slow diffusive mode and the degree of sulfonation. The branching parameter *g* was determined for the star-branched NaPSS samples and compared to theoretical predictions of *g*, verifying the type and extent of branching and the retention of the molecular structure after polymer-analogous sulfonation.

Having thus determined that the star-branched NaPSS samples were suitable for use as model polymers, static light scattering experiments were performed to elucidate the effect of varying ionic strength on the $R_g$, where it was determined that $R_g \sim C_s^{-0.11}$ for the whole range of samples. The apparent persistence length of each sample was determined using the combinatorial wormlike star theory, and relations were established for its variation as a function of $C_s$, *f* and degree of arm polymerization. Additionally, no agreement was found between theoretical predictions of *g* and experimentally determined ones. No slow diffusive mode was observed for very dilute solutions of the samples in solutions with $C_s$. A novel method was developed that enabled the determination of molecular dimensions of star-branched NaPSS using AFM with a high degree of

agreement with the radii established using scattering methods on solutions of the polyelectrolytes. The method was found to be applicable over a wide range of $C_s$.

We also examined the viscometric behavior of star-branched NaPSS in a range of aqueous solutions of varying ionic strength. The intrinsic viscosity could reliably be determined in solutions with $C_s$ using either a Huggins equation or a Wolf equation. For aqueous solutions with no $C_s$, the fit of the Wolf equation to the viscosity data was poor, whereas utilization of the Huggins equation over the linear portion of the data at low $C_p$ enabled an alternative determination of the intrinsic viscosity. This hypothesis was tested by AFM measurements of the dimensions of the polyelectrolyte and comparisons to the viscometric radii determined from the intrinsic viscosities calculated using the two equations. A very close fit between the $R_{afm}$ and the $R_v$ calculated from intrinsic viscosities determined by the Huggins equation led to the conclusion that this method of analysis can be used in the regime of $C_p$ significantly below the maximum known as the viscosity polyelectrolyte effect. The observation that the $R_v$ of the 50s and 60s series of stars did not vary significantly with *f* in dilute aqueous solutions with no $C_s$ was correlated to predictions for the dilute osmotic regime with counterion condensation. Several observations support the hypothesis that small, densely branched NaPSS stars display viscosity behavior distinctly different from stars with longer arms, displaying aggregation phenomenon on AFM images and unusual increases in viscosity at very low $C_p$. The values of g' were calculated for solutions of the NaPSS stars in water, where it was observed that sets of stars with shorter arms had much smaller values of g' than that calculated by theory, but the set of stars with the longest arms showed good agreement with the theoretical g' values predicted by Fixman. The maximum in the $[\eta]_{red}$ vs. $C_p$

relation known in the literature as the viscosity polyelectrolyte effect was observed for all star branched NaPSS samples studied.

### *Future Work*

Though the results summarized in the previous section constitute a good start towards understanding the phenomenon of branching in polyelectrolyte solutions, several different avenues for future research are naturally suggested as continuations of the present work. Some of the most obvious are:

(1) The TGA methodology demonstrated in Part 3 could become a quantitative method of determining the sulfonation degree of NaPSS samples. A set of linear NaPSS with degrees of sulfonation and molecular weighs extending over a wider range than was studied in this thesis could be examined to this end. A TGA coupled with a gas chromatograph could elucidate the decomposition products resulting from each portion of the curve, resulting in a deeper understanding of the reactions involved at each step of the decomposition.

(2) To extend the work in Part 4 and confirm that the combinatorial wormlike star is an appropriate model for use star-branched NaPSS, small-angle neutron scattering could be conducted on the samples to determine the persistence length of the samples independently.

(3) To extend the work in Part 5, a more detailed rheological study of the star-branched NaPSS is appropriate. Such a work would have as its aims the examination of the effect of shear on the solutions of varying $C_s$ and how

it compares to the effects previous seen for linear NaPSS. The determination of relaxation times and terminal moduli would also be of interest in terms of comparison. The anomalous viscosity behavior of samples 44s and 46s also merit more study, to study the abrupt increase in viscosity at very low $C_p$ and determine whether its origin rests in an aggregation phenomenon, as suggested by AFM measurements.

The work in this thesis has elucidated many of the properties of solutions of star-branched NaPSS, but, as illustrated by the above points many questions remain unanswered. Hopefully, many of these questions can be addressed with the set of polyelectrolyte stars painstakingly synthesized and characterized herein.

# Vita

D. Wade Holley was raised in the small town of Hartford, Alabama by his loving parents Martha and Nick Holley, who encouraged him to read and study from an early age. After high school, Wade attended Troy University, where he discovered a love for chemistry inspired by the excellent teaching of the Chemistry department faculty. After earning a B.S. in Chemistry, Summa Cum Laude, Wade continued his studies at the University of Alabama-Birmingham with Dr. Jimmy W. Mays where he was awarded a NASA Fellowship. When Dr. Mays transferred to the University of Tennessee-Knoxville, Wade followed and was awarded a TAML Fellowship. During his time at U.T., Wade presented posters at several international polymer science conferences and a talk at Pacifichem in 2005. Wade successfully defended his dissertation on July 29, 2009, and will graduate in December 2009 with his Ph.D. in chemistry.